DOE/ER/10471-2

Illinois Institute of Technology, Chicago, Illinois 60616

STUDY OF THE INTERACTIONS BETWEEN FRICTION, WEAR AND SYSTEM RIGIDITY

FINAL REPORT

FOR PERIOD JULY 1, 1979 - JUNE 30, 1981

V. ARONOV, A. F. D'SOUZA, S. KALPAKJIAN AND I. SHAREEF

MARCH 1982

PREPARED FOR
THE U. S. DEPARTMENT OF ENERGY
UNDER CONTRACT NO. DE-AC02-79ER10471

DOE/ER/10471-2

STUDY OF THE INTERACTIONS BETWEEN FRICTION, WEAR AND SYSTEM RIGIDITY

Final Report

For Period July 1, 1979 - June 30, 1981

V. Aronov, A. F. D'Souza, S. Kalpakjian and
I. Shareef

Illinois Institute of Technology
Chicago, Illinois 60616

MARCH 1982

Prepared For

The U. S. Department of Energy

Under Contract No. DE-AC02-79-ER10471

TABLE OF CONTENTS

ACKNOWLEDGEMENTS

We gratefully acknowledge the financial support and guidance by Dr. Oscar P. Manley of the Office of Basic Energy Sciences of the U.S. Department of Energy. We would also like to acknowledge the assistance of Mr. Eugene G. Johnson of the MMAE Department at IIT in the construction of test facilities and the help of Mr. F. Dream, graduate student in the department, in obtaining some of the experimental data. We would also like to thank Ms Christine Gillotte for typing this report.

I. ABSTRACT

This study was undertaken to investigate the interrelationships between system rigidity and friction and wear. A special apparatus was designed and constructed where the system rigidity could be changed, and experiments were conducted with water lubrication and also under dry conditions. During experiments the wear rate, friction force and normal force oscillations as well as slider vibrations were measured and analyzed. The samples of work surfaces were subjected to the light and scanning electron microscopy analysis and Talysurf roughness measurement. These analyses have shown that three main regimes of friction exist as a function of system rigidity, namely, a) "steady state" friction associated with the smallest rate of wear, b) friction with "self-disturbances" causing highest rate of wear and c) regime of self excited vibrations. The wear behavior and slider vibration in tangential and normal directions are analyzed for all three friction regimes.

II. INTRODUCTION

Friction and wear are being increasingly recognized as important areas of study because of their technological impact, particularly in the conservation of materials and energy. It has been observed that friction can often excite vibrations which, in turn, can affect friction and wear. The subject of the interaction between friction, wear and system rigidity is quite complex and, depending on the particular parameters involved, one or more mechanisms can be responsible for this interaction.

The subject of friction and wear between sliding surfaces has been studied extensively for many years in terms of their controlling factors and parameters such as materials, surface conditions, loads, speed, temperature, environment, and lubricants. Various theories have been proposed concerning the mechanisms of friction and wear, and numerous attempts have been made to establish quantitative relationships between the many parameters involved.

However, little attention has been paid in the past to the effect on friction and wear due to system rigidity, i.e., dynamic characteristics of the equipment, machinery or test facility. Friction induced vibrations have been studied to some extent and the stick-slip phenomenon, which occurs at low sliding speeds, has received much attention. However, the effect of vibrations on wear has not been investigated, although it is recognized that it can lead to not only objectionable noise levels but also it could result in surface damage and eventual failure of machine components.

It appears that several different mechanisms can be responsible for friction-induced vibrations. It has been established that, even within the same system, more than one mechanism of wear can be operative as a result of a change in only one parameter. The traditional models of adhesive, abrasive, oxidation, and fatigue wear are commonly observed. Yet, the conditions under which transitions take place from one mechanism to another are difficult to establish.

The effect of the dynamic characteristics of the system on the mechanism of wear and wear rate is a subject that requires careful study. It would appear that in studies of friction and wear, it is not sufficient to vary only parameters such as load, speed, lubrication, etc., but also to vary parameters such as inertia, stiffness and damping in as many direction as practicable.

Accordingly, an interdisciplinary investigation combining the areas of dynamics, friction and wear was undertaken at the Illinois Institute of Technology under the sponsorship of the Office of Energy Research of the U. S. Department of Energy. The objectives of this study were as follows: a) investigation of friction, wear and vibration regimes encountered under different lubricating conditions; b) investigation of the effect of slider rigidity on friction, wear and vibrations; c) investigation of wear processes including the interactions among friction, vibration and wear; and d) model development of the vibratory system and analysis of self-excited vibrations.

The technical background is given in the next chapter which describes the several friction-induced vibration mechanisms and the interaction between wear and vibrations. In the chapter that follows, a review is given of the experimental set-ups used in tribology research in the recent literature and a description is given of the mechanical design of the test facility that was built for the present study.

Two types of experiments with different lubricating conditions were undertaken in the present study. In the first set of experiments, water was used as boundary lubricant. After some modifications of the test apparatus, a second set of experiments were conducted with dry friction. A description of the test apparatus, materials, measurement techniques and experimental results for the two sets of experiments is given in Chapter V. The model development of the vibratory system employed for the dry friction experiments and analysis of self-excited vibrations are covered in Chapter VI. A discussion of the results of the two sets of experiments and conclusions and recommendations for future work are given in the last chapter.

III. TECHNICAL BACKGROUND

A. Friction-induced Vibration Mechanisms

Although the nature of resistance to relative motion of two surfaces in contact is not completely understood at the present time, it is well known that friction is not entirely a steady state process. Unsteady friction is usually accompanied by vibrations of the machine components. Several different types of friction-induced vibrations have been reported in the literature. It is apparent that there exist several distinct mechanisms that can excite different types of oscillations. This study is not concerned with externally forced vibrations caused by unbalance, worn bearings and other reasons. The following discussion is devoted to the analysis of the various mechanisms of friction-induced vibration and their effect on the rate and mechanisms of wear processes.

a) Stick-Slip. The formation of areas of contact by adhesion of asperities and hence sticking of two surfaces was first reported by Hardy and Hardy [1]* in 1919 and again a decade later by Tomlinson [2] in 1929. Since that time, self-excited vibrations of the stick-slip type have been studied by several investigators such as Rabinowicz [3]. They occur at very low sliding speeds and, as observed by Ko and Brockley [4], they have almost a saw-tooth wave-form, the "stick" part having zero relative motion. As discussed by Brockley, Cameron and Potter [5], the mechanism that causes stick-slip is attributed to the fact that there is a difference between the static and kinematic coefficients of friction and static friction requires some time to build up to its steady-state value after the surfaces in contact come to rest with respect to each other. This behavior of static friction is discussed by Brockley and Davis [6]. As the sliding speed is increased, there is a critical value of the speed above which stick-slip type of vibrations are not induced [5].

b) Mechanism of Negative Slope of Friction-Velocity Curve. The negative slope of the friction versus sliding speed curve in certain regions has been recognized in the past as the cause of instability which supplies energy to the vibrating system, as discussed by Den Hartog [7]. These vibrations are almost sinusoidal in waveform and have been named quasi-harmonic vibrations by Brockley and Ko [8]. Several reasons have been advanced to explain the decrease in the friction force with increasing sliding speed in certain regions of the friction-sliding speed curve. Fuller [9] has noted that the rise in temperature should contribute to the decrease in friction at high sliding speeds. Kummer and Meyer [10] attribute this drop partly to the velocity effect and partly to the temperature effect.

Tolstoi [11] has proposed a very interesting hypothesis to explain the negative slope of the friction-velocity curve. According to him, this is closely associated with the degree of freedom of the slider in the normal direction. He conducted experiments in which sufficiently heavy damping of tangential vibrations alone could suppress these vibrations but failed to affect the negative slope of the friction-velocity curve. On the other hand, when the micro-vibrations in the normal direction were damped, not only did the sliding become uniform but the decrease of the frictional force with sliding velocity disappeared.

The factors through which sliding velocity affects the slider elevation are as follows:

1) When placed on the supporting surface, the slider sinks gradually, a finite time being required to produce the deformations and indentation of the asperities. In the process of sliding, the higher the speed the shorter is the time during which opposite asperities compress each other and the higher is the level on which the slider moves.

2) An increase in speed increases the components of the impulses exerted on the slider asperities in the direction normal to the surface as they collide with those of the opposite surface. This increases the amplitude of the normal vibrations.

As the slider is raised there occurs:

1) A decrease in the total area of actual contact.

2) A decrease in the depth of indentations, if any, of the harder asperities in the softer material.

3) Eventual decrease in the resistance of all types of plastic deformation, including the wearing and rupture of the junctions occuring in the process of sliding.

4) Increase of the atomic separations in the normal direction, with an eventual decrease in the tangential components of the molecular forces.

5) Decrease in the area of contactless adhesion, i.e., the total area of the patches on which the distance between the opposite non-touching asperities is less than the range of molecular forces. This area may be much larger than the area of actual contact so that contactless adhesion may contribute a significant fraction of the total normal and tangential (friction) forces.

c) Mechanism Due to Coupling Between Different Degrees of Freedom. A study of the generating mechanism of frictional noise has been reported by Yokoi and Nakai [12]. In their experiments on sliding dry friction they observed quasi-harmonic vibrations which they named squeal. An interesting point to note is that these vibrations occurred not only in the region where the slope of the friction force versus sliding speed is negative but also in the region where it is positive. They state that their experimental results are inconsistent with the frictional vibration theory that self-excited vibrations are not generated when the slope of the friction force versus sliding speed is positive.

It is likely that the mechanism is a coupling between the normal and frictional degrees of freedom. Our own experimental results concerning high frequency self-excited vibrations, which are discussed later, exhibit this coupling between the normal and frictional degrees of freedom.

Our experimental results obtained in machining at IIT showed that chatter occurred in the region where the slope of the friction-sliding velocity curve is positive and exhibited a coupling between the cutting and thrust degrees of freedom.

The generation of squeal-noise by dry friction has been studied by Earles and Lee [44], where they recognized the importance of the coupling between different degrees of freedom in their linear analysis.

The experimental study of Bhushan [13] has employed a glass slider, sliding over a rubber stave with water lubrication. He observed two types of friction induced vibrations, namely, low frequency oscillations which he has named chatter and high frequency oscillations which he has named squeal. Generally, squeal was generated at low normal loads and high speed whereas chatter was generated at high load and low speed or very high load and any speed. Krauter [14] has presented a linear mathematical model with coupling in three degrees of freedom to predict the onset of squeal/chatter instabilities. It is likely that the low frequency chatter observed by Bhushan [13] corresponds to the friction regime which is discussed next.

d) Mechanism of Intermittent Self-Disturbances. Our experimental results discussed later indicate that in a certain region the steady state friction process is unstable and gives rise to intermittent self disturbances. During a disturbance, the friction force suddenly increases from its nominal value and decreases back to it. This behavior is attributed to intermittent formation of metallic junctions and their subsequent shearing. This unsteadiness causes damped oscillations which are discussed later.

e) Mechanism of Stochastic Oscillations. Due to the general heterogeneity of the mechanical properties of the surfaces and due to wear processes, the asperities are randomly distributed over the surfaces. During sliding the surfaces in contact change with time and give rise to fluctuations in both the normal and frictional forces. It is possible for the power spectral density of the random process to possess a significant component at the natural frequency of the slider. In that case, the slider will vibrate at its natural frequency with random amplitude which may not be negligibly small.

B. Interaction Between Wear and Vibrations

Apart from various mechanisms of wear there are mainly three recognized mechanisms of wear in unlubricated sliding friction, namely, mild (or oxidation), adhesive (or severe), and abrasive.

Mild wear is associated with formation of specific films between sliding surfaces preventing direct metallic contact [15-17]. This film is usually a product of the interaction between metallic surfaces and active components of environment. These products are, in most cases, metallic oxides [17-19]. The break-down process in this case is localized in the film without damaging the bulk material. The slider vibration causes a change in the contact stress distribution and conditions of elasto-plastic deformation of the surface layers. This action can affect both (a) processes of metallic surface interaction with interfacial media and, (b) break-down of formed product. A change in the ratio of their rates can cause a transition to the mechanism of severe wear.

Although the mechanism of mild wear and the parameters involved (load, sliding velocity, materials, medium, and temperature) have been extensively investigated [15,19,20-25] there is little literature available on the interaction between wear and vibration.

Zaporogetz [26,27] has analyzed the oscillation of the friction force with respect to the different mechanisms of wear. The sliding friction force of two lubricated steel surfaces was recorded at various normal loads and sliding velocities. For every given set of sliding velocity and normal load, the rate of wear was measured and the type of wear was determined.

Harmonic analysis of the friction force oscillation shows that the transition from mild to severe wear causes both a change in amplitudes and frequency of the harmonics of the friction force oscillations. The conditions of severe wear differ from oxidation wear in that the amplitudes of the intermediate harmonics (2-5 kHz) decrease while the amplitudes of the low frequency harmonics (300-1000 Hz) increase.

Noticing that physicochemical processes play a major role in friction, the authors [28-30] have proposed to describe the friction force by its dynamic characteristics rather than by its average value.

The friction force depends on the properties of two mating surfaces and their change with time. This change in the surface properties is mostly caused by the inevitable wear (breakdown) process. This is very well shown [28] by the change of the electrode potential in the electrolyte solution. The electrode potential in this case is proportional to the ratio of areas covered by the oxide film and areas where the film is broken [29]. The beginning of the friction process causes an increase in the areas where the oxide film is broken. After this, the electrode potential oscillates randomly, indicating that neither the breakdown process of the oxide film destruction nor the process of the oxide film regeneration are constants. Their rates change with time thus changing the surface conditions which, in turn, affect the friction force.

Not only the magnitude of the slider oscillation may change the conditions of the frictional surfaces but the frequency of oscillation can also play a major role. From Aronov's [30] investigation of 2Hz the rate of wear is lower and wear is of the oxidative type. At the lower and higher frequencies, the rate of wear increases and surface breakdown is due to cold seizure. Thus, the change in the frequency of the normal load application causes repetetive transition from cold seizure to oxidation wear and once again to the cold seizure. One possible explanation is that a change in the frequency of the normal load application causes a change in the rate of elasto-plastic deformation of surface layers thus affecting both the breakdown processes and the processes of surface interactions with interfacial medium. At the lower frequency, the rate of breakdown was higher than the rate of oxidation. With the frequency increase and possible increase in temperature, the rate of destruction was once again higher.

Ever since the terms "mild" and "severe wear" were first introduced by Hirst [33] in order to describe the sudden transitions in wear rates, they have been the focus of many experimental investigations. Lancaster [34] explains the transition from mild to severe wear as arising from competition of two opposing dynamic processes. One of these is the formation of fresh metal surface and the other is the formation of surface oxide film by reaction with the surrounding atmosphere.

In mild wear, the contact surface at any moment of time is dominated with protective (transformed) films, while a small portion is free of these films as a result of their destruction, Figure 1.

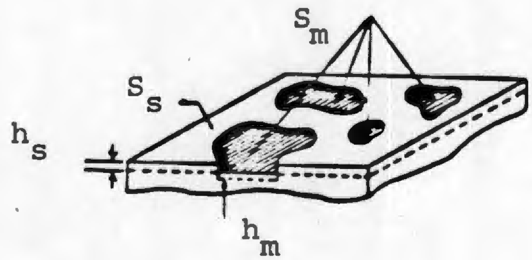

(a)

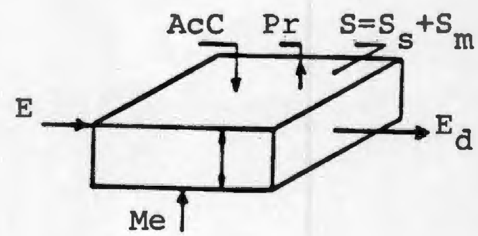

(b)

Figure 1. (a) Model of the Friction Surface: S Area of the Friction Surface; S_s Area of the Film of the Transformed Structure; S_m Area of the Juvenile Metal on Which the Film of the Transformed Structure was Destroyed; h_s depth of Film of the Transformed Structure; h_m depth of the Metal Involved in the Formation Process of the Transformed Structure. (b) Model of the Reactive System: Me, metal; AcC, Active Component of the Surrounding; Pr, Products of the Destruction Process; E, Energy Input; E_d, Dissipative Energy.

In the case of severe wear the situation is vice-versa. In other words, it means that the surface layer comprises of a given spatial zone on which the two processes, namely, formation of protective film and its breakdown take place. Aronov [20], [21] showed that the rate of oxidative wear in this case can be expressed as

$$W = \frac{K_1 K_2}{K_1 + K_2}$$

where K_1, K_2 are corresponding rate constants.

For given materials both K_1 and K_2 are functions of temperature and contact stresses. An increase in the rate of protective film breakdown causes an increase in surface areas unprotected by this film and, thus, direct metallic contact between the two surfaces becomes probable. As this occurs transition from mild to severe wear takes place. Rabinowicz [35, 36] emphasized very strongly the fact that practical interest is mainly confined to low or moderate friction problems. The solution to many of the problems appear to lie in avoiding stick-slip oscillations. The basic mechanism of their occurence and their effect on wear is still not clearly understood.

Kimusa [37] emphasizes the importance of high friction on tribological phenomena such as wear, stiffness, seizure, whose friction coefficients exceed even 100 [38,39,40]. Nevertheless, the possible roles of friction and frictional oscillations in such phenomena have not been properly analyzed in terms of fundamental understanding of friction and its interaction with wear. Further investigation is clearly needed to explain and to control friction and friction-induced vibrations.

Friction-induced vibrations of a tribological system, being a function of the system rigidity and surface conditions, causes energy dissipation through this vibration. The main source of energy dissipation in this case is the friction process itself [41,42]. Thus, it becomes obvious that friction induced vibration, affecting contact stresses and temperature, unavoidably offsets wear. The direct evidence of this is obtained in our experiments where it is shown that the rate of mild wear under water lubrication is a function of sytem rigidity. It is not still clear as to what causes this behavior. It appears that mainly two mechanisms are responsible, namely, i) different sliding distance of the slider due to change in oscillation frequency, and/or ii) different stress distribution in the contact zone.

In any case the normal and tangential rigidities and coupling between them are likely to be controlling parameters. Although transition from mild to severe wear was not affected by system rigidity in our water lubrication experiments [43], self excited vibrations (a strong function of system rigidity) can occur before this transition. Self excited vibration dissipates a large amount of energy through friction that can, in turn, cause an increase in the rate of mild wear, or even transition from mild to severe wear may occur. Once again in this situation the rigidities in normal and tangential directions and their coupling are likely to be controlling parameters.

From the above discussion it is obvious that a systematic study of the effect of tangential and normal slider rigidities on friction induced vibration and their effect on wear rate is necessary for understanding friction and wear mechanisms, so that a safe and reliable tribological design concept could be developed thereby resulting in low energy consumption and reduced cost.

IV DESIGN OF TEST FACILITY

A) Review of Recent Designs used in Tribology Research

As it is evident from the review of the literature on tribology, there are very complex interrelationships between friction, vibration and wear.

It is clear, therefore, that the dynamic characteristics of both the structure of the total system and of the frictional contact should play major roles in friction and wear. In view of the complexities involved in such dynamic characteristics of a tribological system, a great deal of effort was expended in the design of the equipment to be used in this present study. Furthermore, it was felt that a comprehensive study and evaluation should be made of all the various apparatus or equipment described in the available literature on the subject.

A great variety of friction and wear test devices have been developed over the past few decades with a variety of characteristics [31]. A majority of these designs are for somewhat routine testing of materials in sliding contact at ambient temperature and environment. More fundamental studies in the subject have necessitated the use of more sophisticated and instrumented apparatus as described below.

For a considerable period of time the most common friction and wear measurement apparatus has consisted of a pin and disk system. Friction force has been measured through the deflection of the arm supporting the pin. It is obvious that in order to be able to measure small magnitudes of friction force, the arm must not be too rigid. However, this in turn introduces a lack of stiffness in the tangential direction. The stiffness normal to the sliding surface is, in a sense, simply the weight of the arm. Dynamically, however, this mass is very significant because of the inertia effect when asperity movement is taken into account.

Such a system is, of course, useful in studying stick-slip phenomena in one direction, i.e., tangential, only where displacements can be measured by a transducer, as shown in Figure 2 used by Brockley and Davis [6]. Their apparatus was designed to study the time-dependence of static friction. It consists of a variable speed turntable (disc), a cantilever beam to provide both normal load on the specimen and spring force, and a displacement transducer to determine the friction force. The sliding speeds could range between 0.001 and 1 in/sec (0.025 and 25 mm/sec). The length of the cantilever beam was adjustable and thus the spring constant of the system could be varied. The normal load application, as shown in the figure, kept the vibrating mass constant regardless of the load.

Brockley et al. [5] used a similar system in another study on friction induced vibration, with the exception that the sliding was linear and damping of the slider was provided for by permanent magnets, Figure 3. The driven surface was 6 ft. (183 cm) long with speeds ranging from 0 to 9 in/sec (0 to 230 mm/sec) with great rigidity and large mass. Different damping ratios were obtained by reducing the flux gap and tests revealed that damping was essentially viscous in nature. The stiffness of the slider assembly could be altered by changing the length

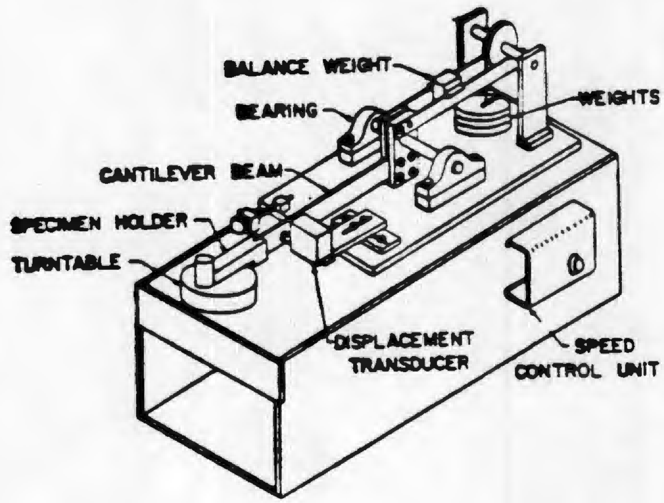

Figure 2. Diagram of the Apparatus used
by Brockley and Davis [6]

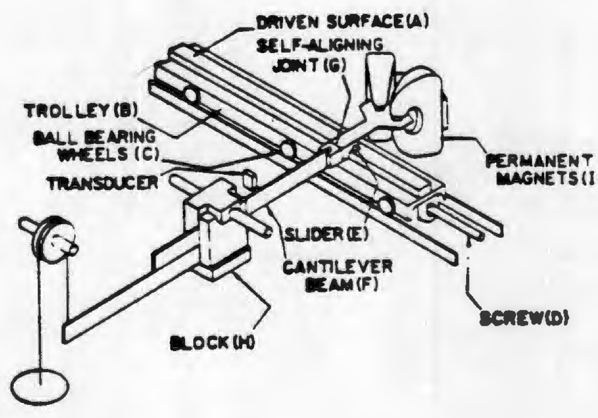

Figure 3. Diagram of the Apparatus used
by Brockley, Cameron and Potter [5]

of the cantilever beam.

In further studies on friction-induced vibration by Ko and Brockley [4], special attention was paid to careful isolation of vibrations arising from the test apparatus or the surroundings. They also used accelerometers, velocity transducers and strain gauges for measurement of various quantities in the vibrating system, Figure 4. One feature of this system was that the apparatus was placed on a massive table resting on a rigid foundation. Note also, in the insert to the figure, the design of the slider support mechanism which assures uniform contact with the rotating disk.

Even though the designs discussed above are among the most advanced, it will be noted that only the rigidity in the tangential (sliding) direction can be changed. There appears to be no attempt to make provisions to make the stiffness normal to the sliding surface another variable in the system. In these apparatus, "resistance" to any transient vertical, i.e. normal to sliding surface, displacement is obtained through the inertia effect of the equivalent mass of the slider arm. It can easily be visualized, of course, that in addition to this mass there can also be a stiffness incorporated in the system.

Although not a part of their study, Swinnerton and Turner [32] used an apparatus which involved a compression spring between the slider and the point of load application, Figure 5. This system was used to simulate sliding electrical contacts used in practice. It is obvious, of course, that even

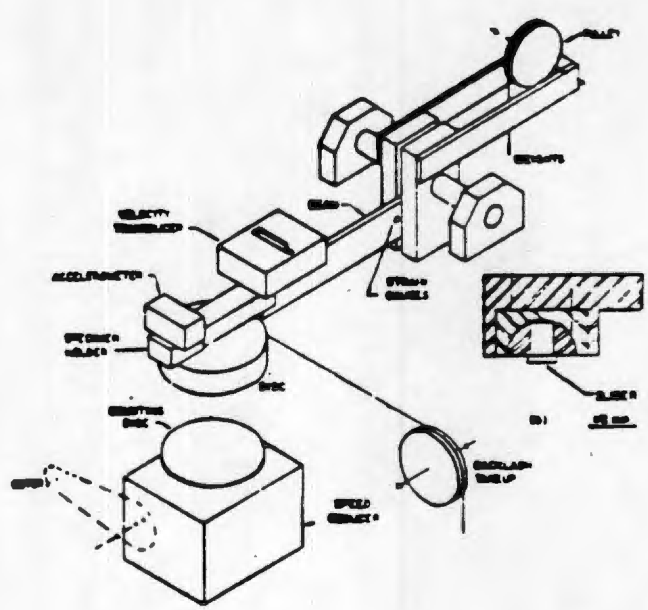

Figure 4. Schematic Diagram of (a) the Apparatus and (b) Self-Aligning Slider Mount used by Ko and Brockley [4]

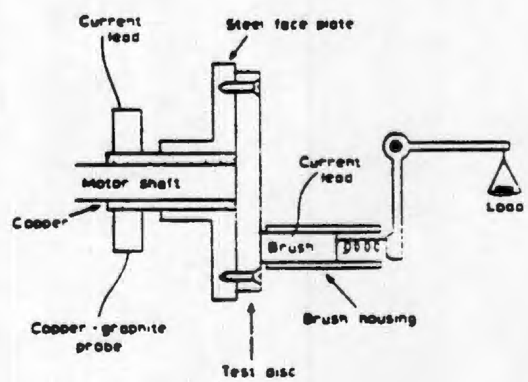

Figure 5. Experimental Apparatus used by Swinnerton and Turner [32]

though the load on the slider may be the same, this load could be transmitted through a spring with different spring constants, i.e. stiffnesses. Thus, the masses would remain the same but the stiffness could be changed over a wide range. The authors do not comment on the role of the stiffness of this spring.

Tolstoi [11] has pointed out the significance of the normal degree of freedom and natural normal vibrations in contact friction. Although conducted at very low sliding velocities of the order of 10^{-9} cm/sec, he showed that both negative friction-velocity slope and frictional self-excited vibrations are closely associated with the freedom of normal displacements of the slider. Whenever the latter is absent, self-excited vibrations disappear. Direct interferometric observations showed that, in self-excited vibrations, the tangential "darts" of the slider are invariably accompanied by simultaneous upward, i.e. normal, jumps.

His apparatus, Figure 6(a), involves a slider (6) in the shape of a circular ring rotating over a disk (5) whose angular velocity was held steady by the damping system below the disk. The normal displacements of the slider were determined interferometrically by the device shown in Figure 6(b). Damping of the slider in the normal direction is accomplished by the damping device (9,10) where bent blades are immersed in a viscous oil, thus causing damping in the vertical direction. Damping can be removed by simply sliding downward the containers (10) filled with the oil.

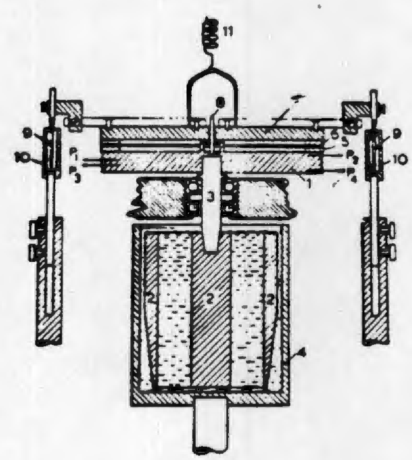

(a)

(b)

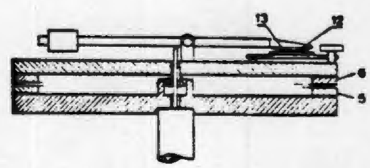

Figure 6. Low-speed Sliding Friction Apparatus (a) used by Tolstoi [11] and the Interferometric Device (b) for Measuring Vertical Slider Displacements

Yamada et al. [45] observed that to analyze friction and wear mechanisms it is necessary to represent the configuration of a surface by the surface density of asperities and the distribution of asperity heights. For experimental analysis of this, they used a test apparatus as shown in Figure 7. It is essentially a pin on disc system with gravity loading mechanism. It includes a damper in the system which cannot be changed easily and is effective only in the tangential direction. Further, with this system the system rigidity cannot be changed.

Tadashi Sasada et al. [46] also used a pin on disc type apparatus similar to the one shown in Figure 8. The design of the apparatus is horizontal type and the pin specimen is loaded against the rotating disc through a hydraulic piston. An aluminum plate is fixed on the piston perpendicularly to the pin axis; the parallel movement of the plate is measured by a non-contacting gap sensor and recorded on a pin oscillogram.

Kato et al. [47] used yet another modification of pin on disc system shown in Figure 9. Here a steel ball is used as a single protuberance, which is pressed against the surface of a rotating disk to measure frictional force. An arm and a lever arrangement actuated by dead weights is used for normal loading. The system is so arranged that the point of frictional contact lies vertically below the point through which the lever applies force. This ensured constant normal loading to be maintained at all times.

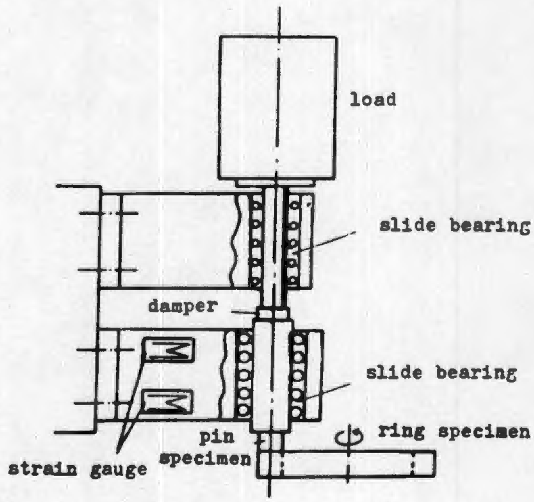

Figure 7. A Schematic Diagram of the Apparatus used by Yamada et al. [45]

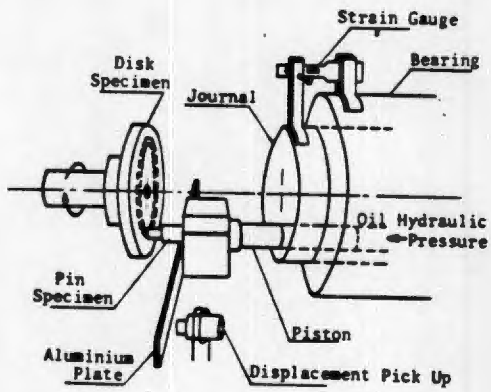

Figure 8. Experimental Apparatus used by Sasada, et al. [46]

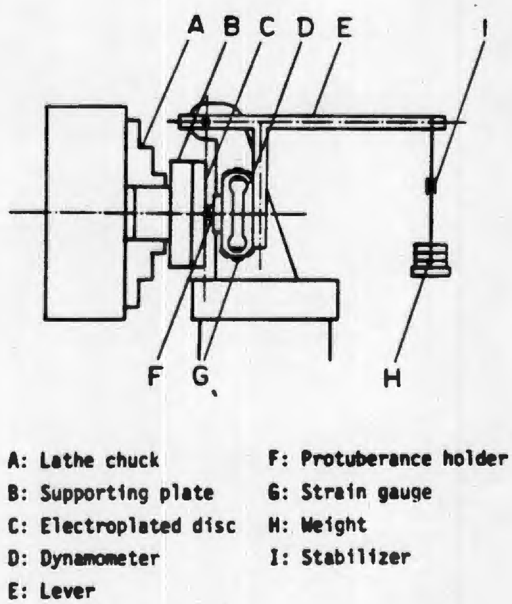

Figure 9. Experimental Apparatus used by Kato et al. [47]

Recent trend in the development of tribomachines has been towards more sophistication and automation. Two such meachines have been designed by Moore [48,49]. The first one is a precise wear screening machine which can test six pin samples simultaneously. Wear of the test pins is measured in situ by detecting the linear dimensional changes by a precision travelling microscope. By taking several readings during a test at preselected time intervals, it is also possible to plot wear rate of the test pin samples. An isometric sketch of the design is shown in Figure 10.

The second tribomachine recently designed by Moore and Noah [49] is a simple reciprocating friction and wear tester. It is a simple and accurate bench machine, which can also be used for fatigue testing. It essentially consists of a variable speed drive unit with built in loading and friction head which reciprocates within a frame work containing the test surface. A scale assembly drawing of the machine is shown in Figure 11. Sample loading is pneumatic or by gravity. Pneumatic loading has the advantage that a restoring force exists to keep sample and track in contact at all times during relative sliding. Hence on rough or undulated surfaces, the speed can be increased to maximum values at the same time; the load capacity is greater than can be accomplished with gravity loading. The machine is also capable of varying both the speed and stroke. The major disadvantage is that the machine may be used only to evaluate the friction and/or fatigue performance of elastomer materials.

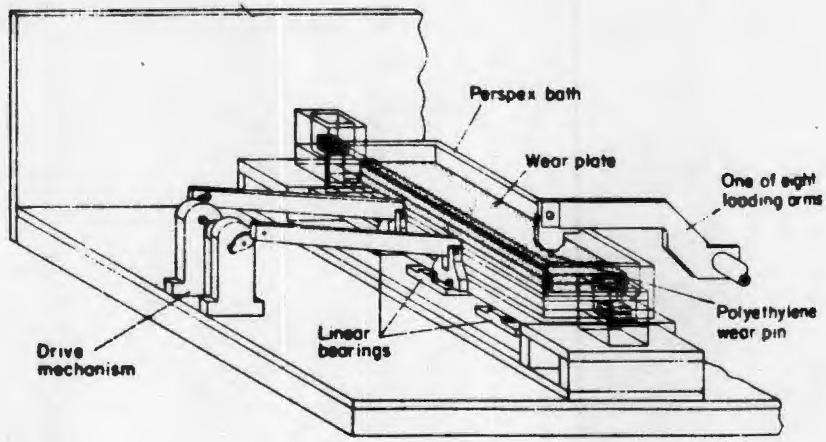

Figure 10. Isometric Sketch of the Machine used by Moore [48]

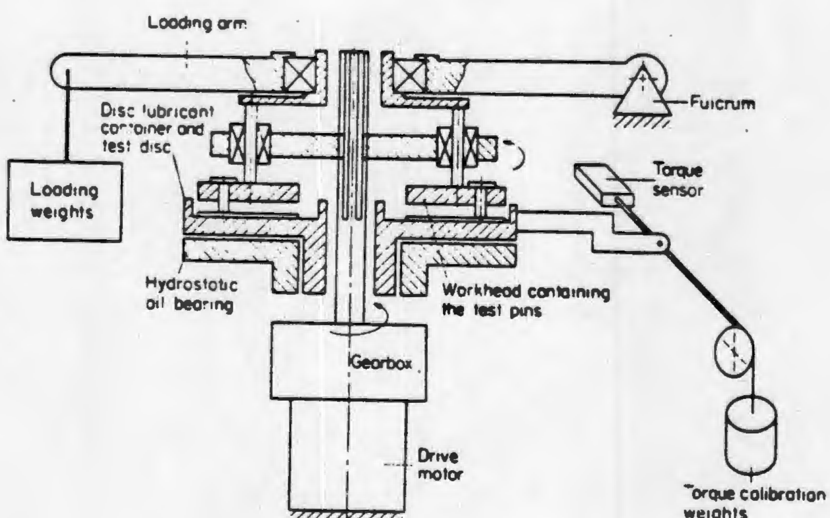

Figure 12. Basic Design of Tribometer used by Throp [50]

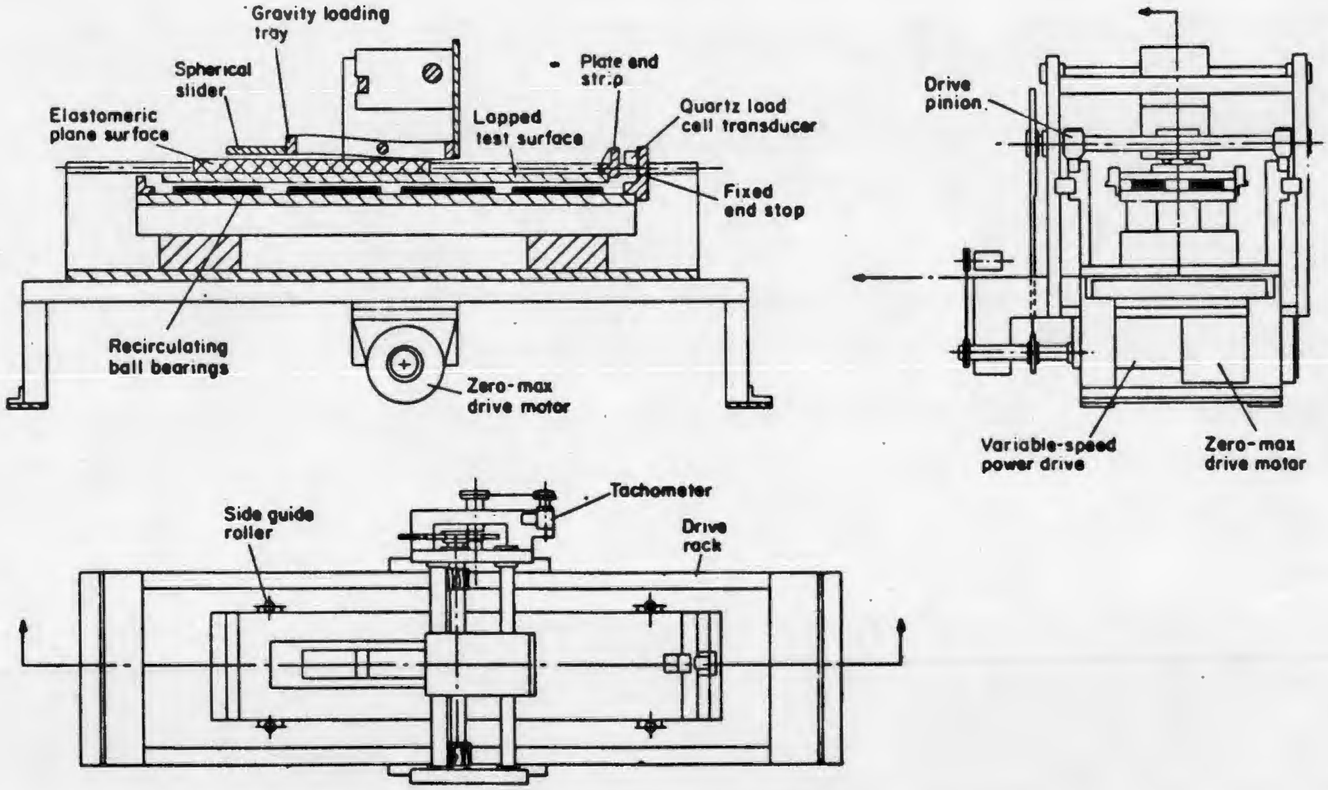

Figure 11. Scale Assembly Drawing of the Machine used by Moore and Noah [49]

A conventional pin-on-disc tribometer is, in general, unsatisfactory for the evaluation of the friction and wear behavior of material interfaces lubricated with fluids. The centrifugal forces cause liquids to be flung off the rotating disc at speeds well below those typical of many industrial applications. A novel tri-pin-on-disc tribometer has been designed and built at Physics & Engineering Laboratory, Lower Hutt, New Zealand [50] which overcomes this problem by rotating three pins on a restrained horizontal disc. A schematic picture of the tribometer is shown in Figure 12. This arrangement allows the retention of small quantities of fluid up to high pin sliding speeds. The design also facilitates lubricant temperature control. The tribological behavior of wide range of material/lubricant/additive systems can thus be determined with this tribometer under a wide range of load, speed and temperature conditions.

B) Mechanical Design of Test Facility for Present Study

Selection of Frictional Contact Geometry.

Seven different types of frictional contact geometry were considered for this project, Figure 13 (a to g):

a) Line contact formed between two rollers rotated at different angular velocities.

b) Contact areas formed between a rotating roller and a brake shoe.

c) Line contact formed between rotating cylinder and a flat surface.

d) Point contact formed by two rotating cylinders placed orthogonally.

e) Flat area formed between rotating disk and a reciprocating pin.

f) Flat area formed between rotating disk and a stationary pin.

g) Flat area formed between rotating and stationary cups.

The following criteria were evaluated in order to select the proper design:

1. Ability to achieve constant apparent contact area.
2. Ability to achieve constant normal stress.
3. Simplest way to apply load.
4. Simplest way to control load, rigidity and damping.
5. Simplest mechanical design without loss of any essential features.

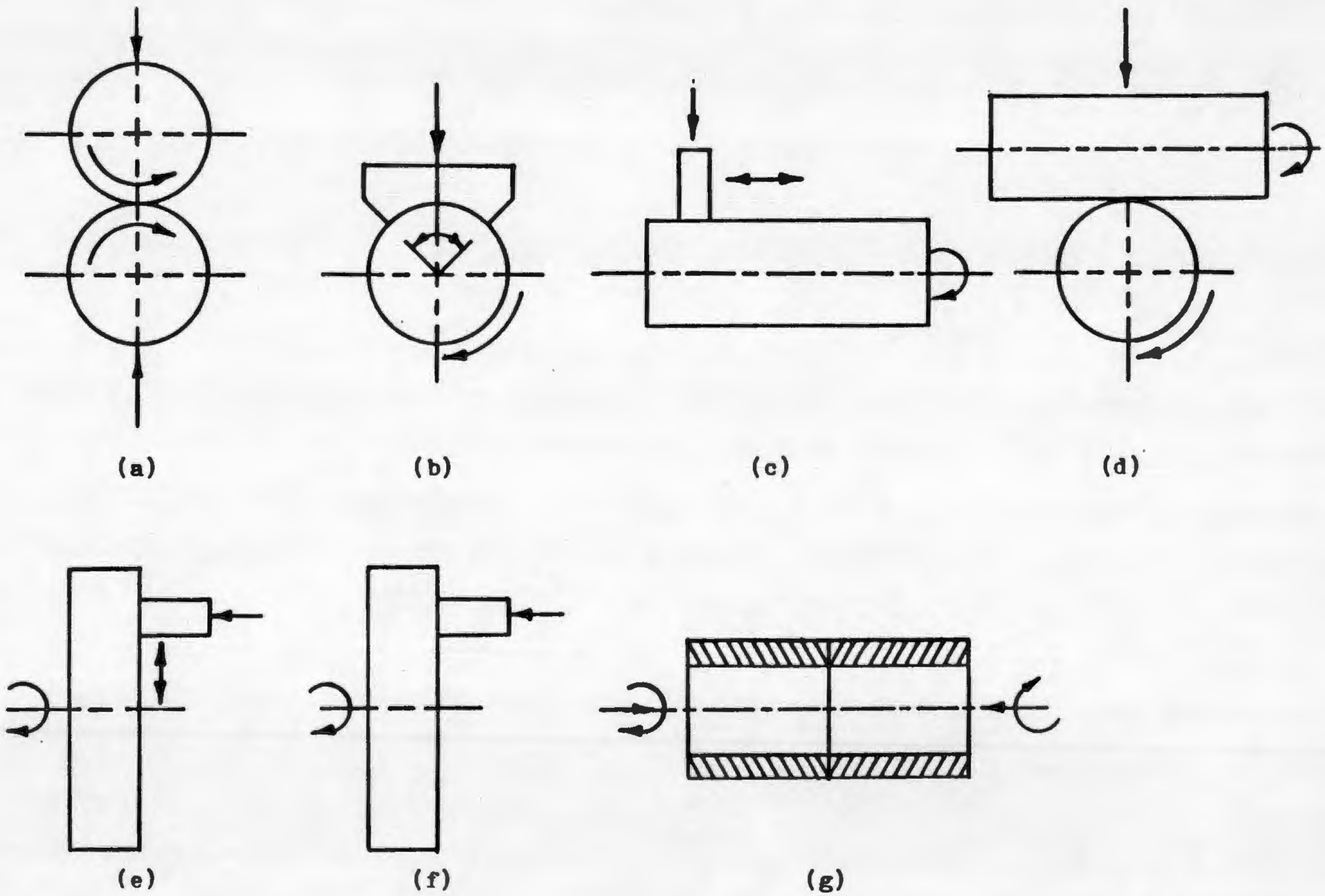

Figure 13. Different Types of Frictional Contact Geometry

It was decided to use a rotating disk and a stationary pin rubbing against it to obtain frictional contact. Various configuration of disk and pin contact were considered, as shown in Figure 14 (a to e).

While evaluating the type of contact geometry, the possibility of using the spindle and bed of a lathe was checked. The lathe spindle was not vibrating from 0 to 1500 rpm when all gears from the gear box were taken apart. With the possibility of using the spindle and bed of a lathe as a part of the testing device and on the basis of the above mentioned criteria, the design shown in Figure 15 was finally selected.

This particular design is the result of extensive discussions extended over a long period. Four different designs (not shown) varying in the degree of complexity were drafted. Out of these, the simplest was the one selected for fabrication. The design was made sufficiently versatile with respect to flexibility and ease in changing process parameters. For instance: a) The spring length could be changed from 19 to 152 mm (3/4 to 6 inches), b) The normal load could be very easily and quickly changed. Linear bearings permit application of constant normal force without introducing inertia effects, c) The infinitely variable torque drive permits variation of sliding speed from zero to 610 cm/sec (240 inches/sec), d) Spring cross sections could be changed by just replacing the cup-spring assembly, e) Also the effect of damping can be studied by a change of damping fluids.

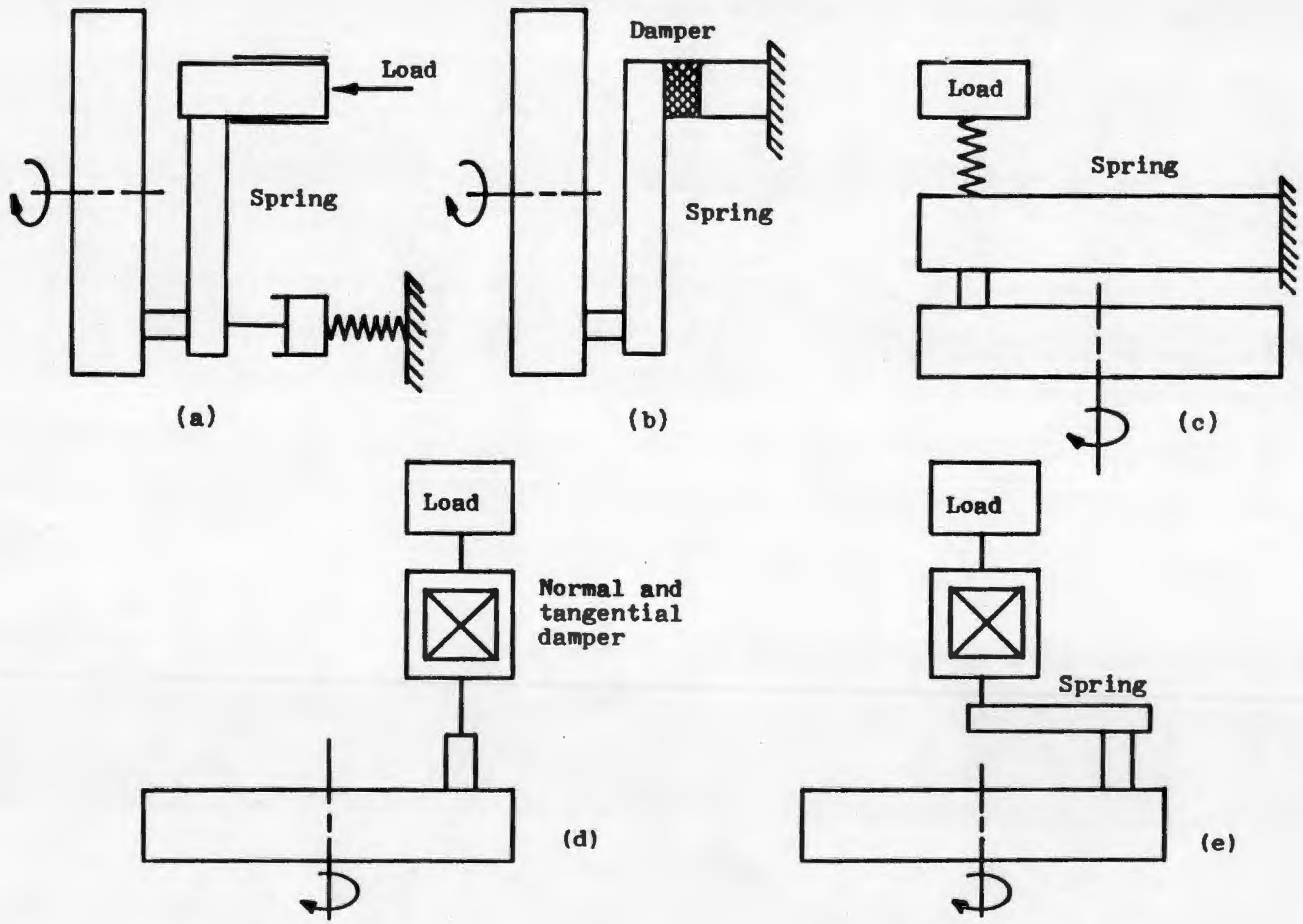

Figure 14. Various Design Configurations of Apparatus for Sliding Contact

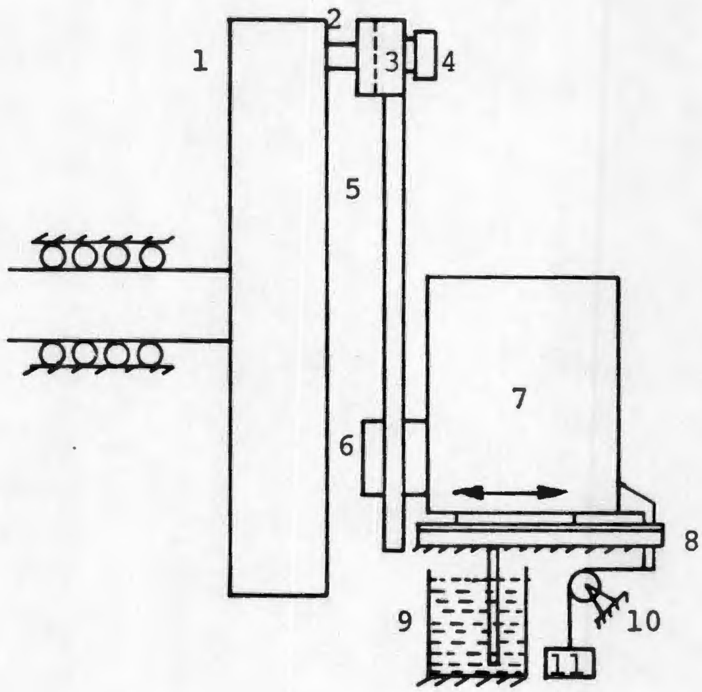

Figure 15. Schematic of the Friction Set-up used in Water Lubrication Experiments. 1) Rotating Disc, 2) Pin, 3) Triaxial Load Cell and Cup Assembly, 4) Triaxial Accelerometer, 5) Spring, 6) Clamp for Adjusting Spring Length, 7) Massive Block Sliding on Linear Bearings, 8) Linear Bearings, 9) Damping System, 10) Pulley System, 11) Dead Weights.

In the early part of the discussions which eventually lead to the evolution of this design, it was arbitrarily fixed that a specimen of 5 mm in diameter will be used as a sliding element. Since the pin is mounted on a spring whose deflection is dependent on the dead load applied through the linear bearings, it was observed that the contact area between pin and disk is not the same for different loads.

Since large variations in the apparent area of slider cannot be permitted, a change of 5% maximum in area of the pin was allowed. The max normal load to be used is 20 kg. Having fixed these values the cross-sectional area of the spring was calculated for the case of the most flexible configuration. That is maximum load, maximum deflection of spring and 5% change in contact area. This provided the minimum cross section of 92 mm^2 (0.142 in^2). The first cross section selected was square, since it provides the same spring constant in normal and tangential directions. The maximum cross section was then fixed at 12.5 x 12.5 mm (1/2 x 1/2 in. square) which permitted less than 1% change in area of contact for maximum load and maximum spring length.

After carefully lapping the pin and disk to a smooth finish (0.42 μm CLA) the preliminary experiments were started with 76 mm (3 in) spring length and 12.5 mm (1/2 inch) square spring. Even with such a rigid configuration there was considerable chatter introduced. The spring length was then reduced to 32 mm (1.25 inches) which resulted in a smoother and more stabilized friction process.

As mentioned in section V, two different types of experiments were performed. One with water lubrication, during which four different spring lengths, 1) 3.18 cm (1.25 in.), 2) 6.76 cm (2.66 in.), 3) 10.19 cm (4.01 in.) and 13.97 cm (5.5 in.) were used corresponding to stiffnesses K_1, K_2, K_3, and K_4. (See table of natural frequencies).

In order to conduct dry friction experiments the design had to be modified. A large value of natural frequency (like the ones used in water lubrication experiments, see Table I) increases the probability of scratching the surface faster and would ultimately lead to seizure. Therefore, the natural frequency of the system was reduced by placing a large block at the top of the spring. Further, the pin holding assembly was also modified. Two different views of the new set up are shown in Figure 16. With this system, three arm lengths of 1) 5.1 cm (2 in), 2) 8.9 cm (3.5 in) and 3) 12.7 cm (5 in) were used.

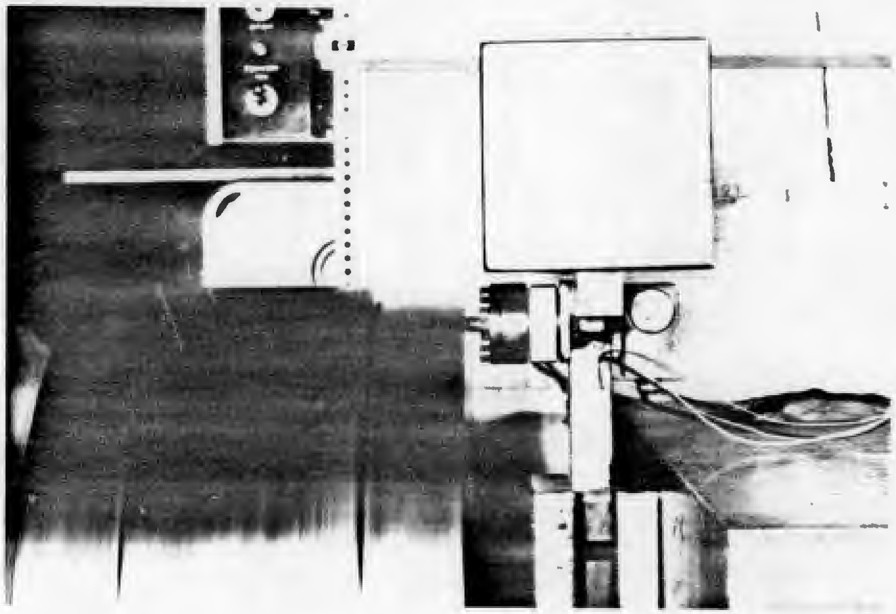

(a)

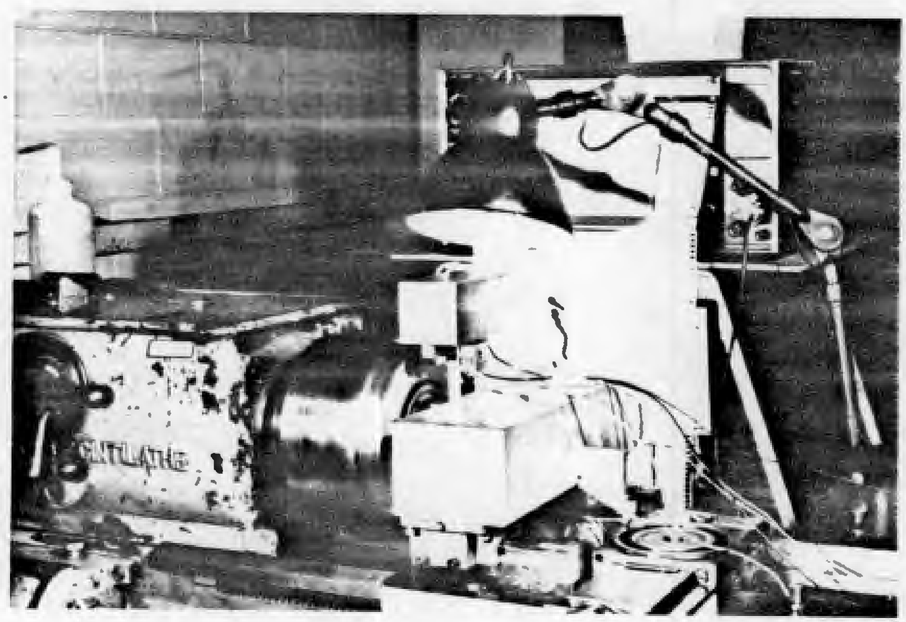

(b)

Figure 16. Two Different Views of the Pin-Spring-Mass Assembly

V. EXPERIMENTAL PROCEDURE AND RESULTS

Under the present D.O.E. contract #AC02-79ER10471, an investigation of the effect of system rigidity on friction and wear was carried out for the following two conditions:

i) Friction with water lubrication, and

ii) Dry friction

A. FRICTION EXPERIMENTS WITH WATER LUBRICATION

The following is a brief description of the techniques and results of the investigation[43].

a) Test Apparatus. A schematic of the test apparatus is shown in Figure 17. The design consists of measuring and loading systems.

The loading system primarily consists of a massive block (3) pulled over the antifriction linear bearings (4) by virtue of a dead weight (1) and a rope and a pulley system (2). The massive block is damped by a damper (5) (using a viscous oil) at the bottom and incorporates an adjustable clamping system (6) in the front. The stiffness of the spring can be changed by changing the distance between the clamps and the sample (9) as well as changing the cross-section of the spring. In this phase of the study the cross-section of the spring was kept constant (1.25 x 1.25 cm).

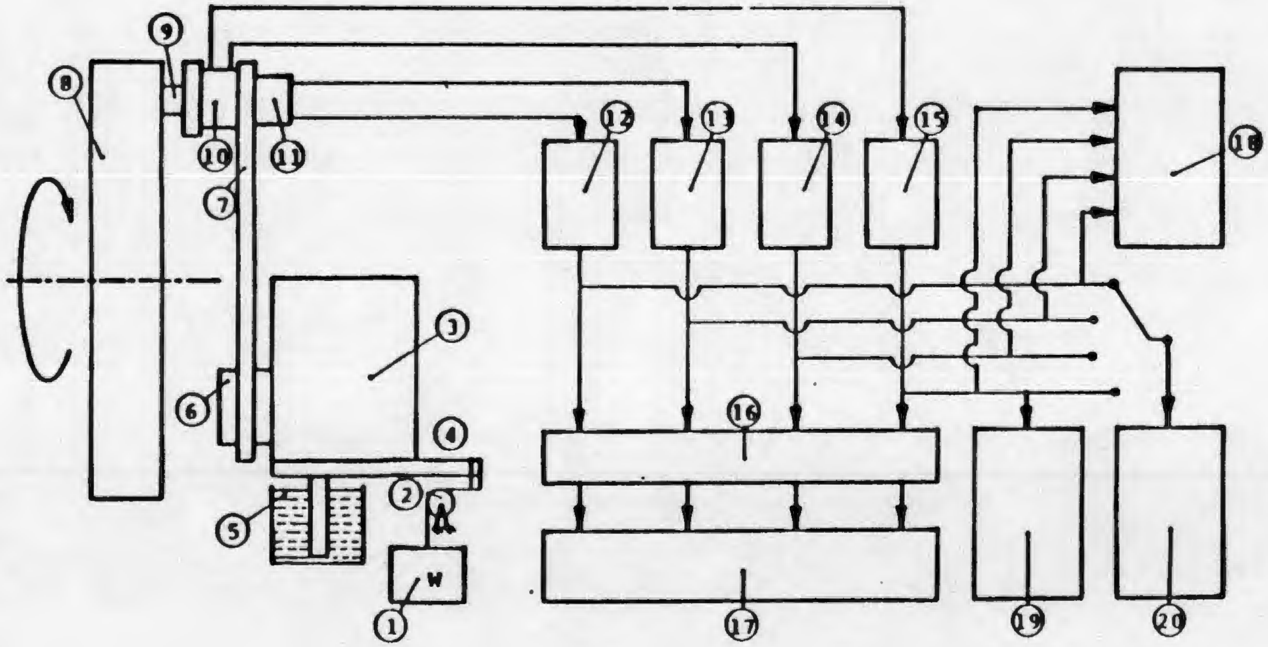

Figure 17. Schematic of Test Apparatus

The measuring system consists of a spring (7) flexible in frictional (tangential to disc (8) and normal (normal to the disc) directions. The load cell (10) is placed between the sample and the spring (7) by means of an expansion bolt, whose other end holds the accelerometer (11). The preamplifiers (12) and (13) are comprehensively equipped, charge conditioning amplifiers intended to take input charge from piezoelectric accelerometer to give an output in the form of acceleration. The device incorporates built-in double integrators which provide velocity and displacement outputs. The preamplifiers (14) and (15) take the input charge from the piezoelectric load cell. The charge outputs from the load cell and accelerometer in frictional and normal directions are connected to pre-amplifiers (15)-(13) and (14)-(12), respectively. The outputs from the preamplifiers are connected to 1) four channel visicorder (17) via the main amplifier (16), 2) dual trace storage oscilloscope (18), 3) strip chart recorder (19), and 4) micro FFT Analyzer (20).

b) Materials and Lubrication. The materials were selected in such a way as to investigate the process of mild wear and the processes of transition from mild to severe wear, both in dry and boundary lubrication regimes. RY-ALLOY, an oil hardening AISI-SAE 01 steel consisting of 0.9%C, 0.58%Cr, 1.35%Mn, 0.5%W, 0.35%Si, was chosen for disc material which was subsequently oil hardened to 59 Rockwell C. A special quality 1045 steel consisting of 0.5%C, 0.85%Mn, 0.04%P and 0.05%S, was hardened to 45 Rockwell C to be used as the pin material.

Water was used as the lubricant because of its low viscosity which readily provided boundary lubrication condition, thereby resulting in desired higher wear rates. Moreover, water lubrication allowed also to continue experiments after transition from mild to severe wear.

c) Testing Technique. In order to investigate the effect of system rigidity on the transition from mild to severe wear, four different arm lengths 3.18cm (1.25 in), 6.76cm (2.66 in), 10.19cm (4.01 in) and 13.97cm (5.5 in) corresponding to stiffnesses K_1, K_2, K_3 and K_4 respectively, were chosen. The arm was clamped at any one of these four lengths. The natural frequencies in the normal and frictional directions corresponding to the four stiffnesses K_1, K_2, K_3 and K_4 were obtained with the disc not rotating and for both cases of the pin in contact with the disc and not in contact with the disc.

The pin was hit impulsively by a force in the normal and frictional directions, respectively. The spectrum of the impulse responses of the accelerometer in both the normal and frictional directions were analyzed by the Fourier analyzer and also observed on the storage oscilloscope. The values of the natural frequencies and damping ratio are given later in the next section.

The pin (1.10 cm (0.435") diameter) and the disc were lapped in situ to a smooth finish (0.42μm CLA) under a normal load of 9 N (2 lb). After cleaning and introducing water drops, the pin was brought in contact with the rotating disc under a normal load of 9 N (2 lb). The disc was set at 76 rpm in all the experiments corresponding to a sliding speed of 73 cm/sec. Under this condition extremely smooth and stable friction process was achieved. This state was continued for 10 hours in order to doubly make sure that full contact of the pin surface has been achieved. After achieving this, the load was applied in steps of 9 N (2 lb) and at intervals of 40 minutes. In-between each load, the friction force (F_x), normal force (F_z), frictional velocity (V_x), normal velocity (V_z) and their corresponding spectra were recorded on Visicorder chart. A trace of the friction force variation on strip chart recorder was also obtained.

Wear experiments were carried out on the same pin-on-disc setup. The pin diameter was 1.1cm (0.435") with a flat wear surface. In the beginning of each experiment the pin and disc were lapped with 600 grit size clover lapping compound and were subsequently cleaned thoroughly by methanol and acetone. Taking all precautionary steps, the pin and disc were brought in contact and maintained so for sufficiently long time (usually 4 to 6 hours) to ensure full contact of the pin surface. The pin was then removed, weighed accurately (up to five decimal places of a gram) and replaced back in the same position. After wearing out the pin over a sliding distance of 15000 to 16000 meters the pin was re-weighed and the difference taken as weight loss.

In all experiments the disc surface speed was maintained at 73 cm/sec and water was introduced as lubricant at the rate of one drop per second. Wear data was obtained for spring stiffnesses K_1, K_3 and K_4 where $K_1>K_3>K_4$.

Recently the following changes of the testing machine were made. The pin holding system was remodeled so as to achieve a more rigid configuration. The pin diameter was reduced from 11 mm to 5 mm. "Micro Measurements 250UT", 'C' Feature strain gages were installed on the pin holding arm. These gages were mounted such that full bridge gage circuitry is obtained which could measure friction force and normal force. A BLH digital strain indicator is used to amplify the gage signal. An analog output of the amplifier is displayed simultaneously on a strip chart and a storage oscilloscope. Provision is also made to obtain steady state forces along with different combinations of dynamic components, on visicorder charts.

d) Experimental Results

i) Effect of Normal Load

As the normal load was increased, with the disc rotating at the constant speed of 76 rpm, three different regions of operation were characterized by the behavior of the friction force F_x, the normal force F_z, the pin velocity components V_x, V_z, the nature of pin surfaces as examined under scanning electron microscope and the wear rate measured as weight loss per unit sliding distance.

1) Region of Stable, Steady-State Friction.

When the normal load is low and below a certain critical value, the steady state friction process is stable with small fluctuations of the two force components and the two pin velocity components as shown in Figure 18. The scanning electron microscope (SEM) photos of the pin surface are given in Figure 19. The pin surface after lapping and before starting the experiment is shown in Figure 19(a). At this stage, the surface is uniform with a roughness of 0.42 μm CLA.

A SEM photo of the pin surface after 10 hours of operation in the region of steady-state friction with a normal load of 9 N (2 lbs) is shown in Figure 19(b). Here, the surface appears to be smooth, without any significant damage, covered with oxide film. In this region, the wear is mild or oxidative wear.

The variation of the wear rate with normal load is shown in Figure 20 for three values of the stiffnesses. In this region of steady-state friction process, the mild wear rate is seen to increase with the normal load and also with the system rigidity. The increase in the mild wear rate with the increase in the square of the natural frequency, which is a measure of the system rigidity, is also shown in Figure 21 for a normal load of 9 N (2 lbs). Although the wear rate increases with the increase in rigidity, it appears that after a certain stage the increase in wear rate saturates with increasing rigidity.

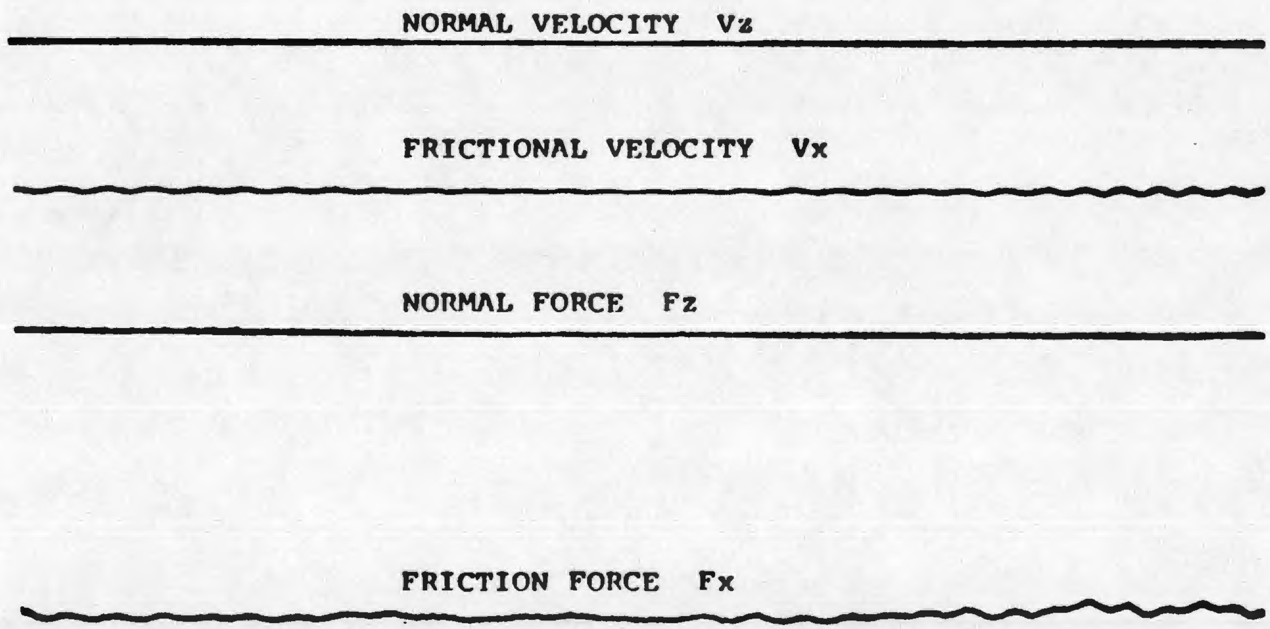

Figure 18. Steady State Friction Process

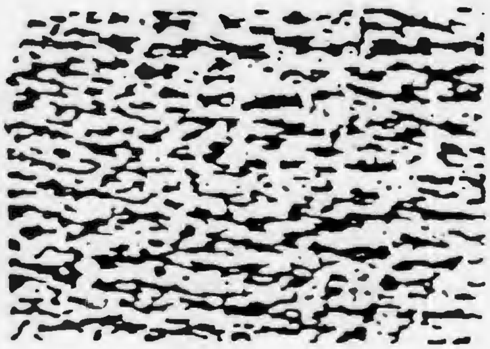

(a) X400

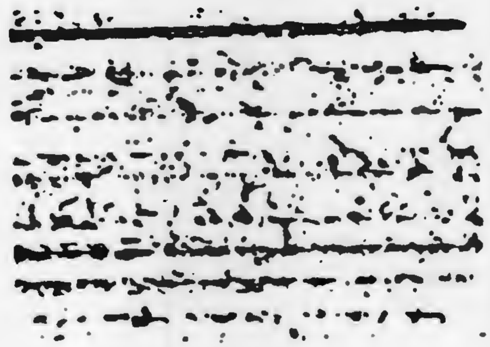

(b) X400

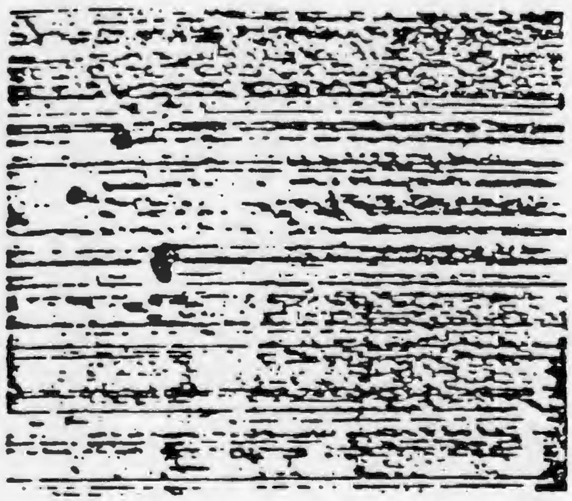

(c) X400

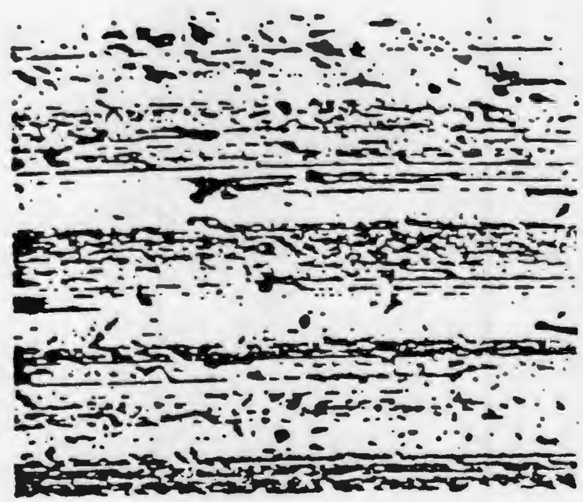

(d) X400

Figure 19. S.E.M. Photos of Pin Surface
a) As lapped, b) After running in Friction,
c) After Self Disturbances, d) After Self-
Excited Vibrations

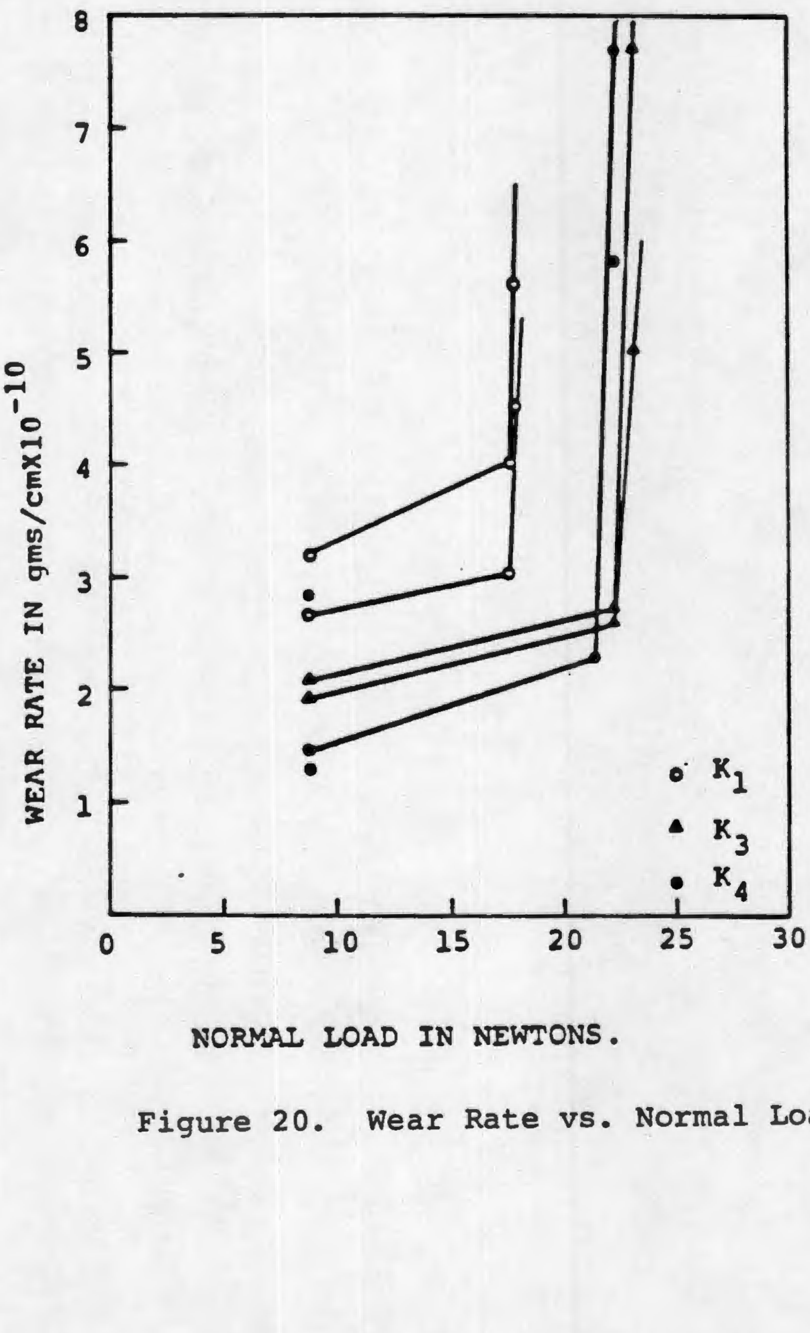

Figure 20. Wear Rate vs. Normal Load

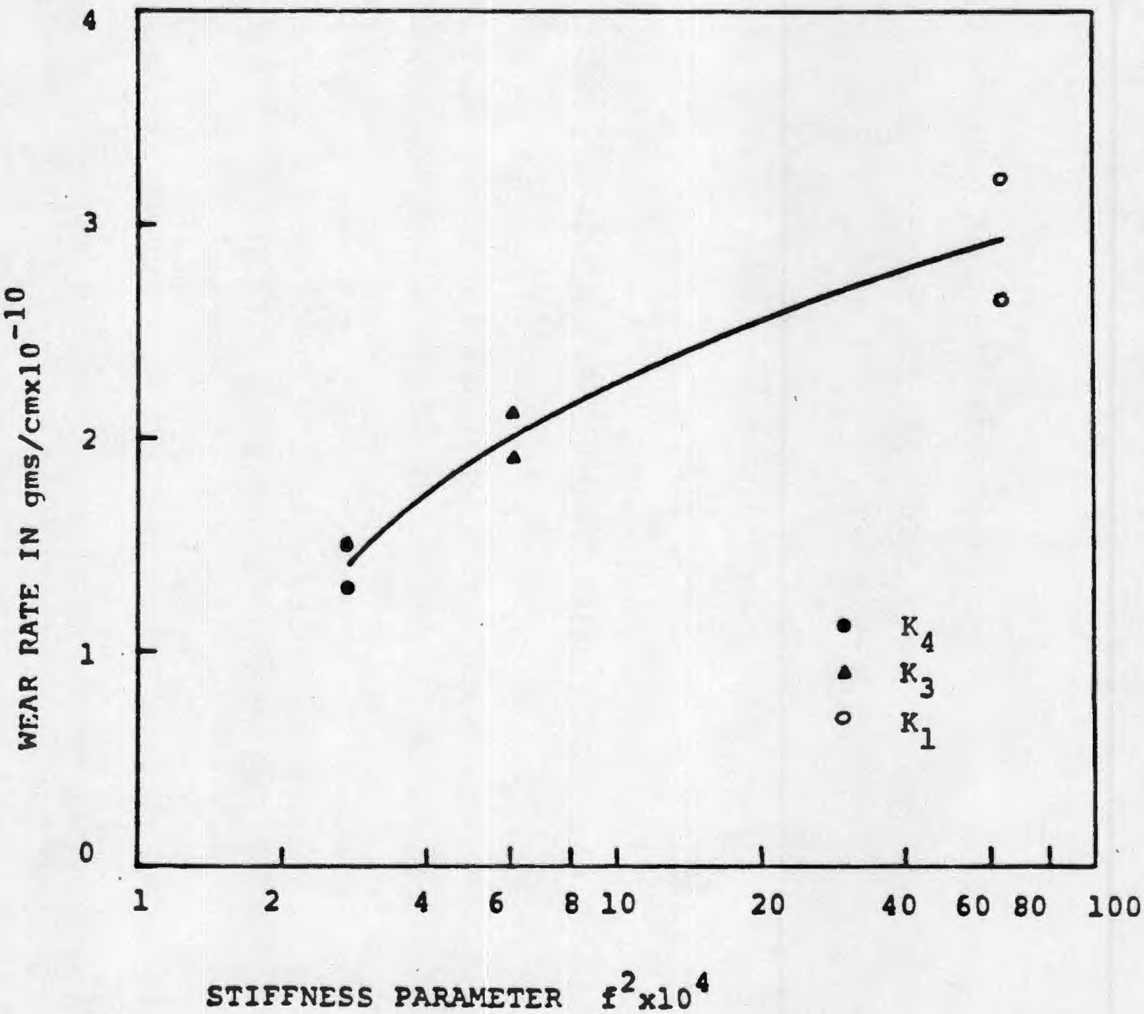

Figure 21. Wear Rate at 9N Normal Load versus Stiffness Parameter f^2 (Squared Natural Frequency)

2) Region of Intermittent Self Disturbances.

As the normal load is increased beyond a certain critical value which in this case is about 18 to 27 N (4 to 6 lbs), a transition occurs from a steady state friction process to an unstable process, characterized by the appearance of self disturbances. During a disturbance, the friction force suddenly increases from its nominal value and decreases back to it, as seen in Figure 22. Oscillations of two different frequencies can be observed in this figure.

The low frequency oscillations appear as soon as the friction force begins to increase from its nominal value. When the friction force has reached its high value, additional high frequency oscillations begin to appear. This high frequency oscillations decay quickly and disappear soon after the friction force decreases back to its nominal value. The low frequency oscillations, however, decay at a much slower rate. In case the time interval between two successive disturbances is sufficiently large, the low frequency oscillations also disappear and a comparatively smooth friction process reoccurs between the disturbances. At this state of friction the two forces and two velocity components appear to be similar to the one shown in Figure 18.

However, when the time interval between two successive disturbances is small, the low frequency oscillations do not have sufficient time to decay and they persist between the disturbances. Both the low frequency and high frequency

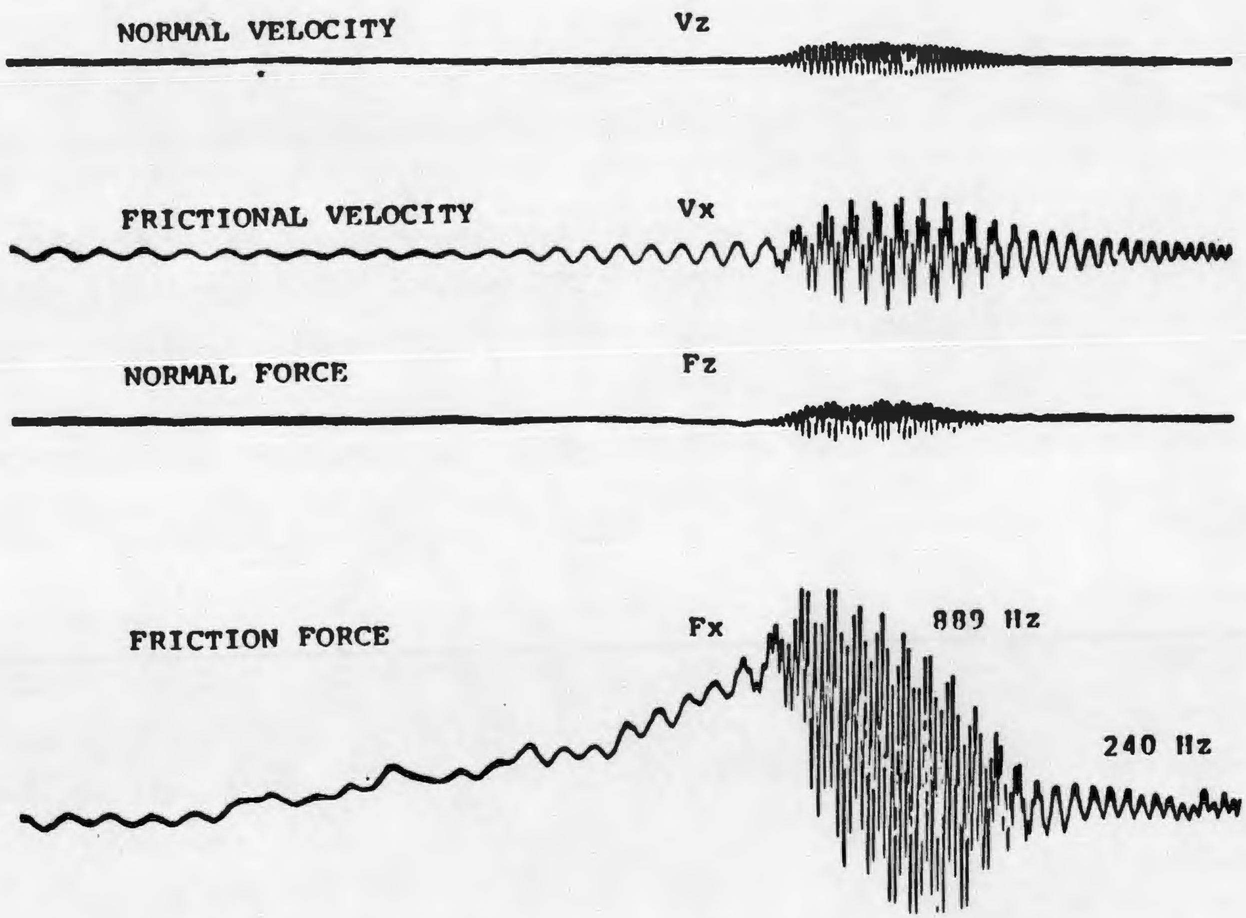

Figure 22. Friction Process at a Typical Disturbance

oscillations have been observed in the published literature [13]. As mentioned earlier, the low frequency oscillation has been named chatter and the high frequency has been named squeal. Both the low and high frequencies depend on the system rigidity and increase as the stiffness is increased. In Figure 22 which is for stiffness K_3 corresponding to the arm length of 10.19 cm (4.01 in), the lower frequency has the value of 240 Hz and the higher 889 Hz. It is seen from Figure 22 that the coupling between the frictional and normal degrees of freedom exists only for the higher frequency oscillations. The lower frequency oscillations occur only in the frictional direction.

The number of self-disturbances occurring during a time interval was also recorded on a strip chart recorder. The frequency of occurrence of disturbances would be high soon after a change in the normal load. As the elapsed time from a change in the normal load increased, the frequency of the occurrence of disturbances would decrease. Using the strip chart records, the number of disturbances per unit time were counted and are shown plotted versus normal load in Figure 23 for all four values of stiffness of the pin arm. It is seen from this figure that the transition from a steady state friction process to an unstable one, characterized by the first appearance of self-disturbances, occurred around a normal load of 18 to 27 N (4 to 6 lbs) for all the stiffnesses investigated. The number of disturbances per unit time is apparently stochastic in its nature.

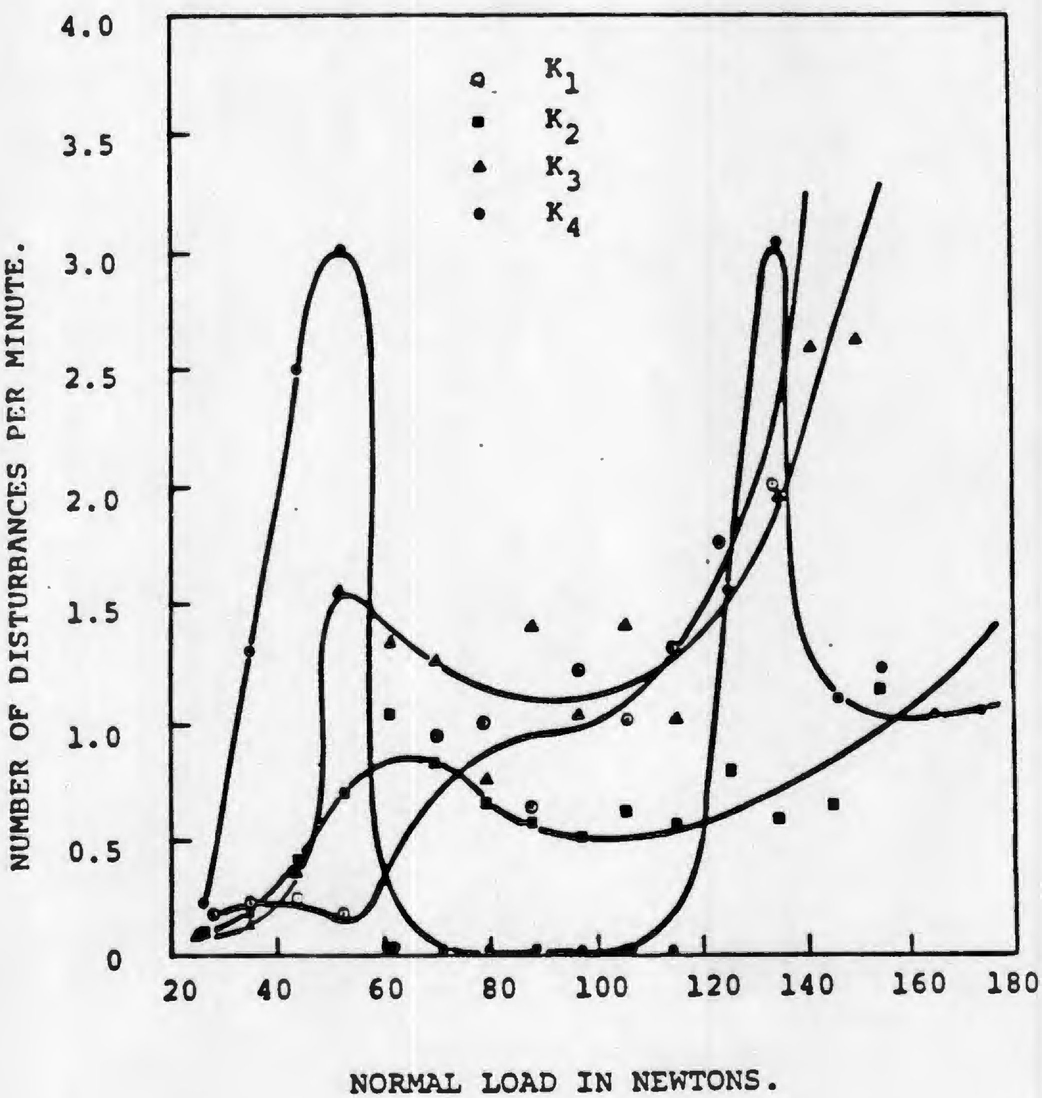

Figure 23. Number of Disturbances Per Minute as a Function of Normal Load for Four Different Stiffnesses

A SEM photo of the pin surface is shown in Figure 19(c) for operation in the region of intermittent self disturbances. In this region of the friction process the surface, in spite of being smooth and covered with oxide film shows deep pits and adjoining scratches. The wear process now is no longer only mild or oxidative wear. As seen from Figure 20, the wear rate sharply increases at the same critical loads (18 to 27 N) that caused transition from steady to unsteady friction process. It is also clear that the wear rate in this region is much higher than that in steady state friction process.

3) Region of High Frequency Self-Excited Oscillations. As the normal load is increased still further, it reaches another critical value at which high frequency self excited vibrations occur and are maintained. It is found that this value of the critical load depends on the system rigidity. This dependence is shown in Figure 24, where the critical load, at which high frequency self excited oscillations occur and are maintained, is plotted versus the square of the natural frequency of the pin.

Figure 25 shows the oscillations in the two force components and in the two velocity components in this region for stiffness K_3. The value of the frequency in this figure is 889 Hz which is seen to be the same as the higher frequency of Figure 22 during a self-disturbance. The value of this high frequency depends on the system rigidity and for stiffness K_2 it is 1045 Hz. These

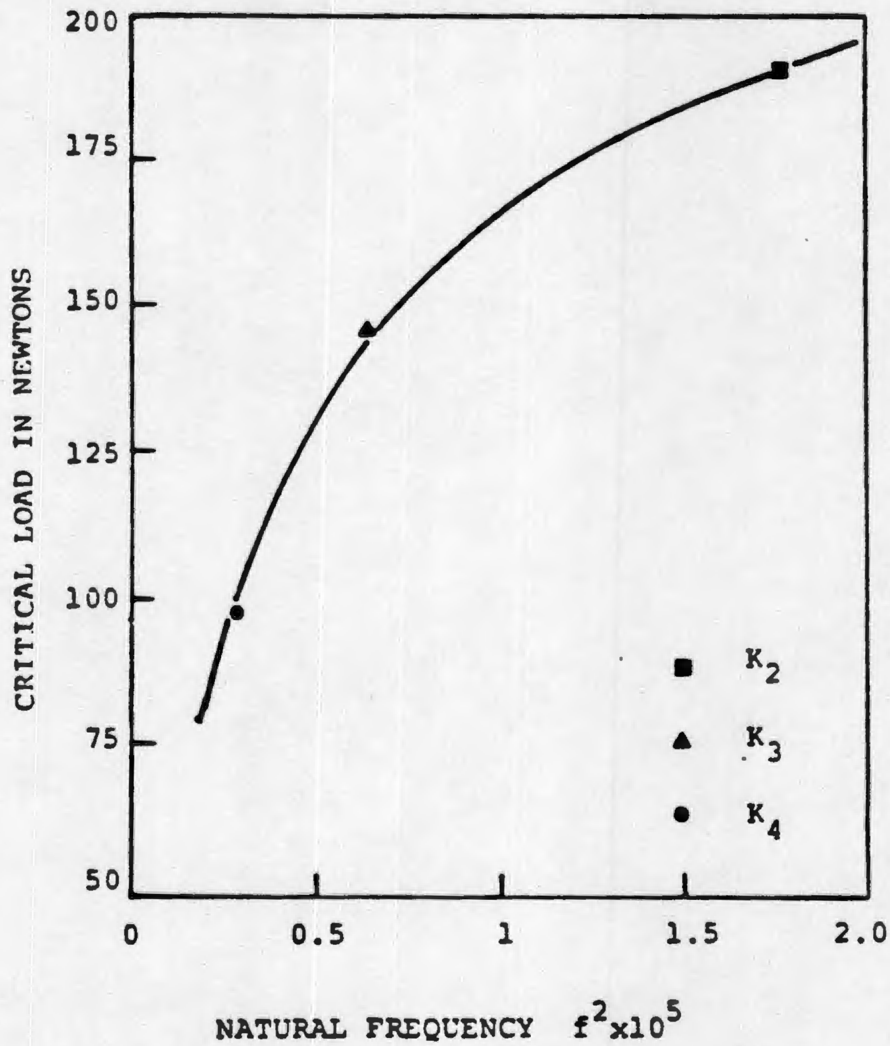

Figure 24. Critical Load Causing Self Excited Vibrations versus the Square of the Natural Frequency

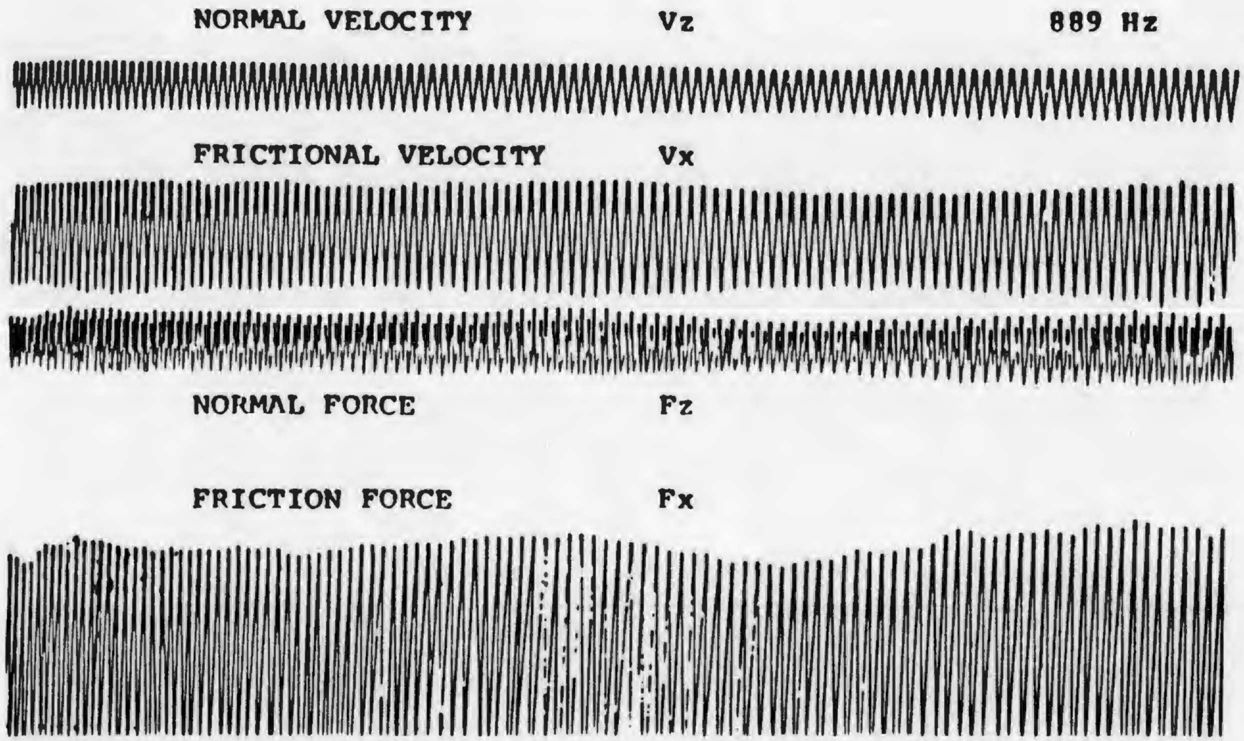

Figure 25. Self Excited Vibrations for Stiffness K_3

oscillations exhibit a coupling between the frictional and normal degrees of freedom. In this region of high frequency self-excited vibrations, it was noted that a few self-disturbances did also occur.

Figure 19(d) shows a SEM photo of the pin surface taken after running in the region of high frequency self-excited vibrations. Some parts of the surface are smooth with shallow pits without adjoining scratches whereas other parts exhibit deep pits with adjoining scratches. It has been mentioned earlier that a self disturbance causes a deep pit with adjoining scratches. Hence, it appears that in the region of self excited vibrations, the shallow scratches formed earlier are smoothened while the deeper pits still remain as shallow pits on a smooth background. The deep pits with adjoining scratches may have been the result of disturbances that occurred just before the picture was taken where sufficient time was not allowed for the surface to smoothen out under self-excited vibrations.

An overall picture of the vibration pattern in above mentioned regions of friction process can be had from Figure 26 where 26(a) is obtained from the region of stable steady state friction, 26(b) and (c) from region of intermittent self disturbances and 26(d) from region of self-excited vibrations.

ii) Natural Frequencies of Pin and Arm.

The natural frequencies of the pin and arm were determined experimentally in order to investigate the relation-

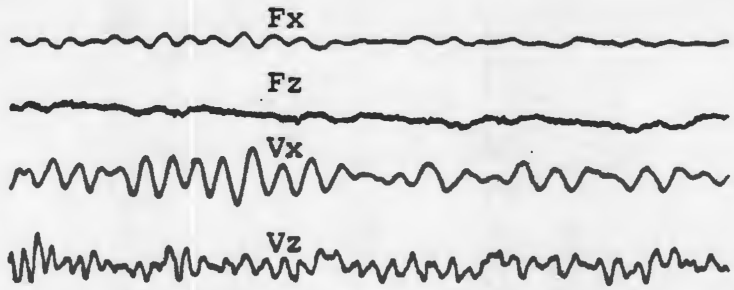

(a) STEADY STATE FRICTION PROCESS.

(b) SELF DISTURBANCES.

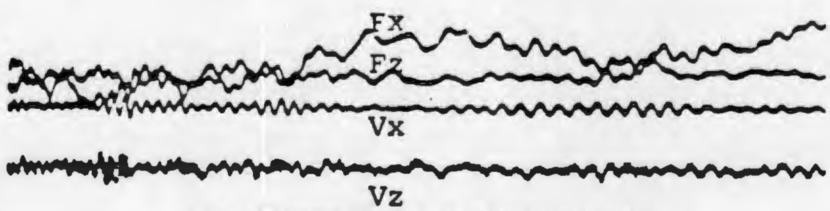

(c) INBETWEEN DISTURBANCES.

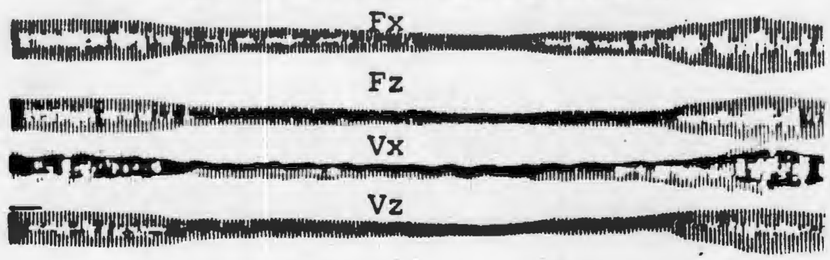

(d) SELF EXCITED VIBRATIONS.

Figure 26. Visicorder Traces of Friction Force (F_x), Normal Force (F_z) and Corresponding Velocities V_x and V_z for Different Friction Regimes

ships, if any, between the low and high frequency self-excited oscillations and the natural frequencies. For each arm length, it was found that the natural frequencies when the pin is in contact with the disc are different from those when the pin is not in contact. Also, the natural frequencies when the pin is in contact with the disc do not depend on the normal load. The natural frequencies are given in Table 1. As expected, there also exist higher harmonics but only the fundamental frequencies are shown in Table 1.

In order to obtain the damping ratios experimentally, the impulse responses of the accelerometer in both the normal and frictional directions were displayed in the time domain on the storage oscilloscope. By employing the method of logarithmic decrement, it was found that the dimensionless damping ratio ζ is approximately the same in both the normal and frictional directions for all the four stiffnesses tested. This value is given approximately by $\zeta = 0.02$.

TABLE I

NATURAL FREQUENCIES

	Pin in contact with disk		Pin not in contact with disk	
Stiffness	Normal Direction Hz	Frictional Direction Hz	Normal Direction Hz	Frictional Direction Hz
K_1	1050	1050	915	815
K_2	575	575	410	420
K_3	435	435	240	250
K_4	355	355	165	170

B. DRY FRICTION EXPERIMENTS

a) Modification of Test Apparatus.

The experimental set up used in water lubrication experiments, Figure 15, was found to be not very suitable for dry friction experiments. This was due to the large values of natural frequency (See Table I), which tend to increase the probability of scratching of surface and/or seizure. Therefore, natural frequency of the system was reduced by placing a block with a total weight of 9.41 lbs. The new set of natural frequencies obtained from this arrangement for three different arm lengths are shown in Table II. (See p. 120)

The pin holding system was also modified to make it more rigid. The load cell, accelerometer and the sample were located on the spring just below the mass. The entire arrangement is shown in Figure 16. For recording steady state friction force strain gages were fixed on the spring at a distance of 5.1 cm (2 inches) from the pin contact. For better response and temperature compensation a full bridge circuit was used. A BLH model 1200 B Digital strain indicator provided both digital and analog output of the friction force. For each arm length the system was calibrated up to 60 N friction force (in steps of 5 Newtons) and the response was found to be linear.

b) Materials.

In dry friction experiments the pin and disc materials were same as those used in water lubrication experiments, described in earlier section. Even the contact geometry was the

TABLE II

NATURAL FREQUENCIES

	Stiffness	Pin not in contact with disc: Frictional Direction Hz	Pin not in contact with disc: Normal Direction Hz
For	K_1	915	815
Water	K_2	410	420
Lubrication	K_3	240	250
Experiment	K_4	165	170
For Dry	K_1^*	75	75
Friction	K_2^*	45	45
Experiment	K_3^*	35	35

same except that the pin was through hardened to 48 Rockwell C scale.

c) Experimental and Measurement Techniques.

The experimental techniques and the equipment used in dry friction experiments basically remains the same as in water lubrication experiments (mentioned in previous section). In this phase of investigation, two series of experiments were conducted:

a) Variable rigidities and constant speed.

b) Variable speeds and constant rigidity.

A series of experiments were first conducted with an arm length of 5.1 cm (2 in) and at sliding speed of 46 cm/sec (50 rpm), 70 cm/sec (75 rpm) and 94 cm/sec (100 rpm). Then the arm length was changed to 12.7 cm (5 in) and experiments were conducted at a sliding speed of 46 cm/sec. The pin and disc were lapped with 400 grit size lapping compound with the disc rotating at the speed at which the experiment was to be conducted. Then the sample and disc were thoroughly cleaned with acetone and methanol. At each spring stiffness and speed a set of two experiments were performed: i) Dynamic Experiment, and ii) Wear Experiment.

Dynamic Experiments

The normal load at the start of this experiment was 8 N. At this condition the experiment was run for 6-8 hours. This was done to ensure that a steady state friction process is obtained. After this the normal load was increased in steps of 4.45 N (1 lb) initially and later on in steps of 9 N (2 lbs).

The loading time was maintained for about 30 minutes between each loading. At each normal load, the analog wave form of the dynamic components of friction for (F_X), normal force (F_Z) and the corresponding frictional and normal velocities V_X and V_Z respectively, were recorded on a four channel Honeywell Visicorder Oscillograph, Model 1508A. A Spectral Dynamics Model SD340 Fourier Fast Transformer was used to analyze the signals from the force, velocity and displacement sensing devices. At each load, spectrum of friction force (SF_X), normal force (SF_Z), frictional velocity (SV_X), and normal velocity (SV_Z) were obtained from the F.F.T. In some experiments additional analog traces and spectra of displacements in frictional direction (SD_X) and normal direction (SD_Z) were also recorded.

Wear Experiments

After lapping the pin and disc in situ, the sample was removed and examined under an optical microscope and photographs of the surface were taken. For examining the surface profile, a Taylor and Hobson Talysurf 10 was used. The Talysurf was set at a vertical magnification of 10,000 and horizontal magnification of 100. Five traces of the surface across the direction of sliding and five traces of the surface along the direction of sliding were taken. Each scan of the Talysurf pickup was displaced across by a distance of 20 μm from the previous scan. After each scan the pickup was made to traverse once more over the same surface to obtain the Ra value of the surface.

After these examinations of the sample surface, the pin was run in at 28 N for a sufficient length of time to ensure full contact of the pin surface. Then the sample was removed for the above mentioned optical microscope and Talysurf examinations. Then the pin was weighed (with an accuracy of up to 0.0001 gram) and replaced in the same position. At the same normal load of 28 N, the pin was run in, generally for 6 to 8 hours. At the end of this running in period analog traces of F_X, F_Z, V_X and V_Z and their corresponding spectra were also recorded. Finally the experiment was stopped and the sample reweighed and the weight loss taken as wear in gms per unit sliding distance. Then the pin was once more subjected to the same optical microscope and Talysurf examinations. In some cases acrylic replicas of the disc surface were also taken and examined for its surface profile and Ra.

This technique of experimentation was adopted for three different stiffnesses, K_1*, K_2* and K_3* corresponding to arm lengths of 5.1 cm (2"), 8.9 cm (3.5") and 12.7 cm (5"). At each of these experiments the disc was run at 50 rpm. Then for stiffness K_1*, i.e. for arm length of 5.1 cm (2"), wear was measured at three different sliding speeds corresponding to the disc rotation of 50, 75 and 100 rpm.

EXPERIMENTAL RESULTS

Figure 27 is a typical plot of the change of friction force with time and normal load for stiffness K_1* corresponding to an arm length of 5.1 cm (2") and sliding speed

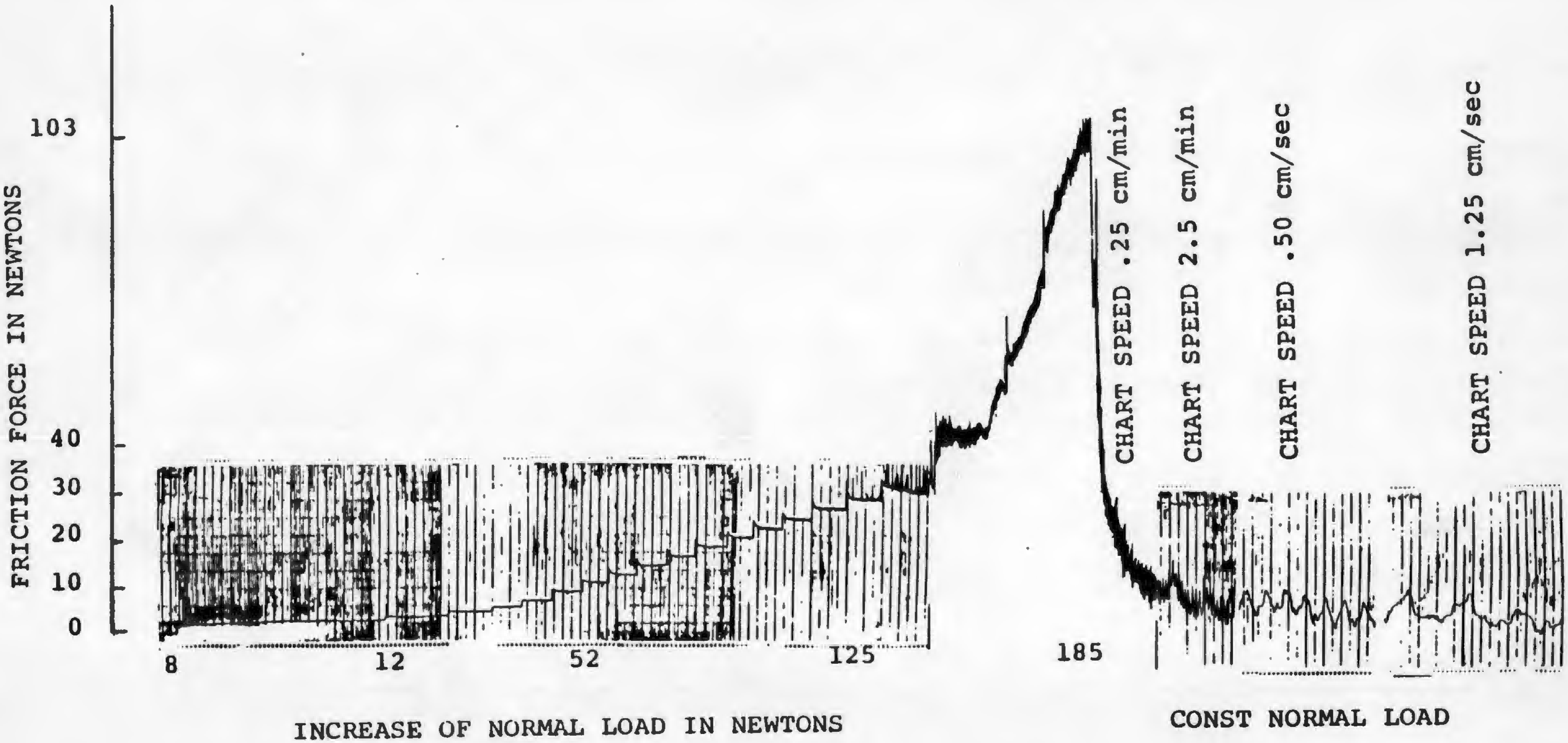

Figure 27. Strip Chart Record of Increase of Friction Force with Increase in Normal Load Obtained from Strain Gages for 5.1 cm Arm Length and for Dry Friction

of 46 cm/sec. As can be seen from the figure the experiment was run in for a period of 5 hours at a normal load of 8 N. At this load, the friction force is 2 N. When the load is increased to 12 N, the friction force immediately increases to 4.88 N. As the load is increased further, we see a proportional increase in the friction force. During the time between loadings, the friction force remains constant. This behavior is seen until a normal load of 125 N is reached. At this load the friction process is no more in steady state. It is now said to have entered the region of self disturbances. As the load is further increased not only the number of disturbances per unit time increases, but also the magnitude of friction force increases. Thus, in this region it is observed that friction force increases with time at a constant value of normal load. This behavior lasts up to 103 N. At this stage the friction force suddenly falls to about 70 N and when the normal load is increased to 185 N, the friction force instantly falls to around 20 N. At the same instant self-excited vibrations start. After onset of self-excited vibrations, the average value of the friction force continues to fall quite rapidly until it has reached almost the starting level. In order to see clearly the variation of friction force, the strip chart speed is increased from 0.25 cm/min to 2.5 cm/min then to 0.5 cm/sec and finally to 1.25 cm/sec, where in the wave form appears as shown. A wave form of the dynamic frictional and normal forces and the corresponding velocities during self-excited

Not obvious from Fig 27

vibrations is shown in Figure 28.

The change in friction force and coefficient of friction with normal load is shown in Figure 29. The friction force behaves almost linearly up to a normal load of 136 N. During the same period there is a sharp initial decrease in the coefficient of friction and then it stabilizes to a near constant value. At a normal load of 136 N the friction force increases sharply along with the coefficient of friction. This point is a transition from a stable to an unstable friction process. As the normal load is further increased in steps, it is seen that the friction force and coefficient of friction continue to increase very sharply up to 185 N normal load. At this load self-excited vibrations suddenly occur and the friction force falls to almost the starting level.

In Figure 30, the friction force and coefficient of friction are shown plotted against the normal load for a sliding speed of 70 cm/sec. The friction force and consequently coefficient of friction increase non-linearly right from the initial state. At a normal load of 88 N and coefficient of friction of 0.58, self excited vibrations occurred and when the normal load is further increased to 97 N, the friction force and coefficient of friction fall drastically to almost the initial level. In order to check the reproducibility of this result, the experiment was repeated three times. The results of each trial coincide very closely.

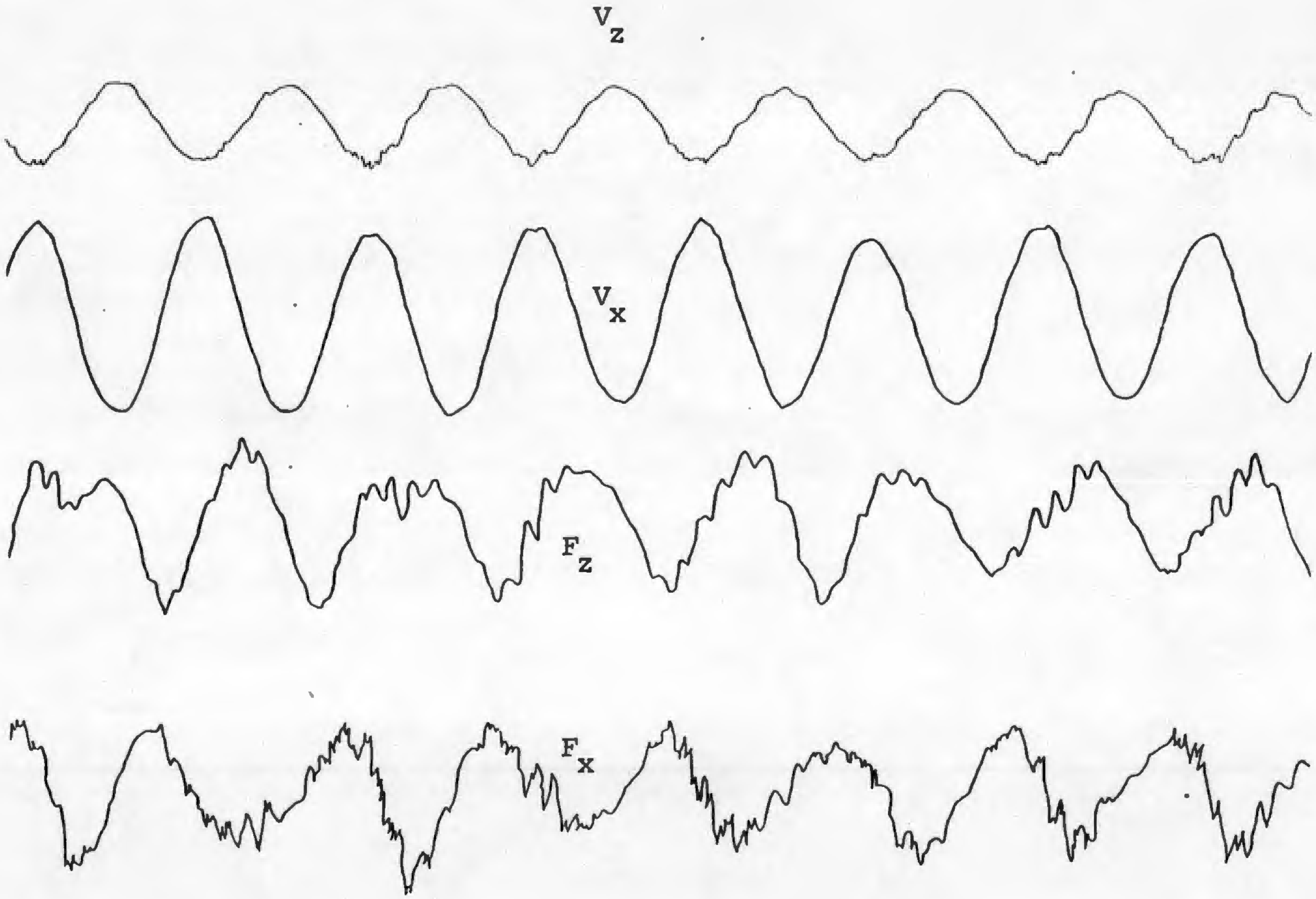

Figure 28. A Typical Trace of Forces and Velocities during Self Excited Vibrations

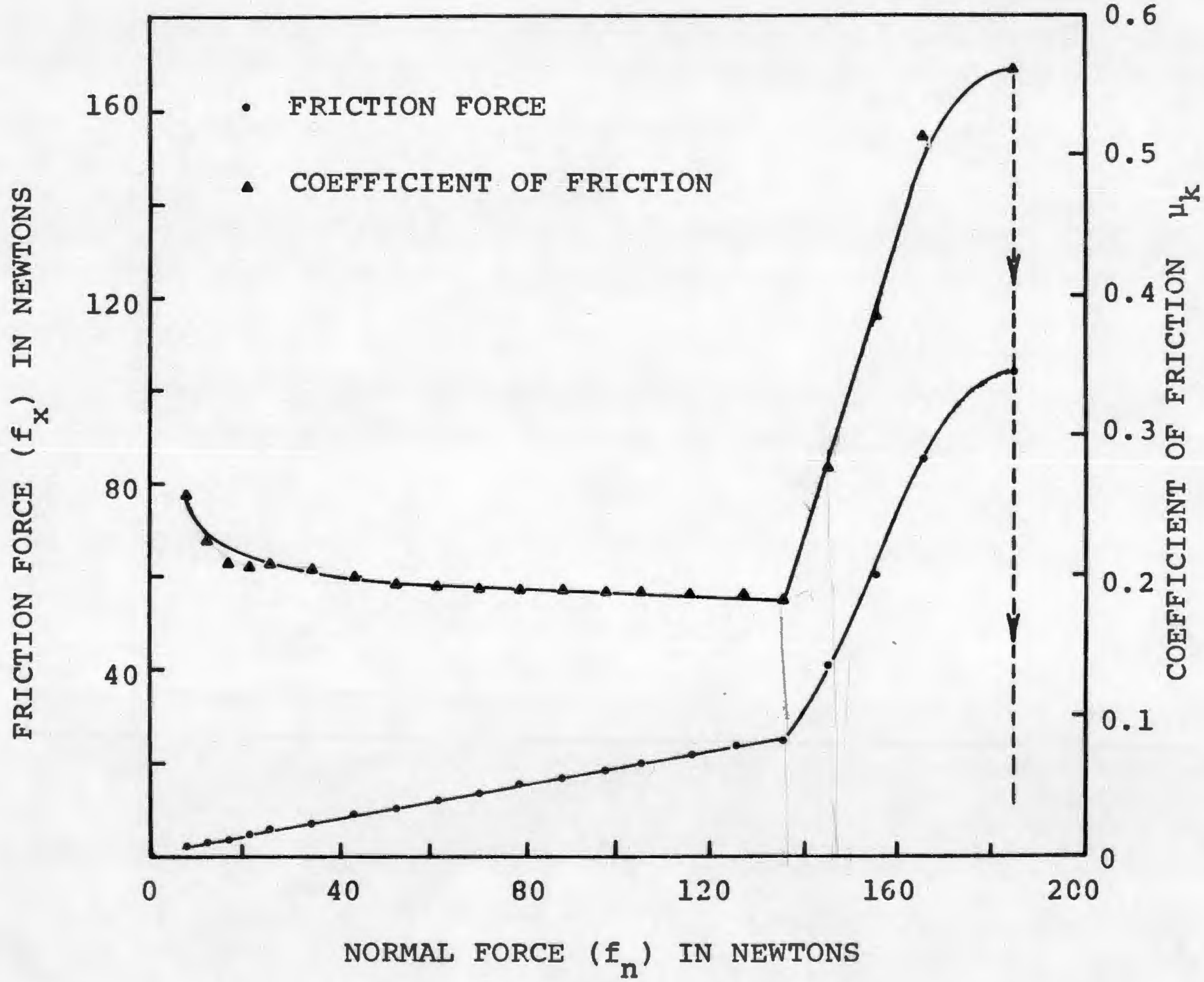

Figure 29. Friction Force and Coefficient of Friction vs. Normal Force for Sliding Speed of 46 cm/sec and Spring Stiffness K_1*

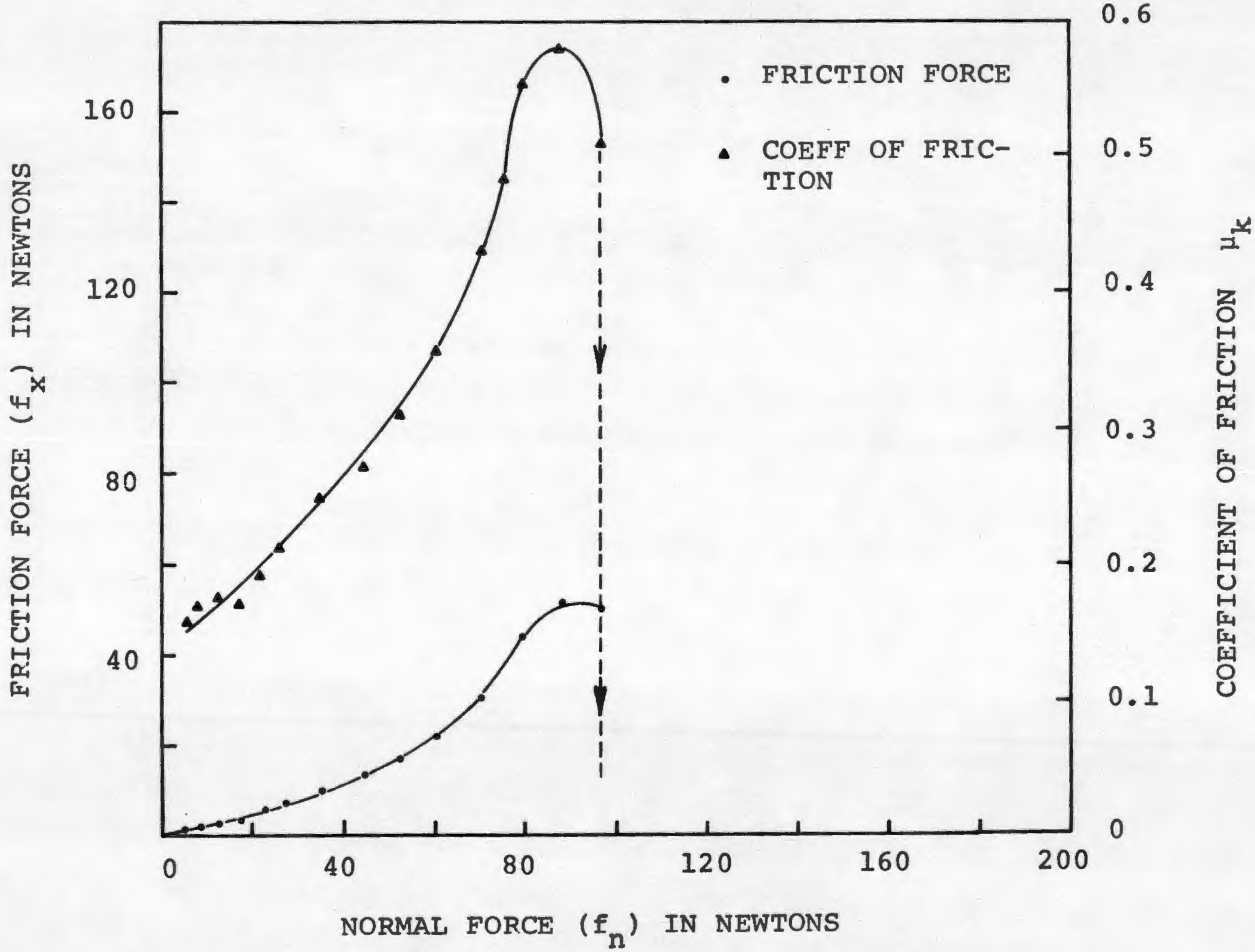

Figure 30. Friction Force and Coefficient of Friction vs. Normal Force for Sliding Speed 70 cm/sec and Spring Stiffness K_1*

A similar graph for a sliding speed of 94 cm/sec is shown in Figure 31. The results of this figure are similar to those in Figure 29. As can be seen from this figure, the friction force increases linearly up to a normal load of 79 N. During the same period, there is an initial sharp decrease in coefficient of friction which stabilizes to almost a constant value. Beyond the normal load of 79 N the friction force and coefficient of friction increases very sharply and at a normal load of 106 N, when the coefficient of friction is 0.45, self excited vibrations occur and the friction force falls to the initial value.

The friction force and coefficient of friction versus normal load for different sliding speeds are plotted in Figures 32 and 33.

Wear was measured at the same three sliding velocities of 46, 70 and 94 cm/sec and at a constant normal load of 28 N. The results obtained are shown in Figure 34. The amount of wear obtained for sliding speed of 70 cm/sec is orders of magnitude higher than that obtained for sliding speeds 46 and 94 cm/sec.

As mentioned in Section V.B.c. on experimental techniques, wave forms of oscillations of dynamic forces and velocities and their corresponding spectra were recorded at each normal load during all experiments.

From the wave forms of dynamic forces and velocities obtained for sliding speed of 46 cm/sec and spring stiffness of K_1* (corresponding to 2" of spring length), the average

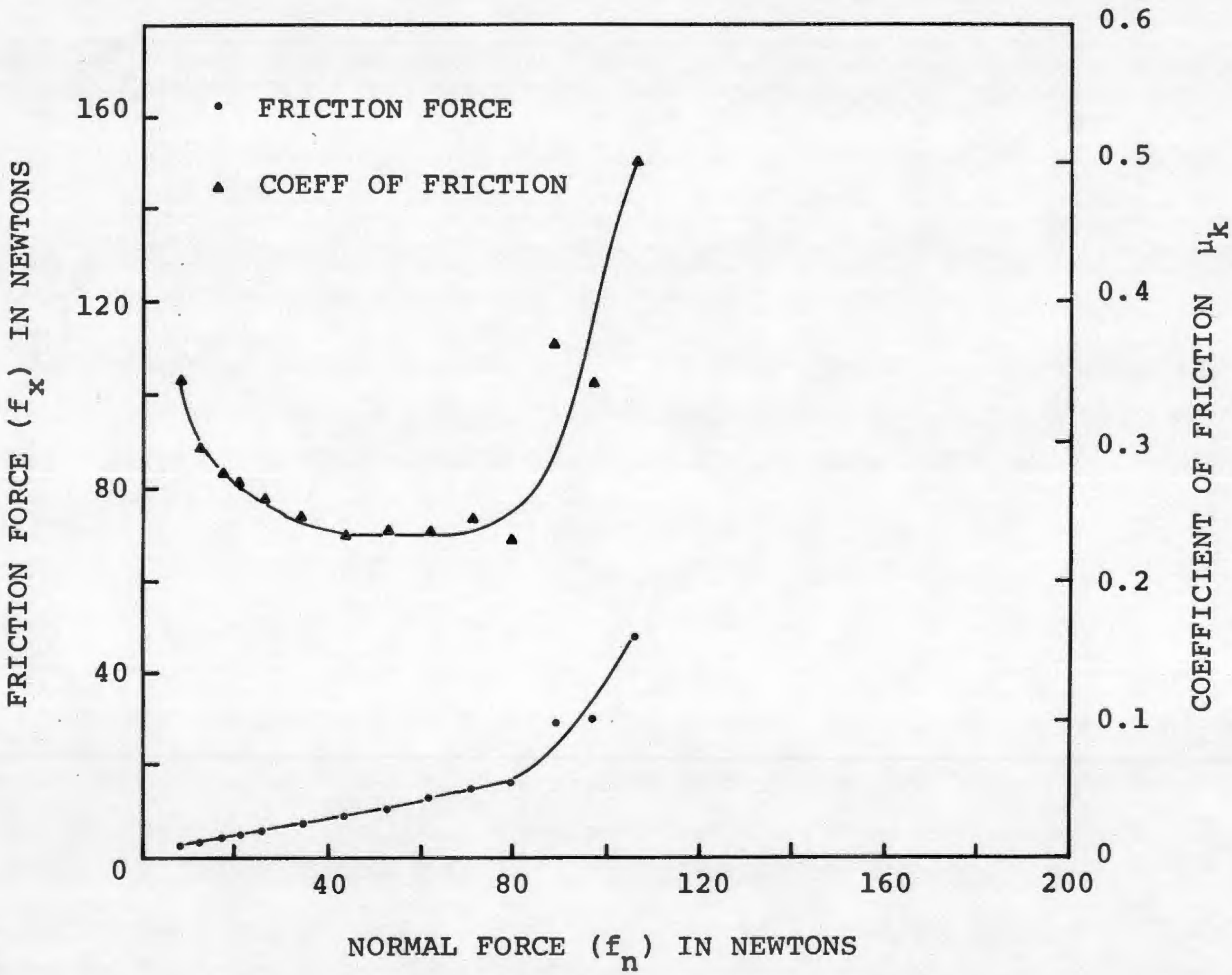

Figure 31. Friction Force and Coefficient of Friction vs. Normal Force for Sliding Speed of 94 cm/sec and Spring Stiffness K_1*

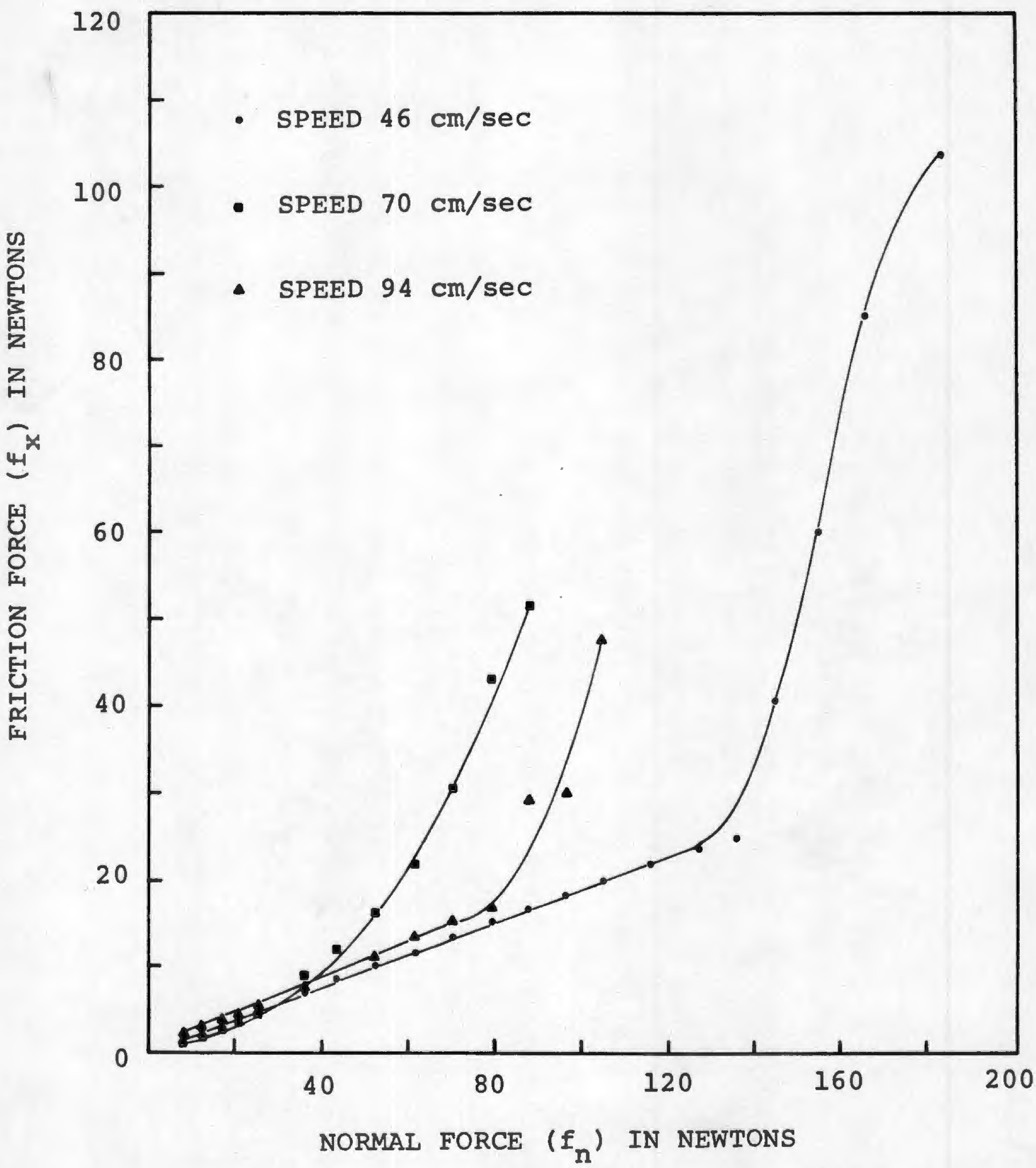

Figure 32. Friction Force vs. Normal Force for Different Sliding Speeds and Const Stiffness K_1*

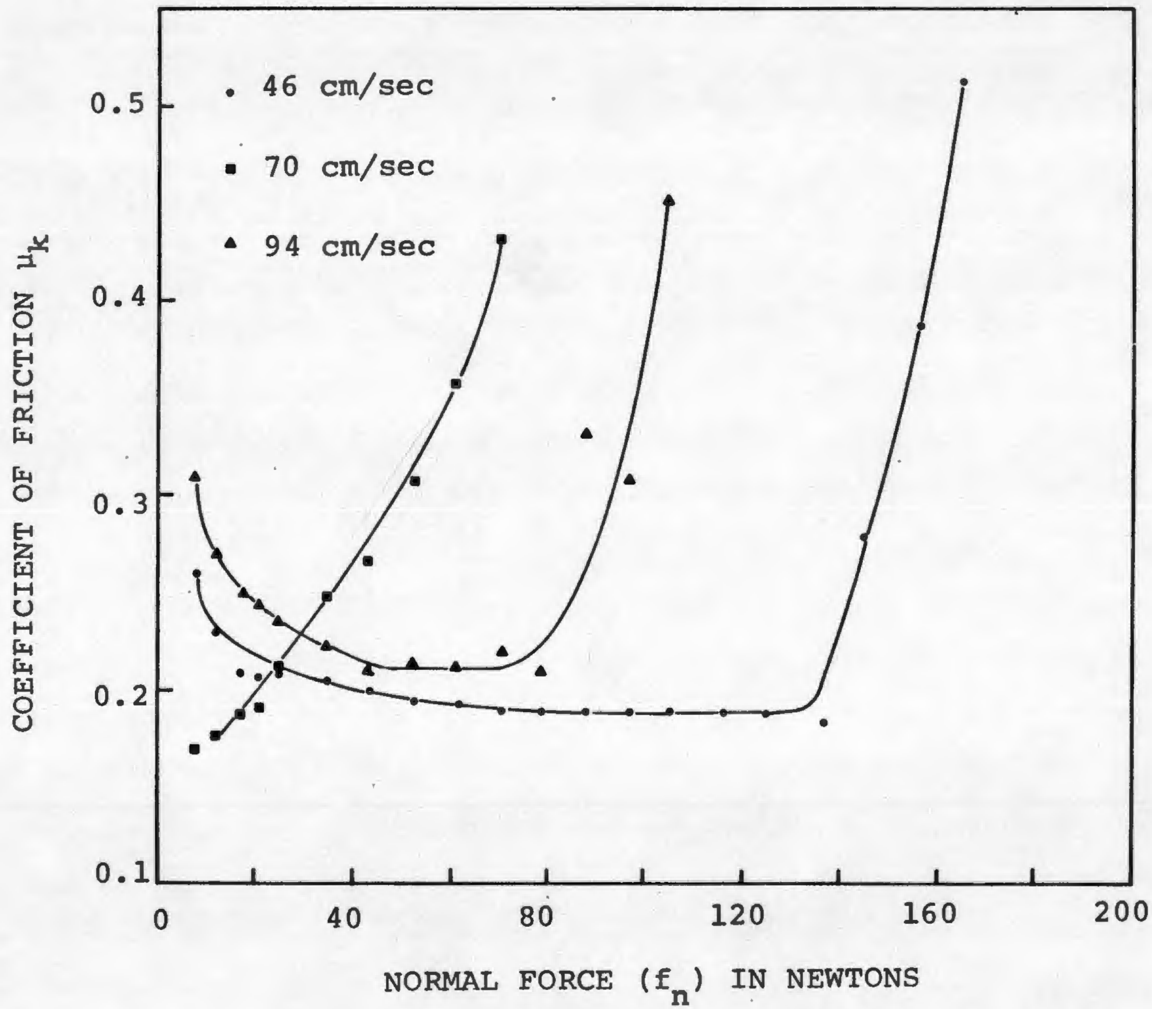

Figure 33. Coefficient of Friction vs. Normal Force for Different Sliding Speeds and Const Spring Stiffness K_1*

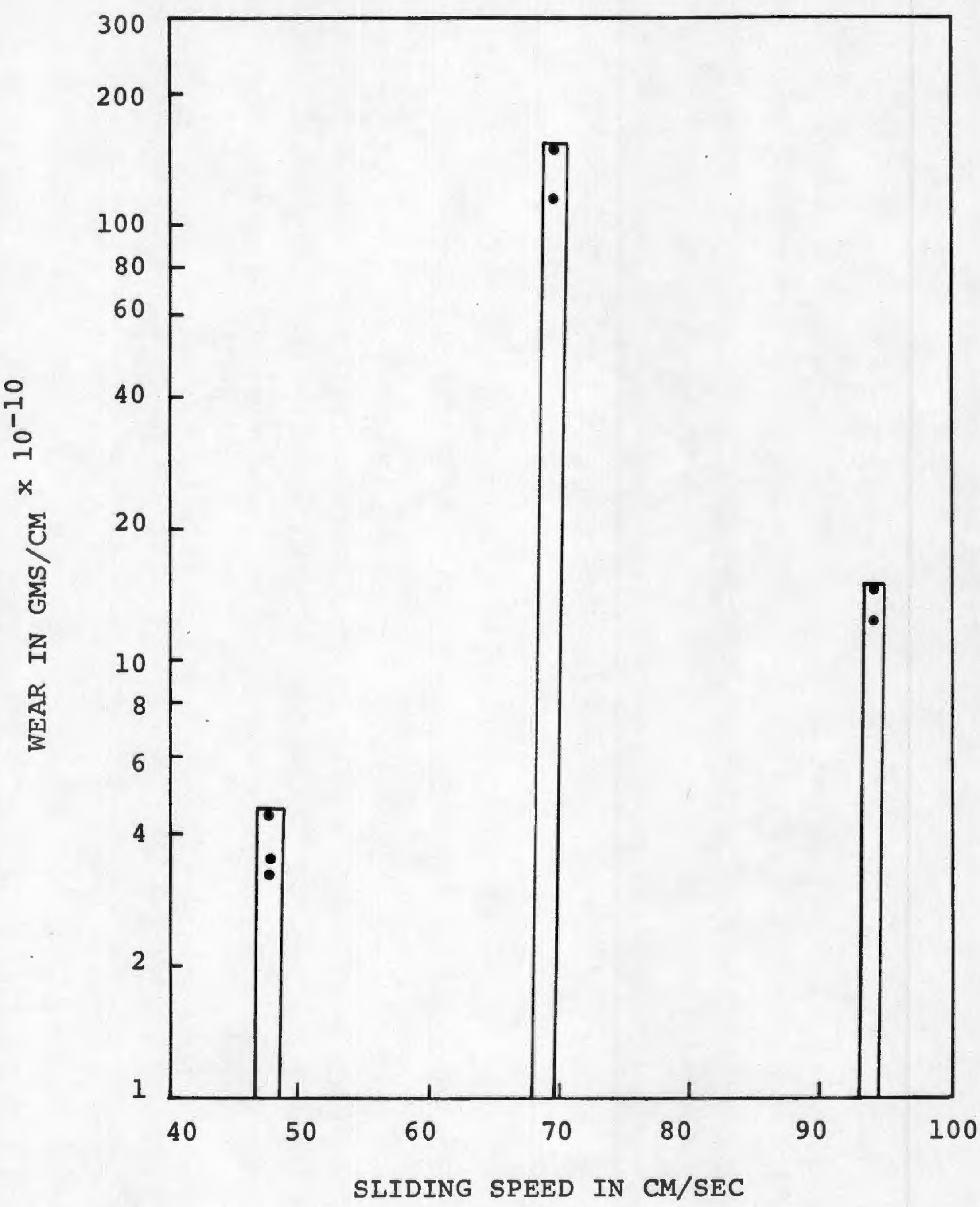

Figure 34. Dry Friction Wear vs. Sliding Speed at Constant Normal Load of 28 Newtons

variations were calculated. The average variation of dynamic friction force (F_x), normal force (F_z) and the velocities in frictional (V_x) and normal (V_z) directions are shown in Figure 35. It is seen in this figure that the forces F_x and F_z decrease with increasing normal load. The velocities V_x and V_z also follow the same trend. This behavior continues up to a normal load of 136 N. Beyond this load there is a sharp increase of F_x, F_z, V_x and V_z with increasing normal load. This is the same load at which transition occurred in Figure 29. At a normal load of 185 N self excited vibrations occur and the variation in force and velocity components is seen to be at a maximum.

The steady state friction force as measured through strain gages is termed f_x and the steady state normal force f_n. The coefficient of dynamic component of friction force (F_x) and normal force (F_z) can be defined by $\tilde{\mu}$ where

$$\tilde{\mu} = \frac{F_x}{F_z}$$

is the average friction coefficient. In Figure 36 dynamic component of friction coefficient $\tilde{\mu}$ is plotted against normal load f_n. The forces f_x and f_n and the dynamic components of these forces are superimposed in Figure 37. Because of the difficulty of presentation of large variations of F_x and F_z, specially after transition, this figure depicts only the steady state region of friction process. It is clearly seen from this figure that F_x and F_z decrease as the normal force (f_n) increases.

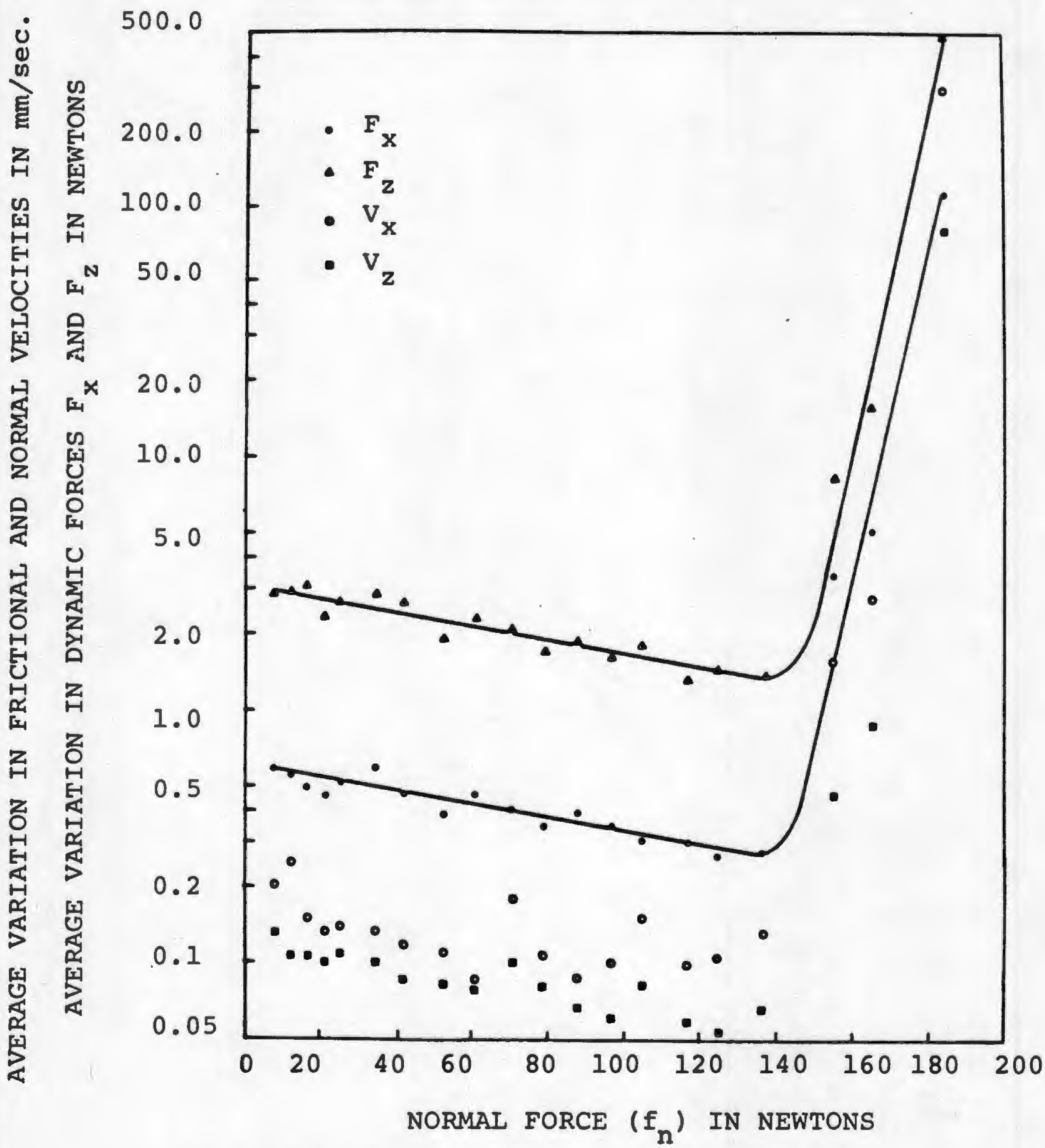

Figure 35. Average Variations of Dynamic Forces and Velocities in Frictional and Normal Directions Plotted against Normal Force at Sliding Speed of 46 cm/sec (50RPM) and for Stiffness K_1*

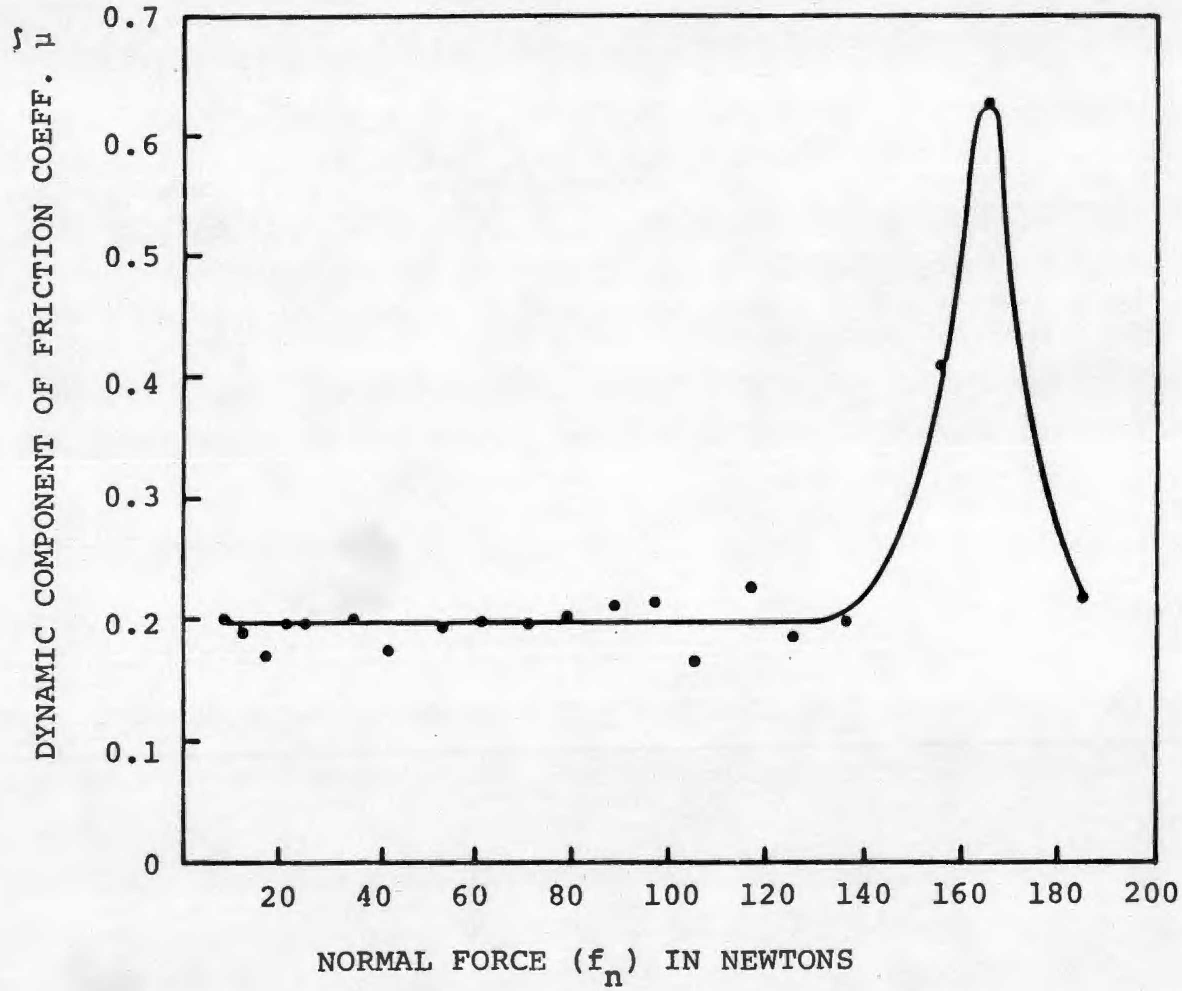

Figure 36. Dynamic Component of Friction Coefficient versus Normal Force for Sliding Speed of 46 cm/sec and for Stiffness K_1* (5.1 cm arm length)

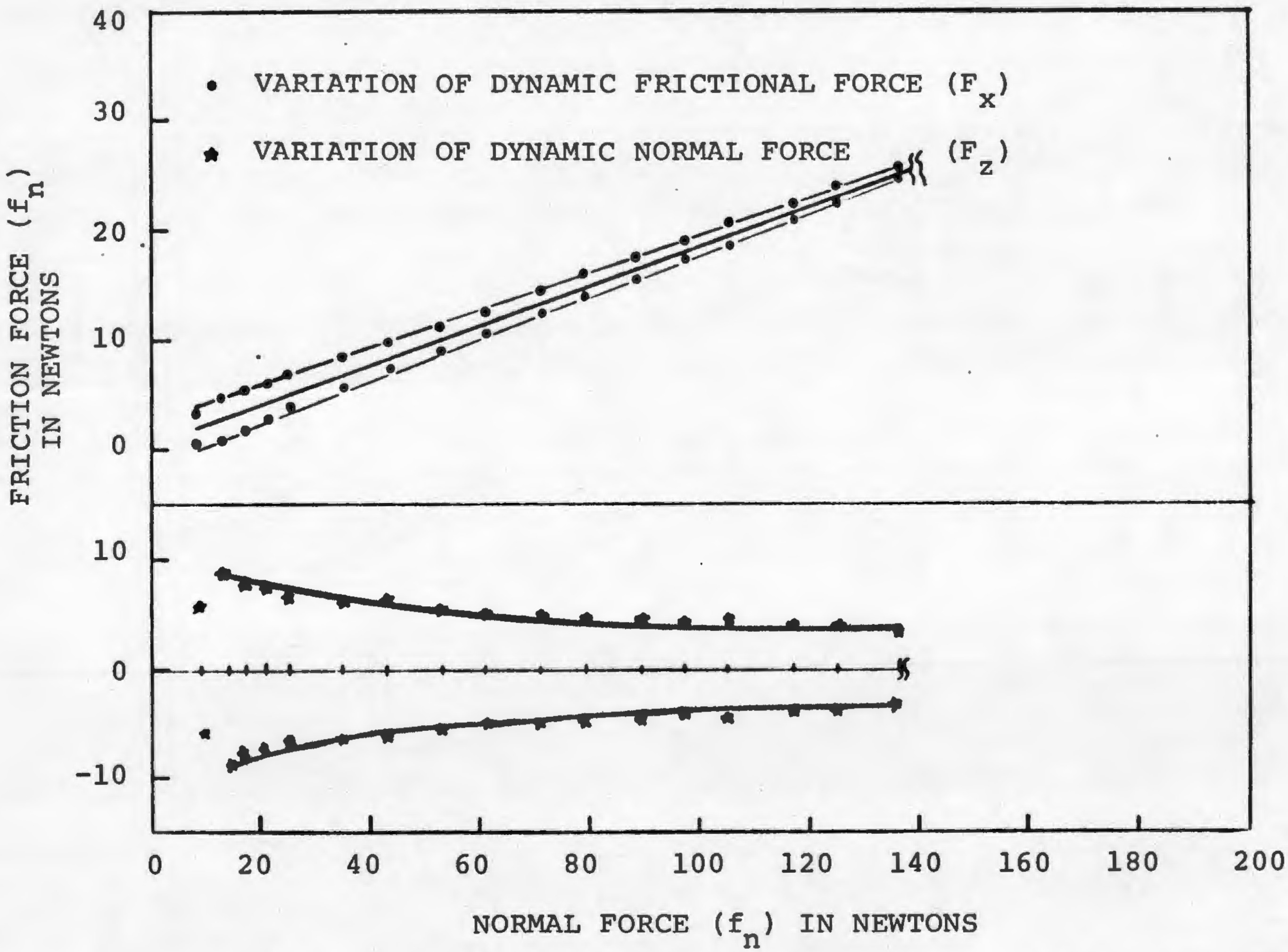

Figure 37. A Plot of Friction Force (f_x) versus Normal Force (f_n). The Corresponding Dynamic Components are Superimposed with Magnification 10X

The average variation in dynamic components of frictional and normal forces (F_x and F_z) and the variation of respective velocities (V_x and V_z) are shown in Figure 38 for a sliding speed of 70 cm/sec. Unlike in Figure 35, we see an increase in F_x with increasing normal load f_n. However, in Figure 39, the same features are plotted for a sliding speed of 94 cm/sec. The results in this figure are very similar to those in Figure 35.

For the purpose of comparison, the average variation of dynamic forces F_x and F_z are plotted for different sliding velocities in Figures 40 and 41. The variation in frictional and normal velocities at different sliding speeds is shown in Figures 42 and 43. It can be seen from these figures that behavior of each component at different sliding speeds is almost the same.

The various frequencies and their amplitudes obtained from Fast Fourier Transformer are shown in Figure 44. These results pertain to friction force spectra (SF_x) obtained for the case when sliding speed was 46 cm/sec. The results from normal force spectra (SF_z) are shown in Figure 45.

The amplitude of various frequencies obtained from friction force spectra (SF_x) at a sliding speed of 70 cm/sec can be seen in Figure 46 and for a sliding speed of 94 cm/sec is shown in Figure 47. The results are very similar to those shown in Figure 44.

For comparison purposes, the behavior of two typical frequencies (60 and 120 Hz) are plotted at different sliding speeds in Figures 48 and 49.

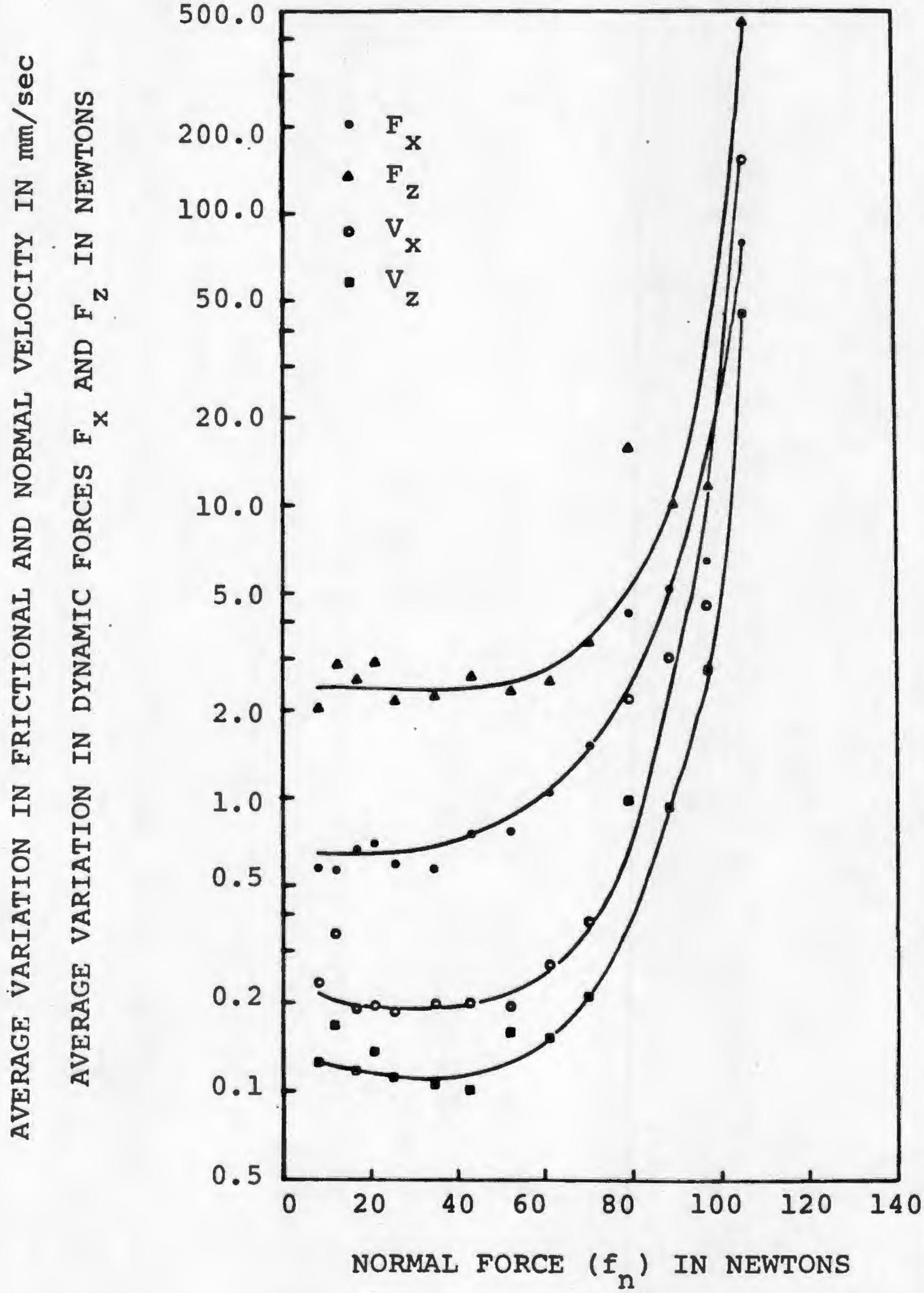

Figure 38. Average Variations of Dynamic Forces and Velocities in Frictional and Normal Directions Plotted Against Normal Force at Sliding Speed of 70 cm/sec (75 RPM) and for Stiffness K_1*

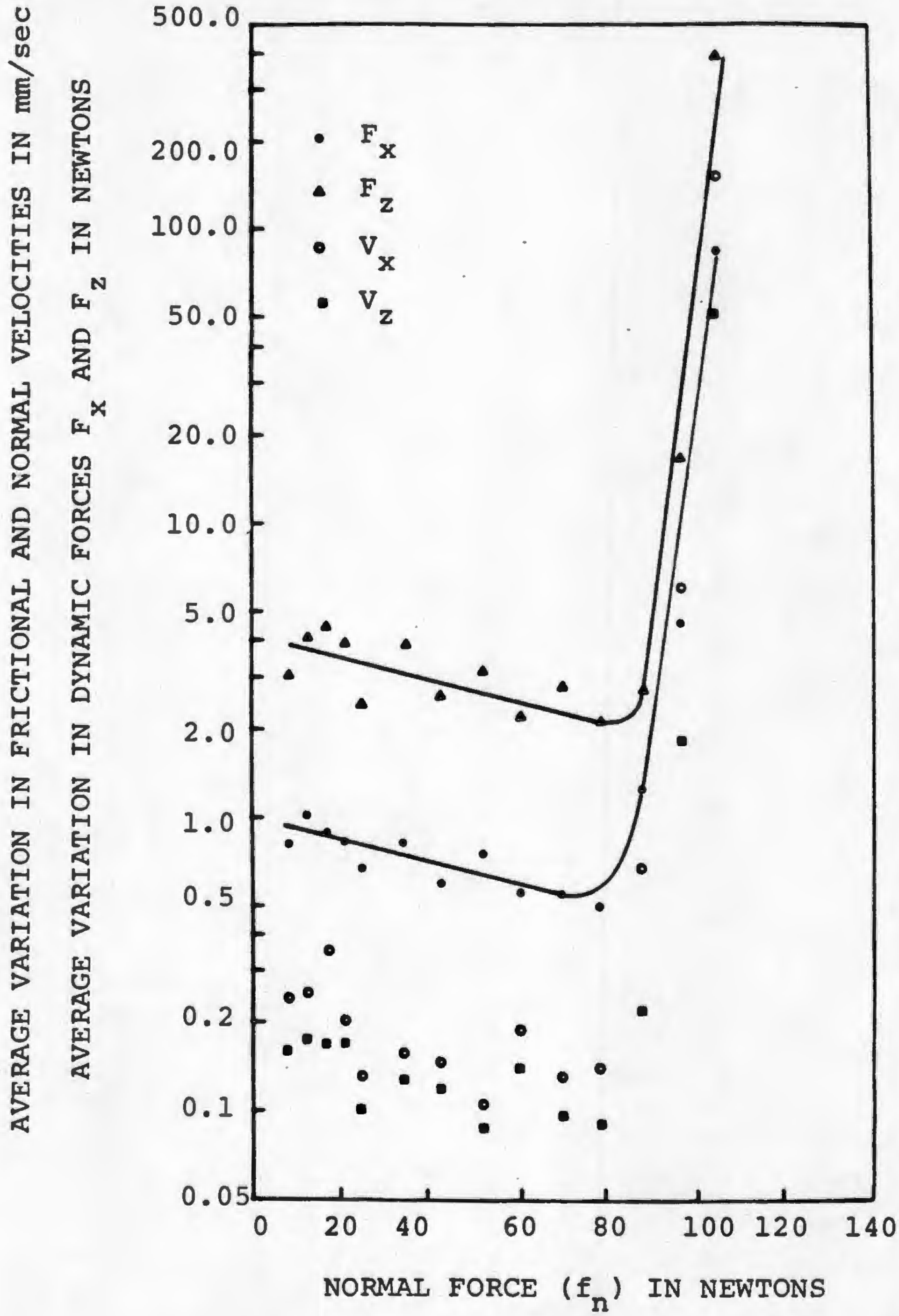

Figure 39. Average Variation of Dynamic Forces and Velocities in Frictional and Normal Directions Plotted Against Normal Force at Sliding Speed of 100 cm/sec (100 RPM) and For Stiffness K_1*

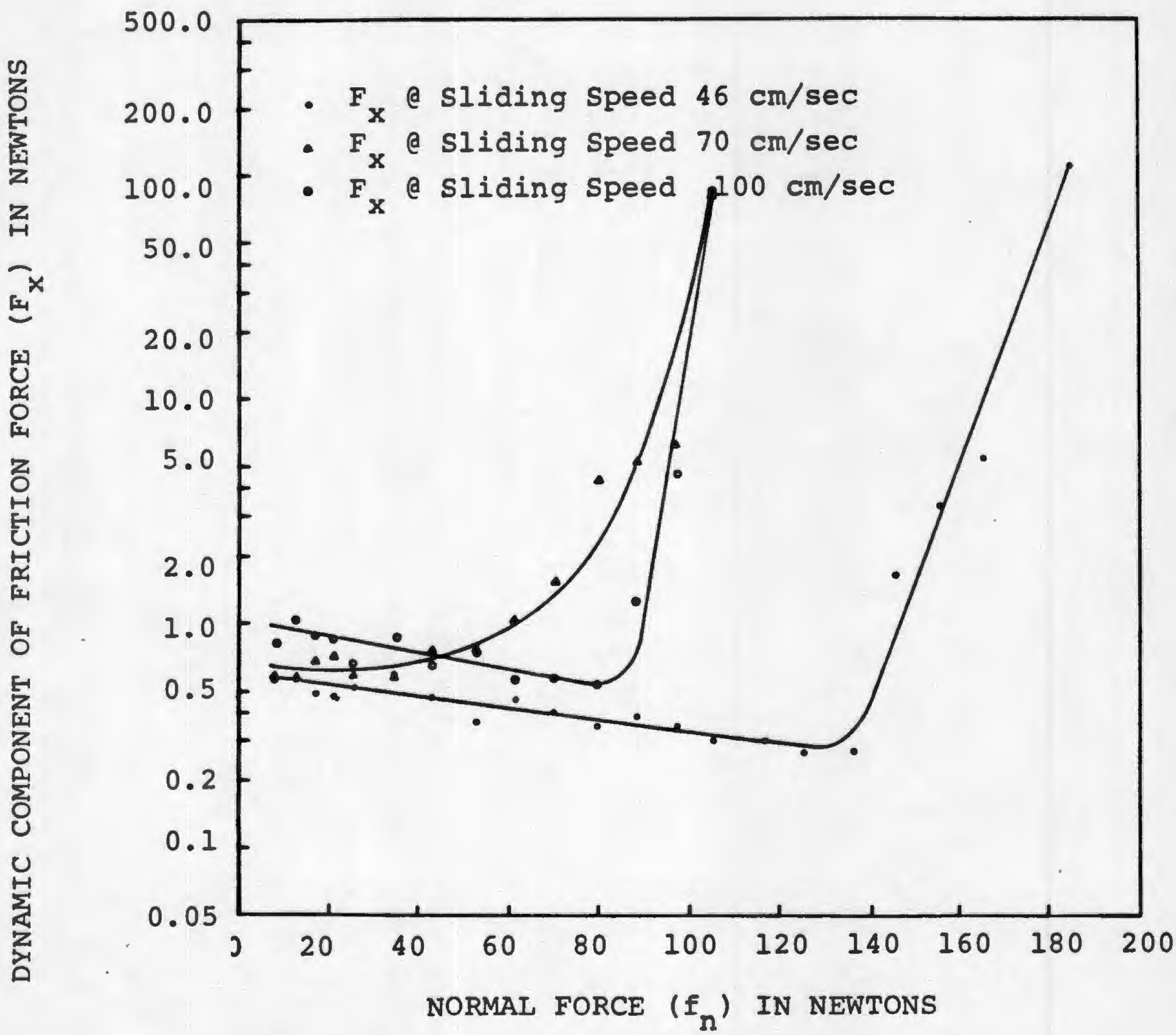

Figure 40. Variation of Dynamic Component of Friction Force (F_x) Plotted Against Normal Force (f_n) for Three Different Sliding Speeds and for Stiffness K_1*

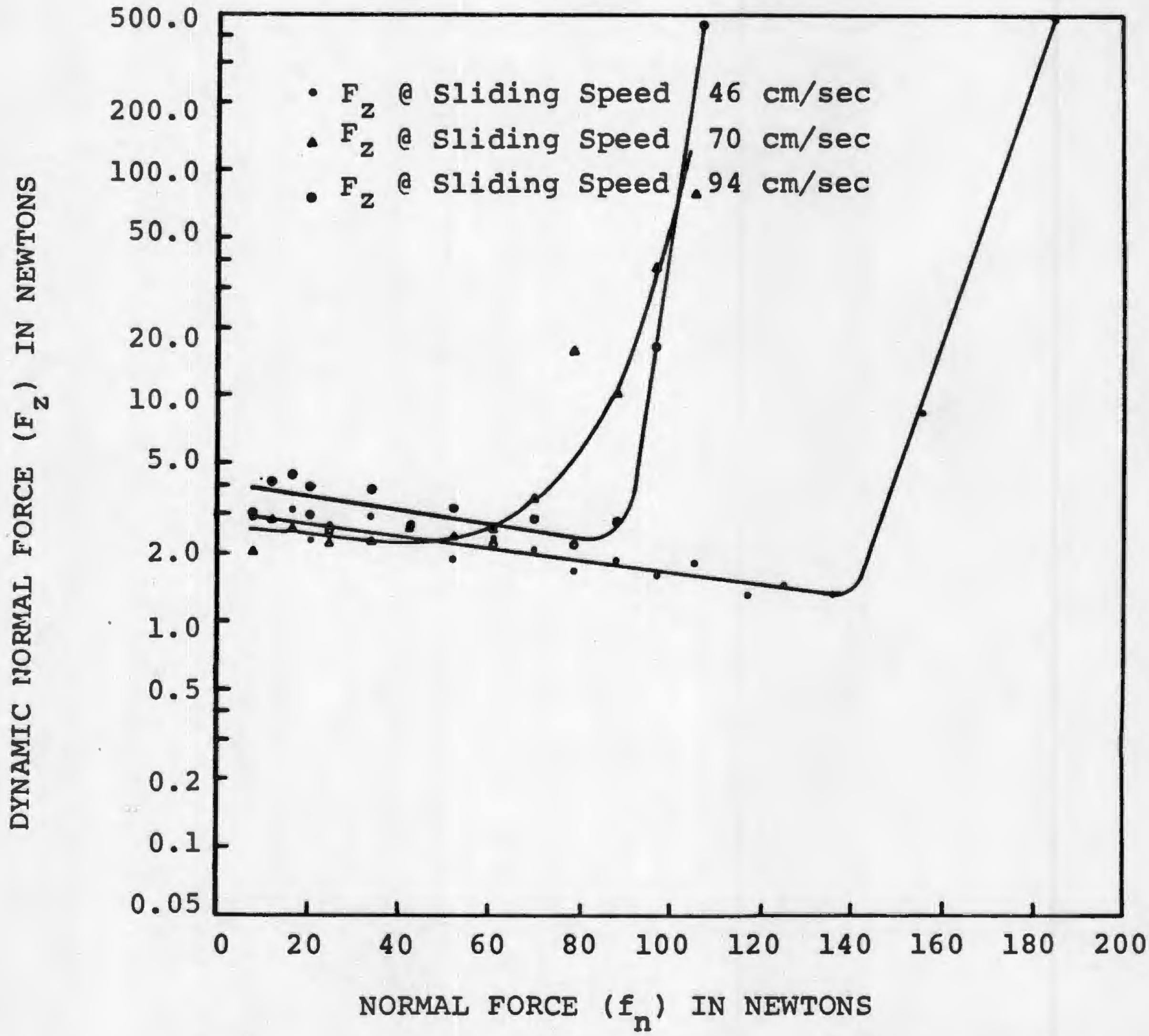

Figure 41. Variation of Dynamic Component of Normal Force (F_z) Plotted Against Normal Force (f_n) for Three Different Sliding Speeds and for Stiffness K_1*

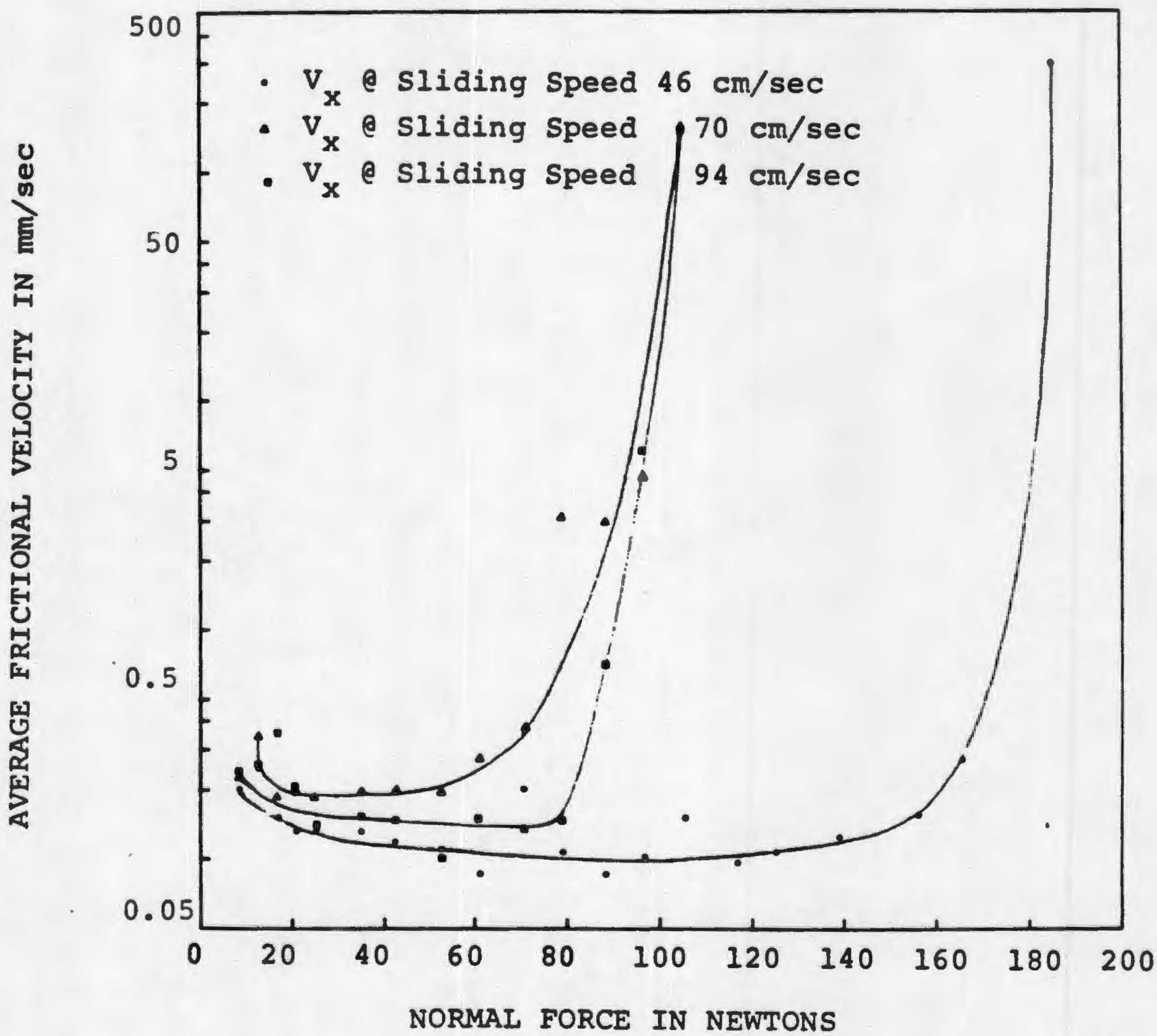

Figure 42. Average Frictional Velocity for Three Different Sliding Speeds versus Normal Force for Arm Length 5.1 cm (K_1*)

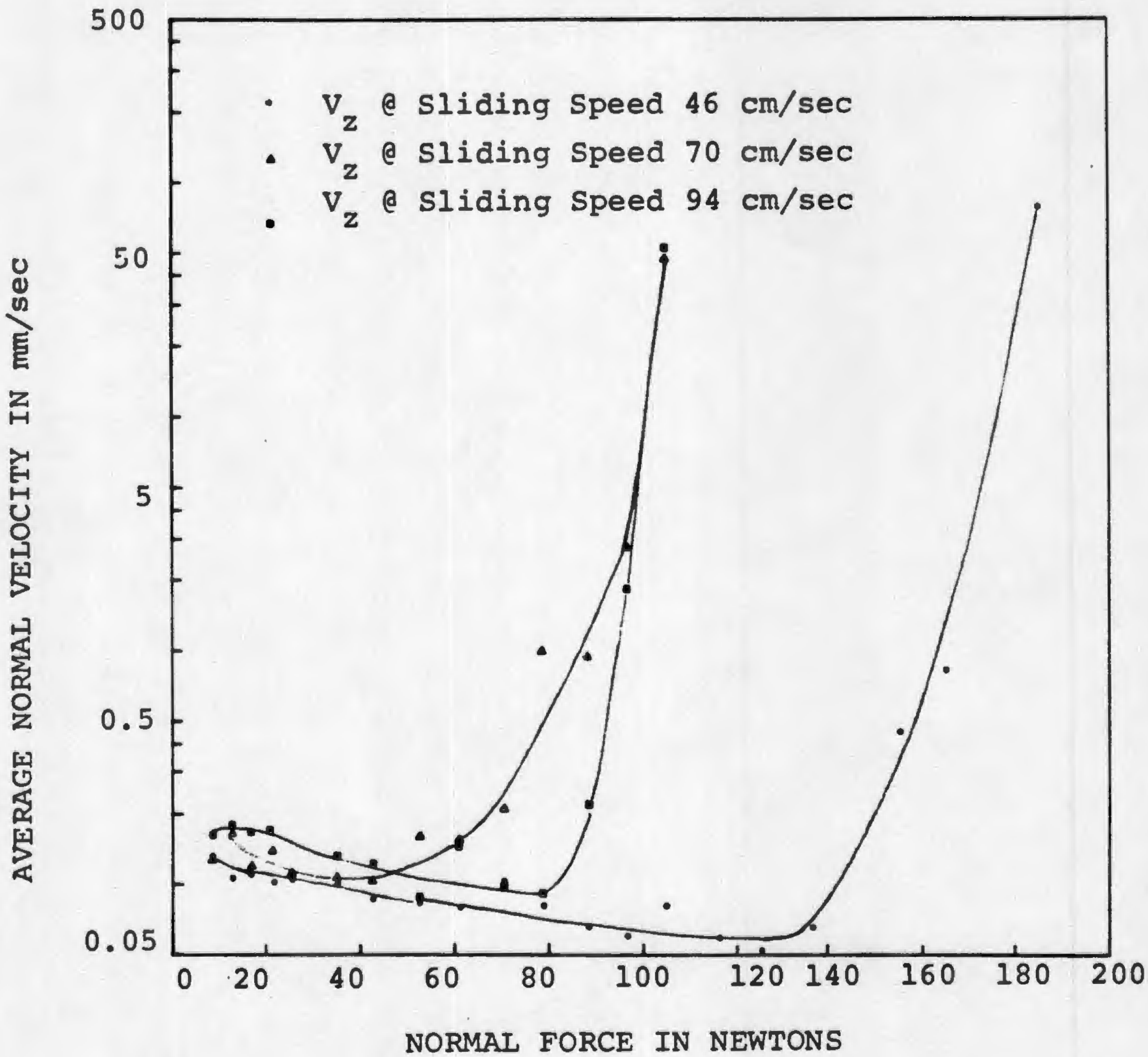

Figure 43. Average Normal Velocity for Three Different Sliding Speeds versus Normal Force for Arm Length 5.1 cm (K_1*)

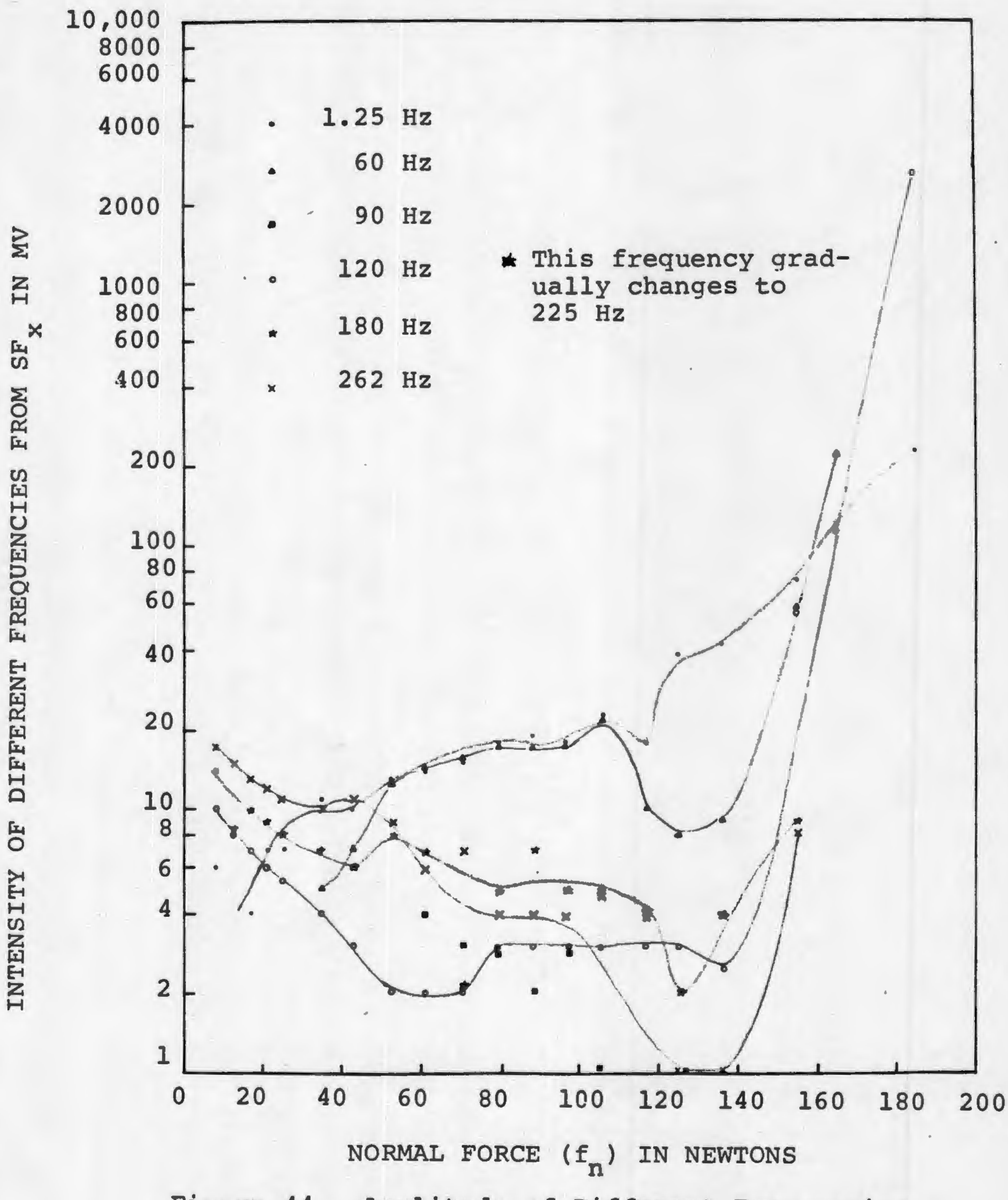

Figure 44. Amplitude of Different Frequencies Obtained from Friction Force Spectrum (SF_x) versus Normal Force for Sliding Speed of 46 cm/sec and Arm Length 5.1 cm (K_1*)

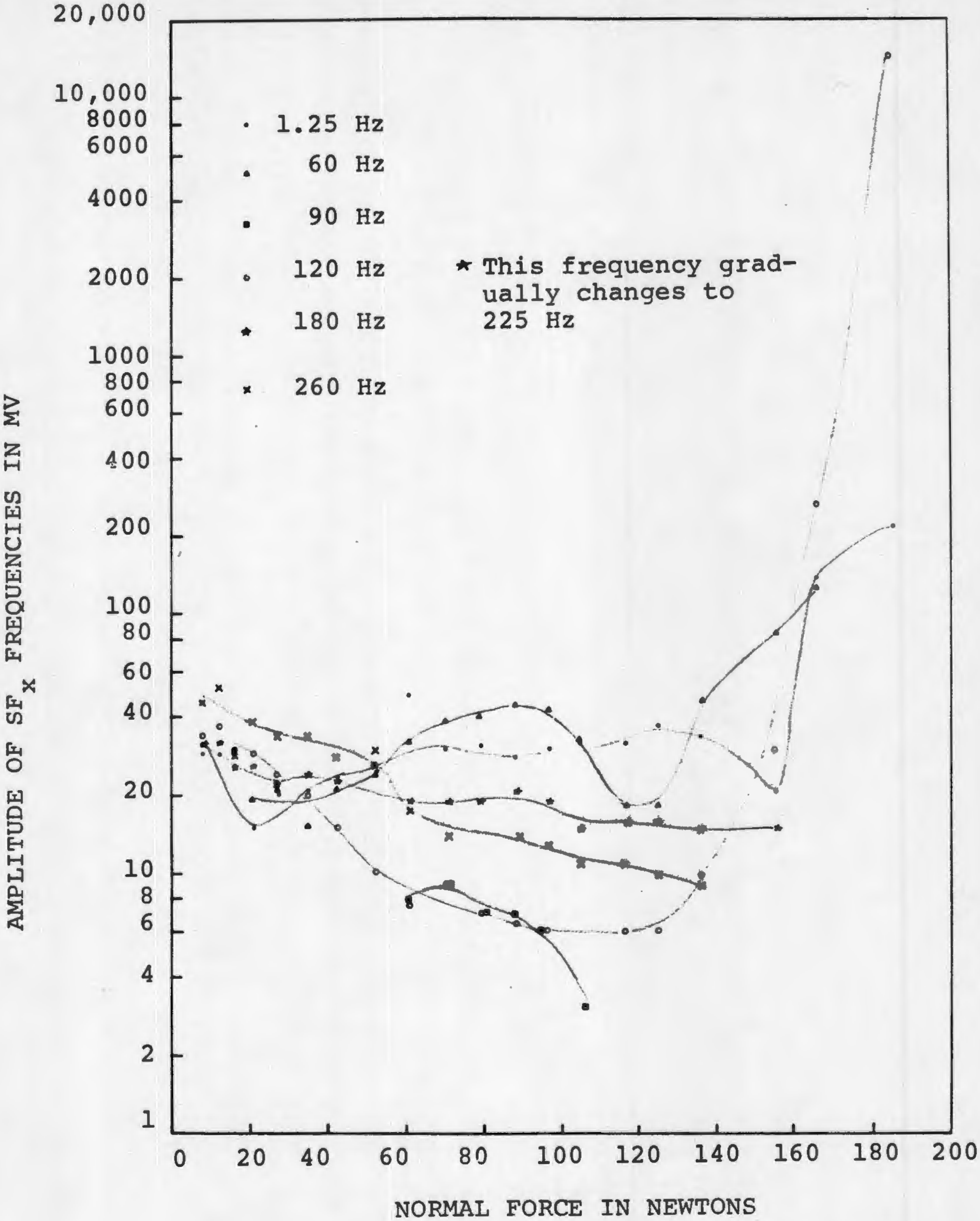

Figure 45. Amplitude of Friction Force Spectrum (SF_x) Frequencies versus Normal Force at Sliding Speed of 46 cm/sec and Stiffness K_1*

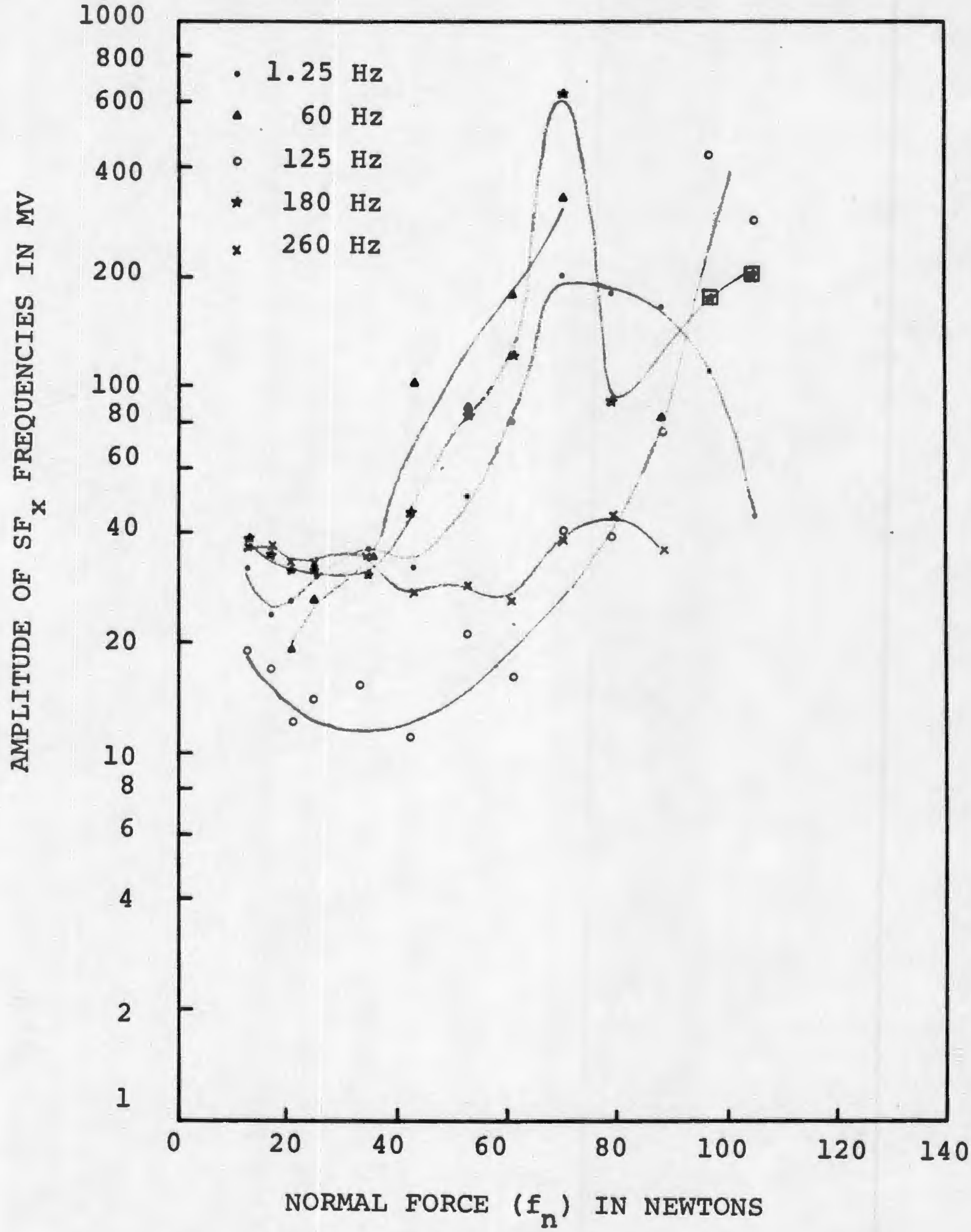

Figure 46. Amplitude of Friction Force Spectrum (SF_x) Frequencies versus Normal Force (f_n) at Sliding Speed of 70 cm/sec and for Stiffness K_1*

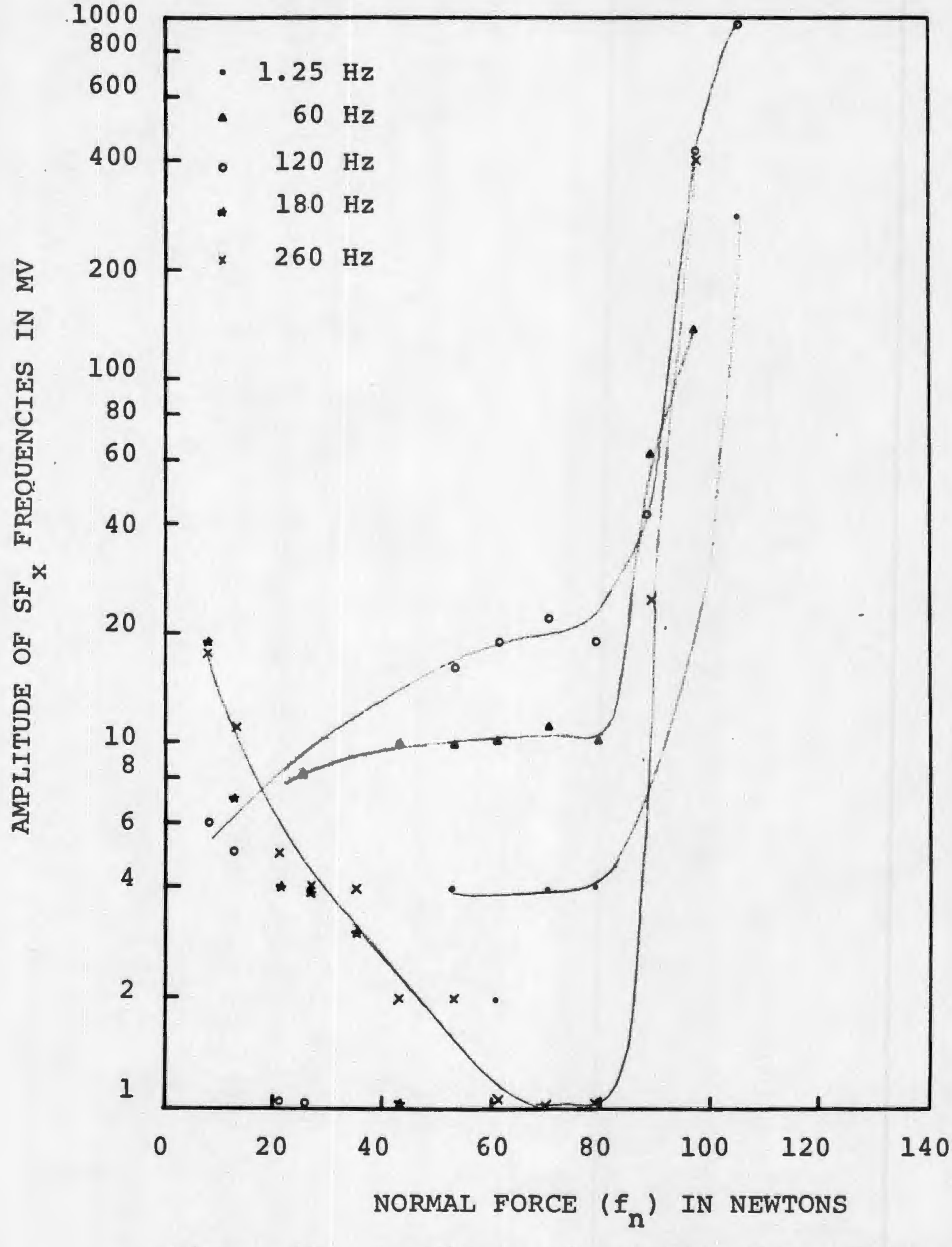

Figure 47. Amplitude of Friction Force Spectrum (SF_x) Frequencies versus Normal Force at Sliding Speed of 94 cm/sec and Stiffness K_1*

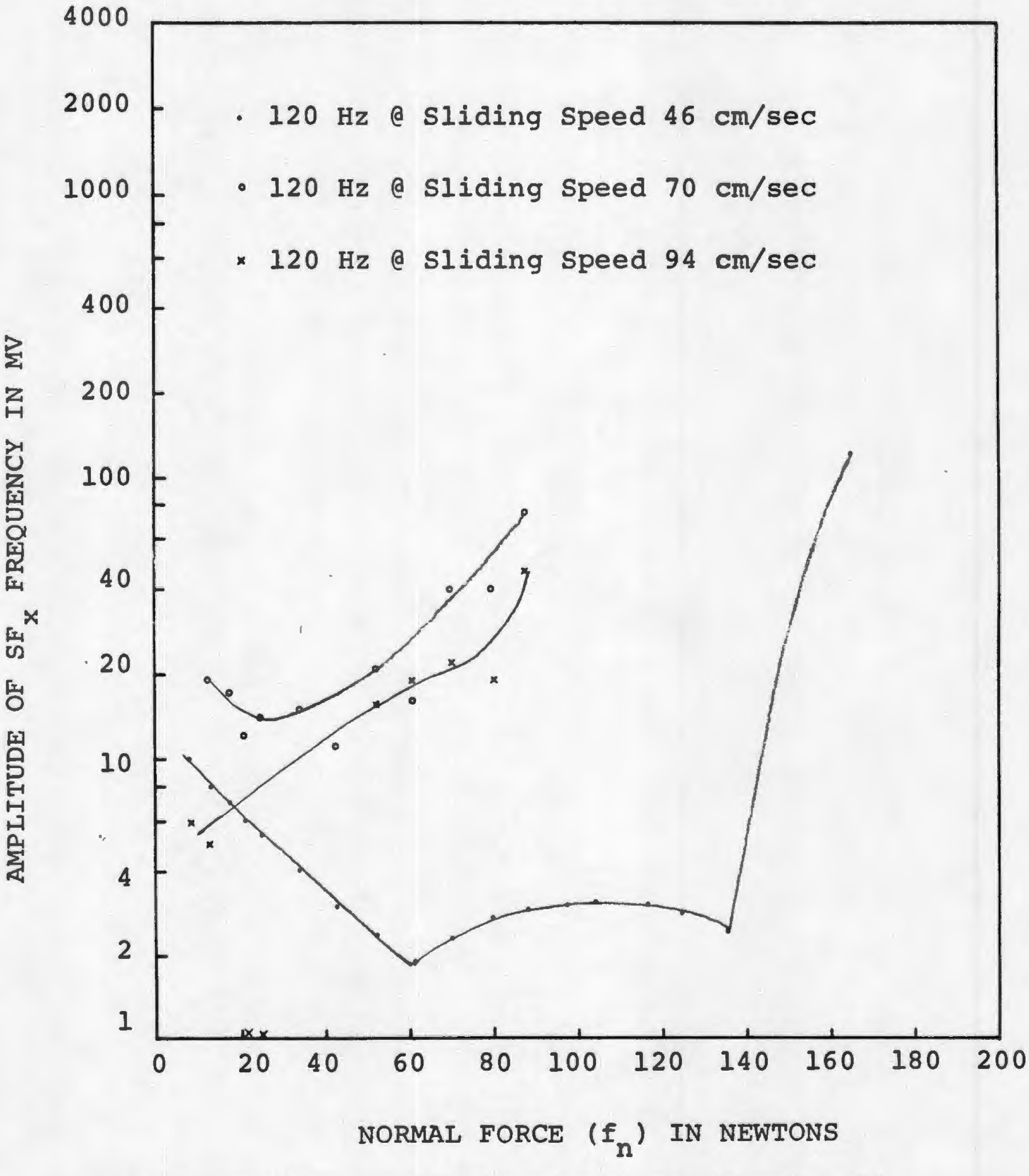

Figure 48. Amplitude of 120 Hz (Tortional) Frequency Obtained from Friction Force Spectrum (SF_x) versus Normal Force at Three Different Sliding Speeds and at Constant Stiffness K_1*

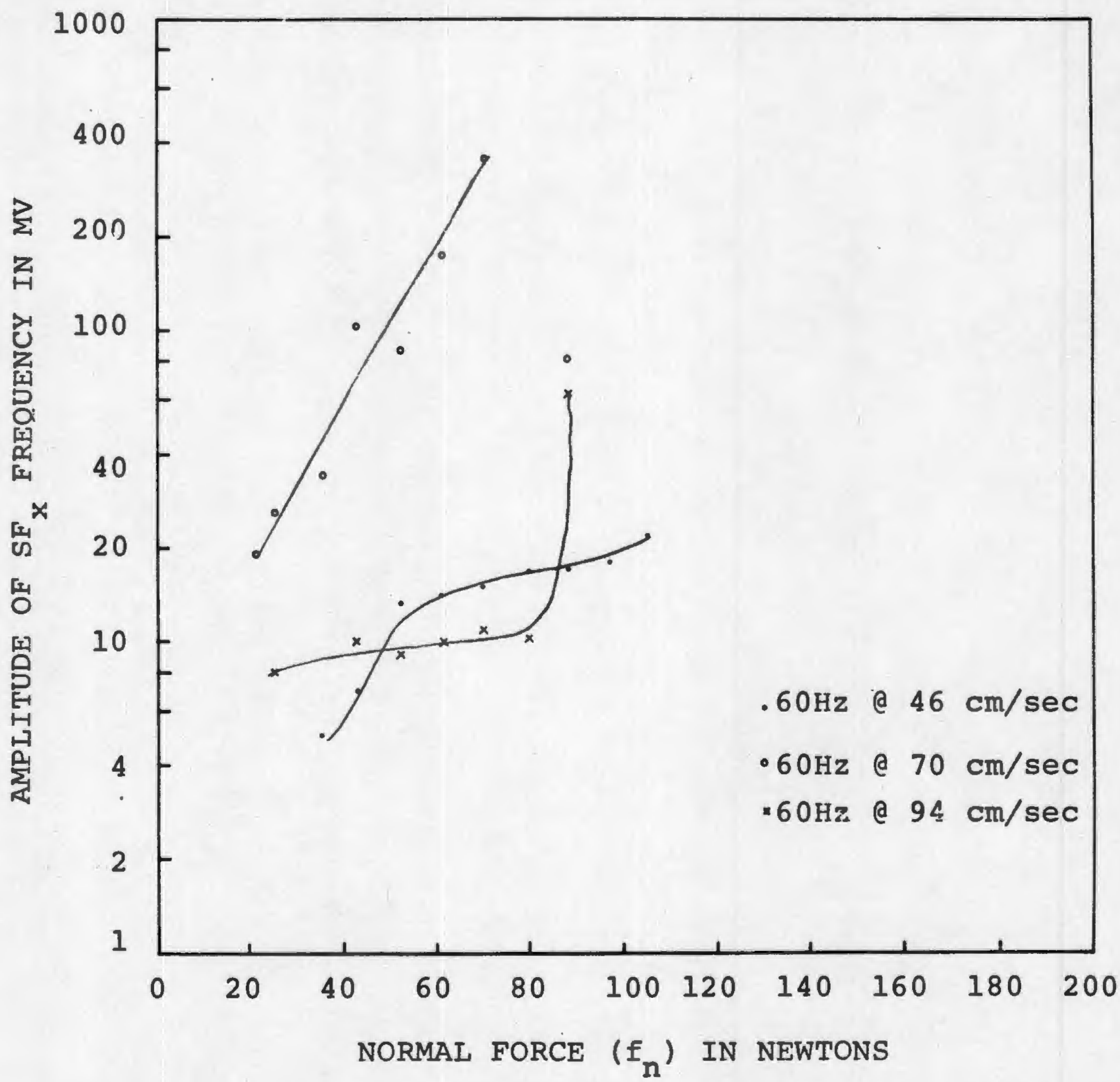

Figure 49. Amplitudes of 60 Hz Frequency Obtained from Friction Force Spectrum (SF_x) versus Normal Force at Three Different Sliding Speeds and at Constant Stiffness K_1*

Out of different frequencies as seen in Figure 40, the frequency of 180 Hz is the only one which changes with a change in normal load. This change and its corresponding amplitude of oscillation in the frictional direction is shown in Figure 50. A typical spectrum of the dynamic friction force (SE_x) is shown in Figure 51. The behavior of the same frequency in the normal direction is shown in Figure 52. From these figures one sees that the frequency of 180 Hz at 8 N increases to around 225 Hz at 80 N and beyond this normal load the frequency does not change. When these two figures are superimposed together in Figure 53, one sees that the change of frequency is very much the same in both frictional and normal directions.

The behavior of 180 Hz frequency at sliding speeds of 70 and 94 cm/sec are shown in Figures 54 and 55.

It was stated earlier that during wear experiments the slider surface was examined under Talysurf for its surface profile and roughness. The results obtained are given below.

Figure 56 shows the rate of wear obtained for spring stiffness K_1* (spring length of 5.1 cm) and sliding speed of 46 cm/sec. Here it can be seen that the wear rate increases rapidly in the steady state region with an increase in normal load. After transition, which occurred around 95 N normal load, the rate of wear suddenly increased from 134.9 x 10^{-10} to 316.55 x 10^{-10} gm/cm.

In order to investigate the effect of rigidity on surface roughness three spring lengths 5.1 cm (5"), 8.0 cm (3.5") and 12.7 cm (5") were used. During all three experi-

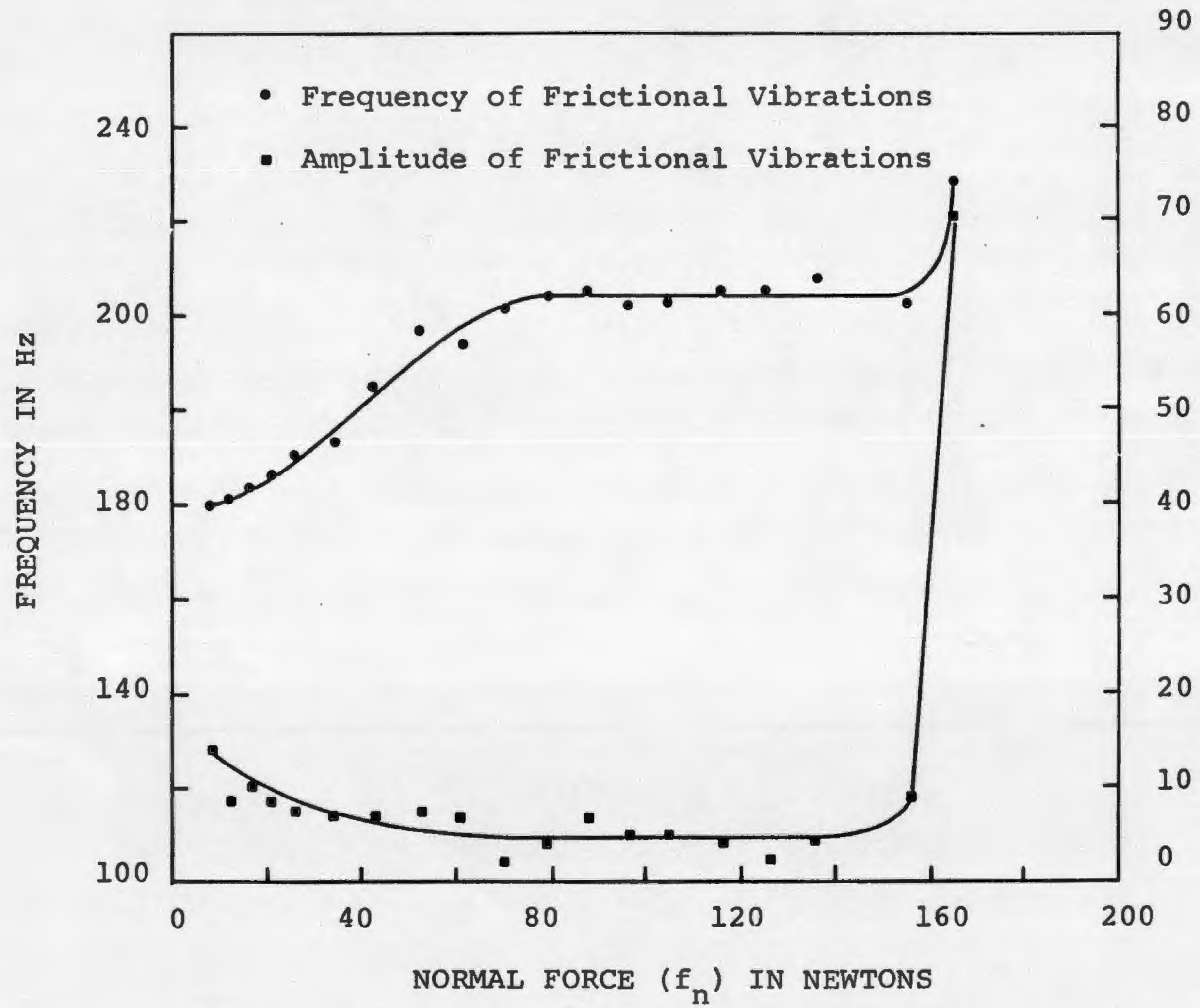

Figure 50. Variation of Frequency and Amplitude of Vibration in Frictional Direction vs. Normal Force for Sliding Speed of 46 cm/sec and stiffness K_1*

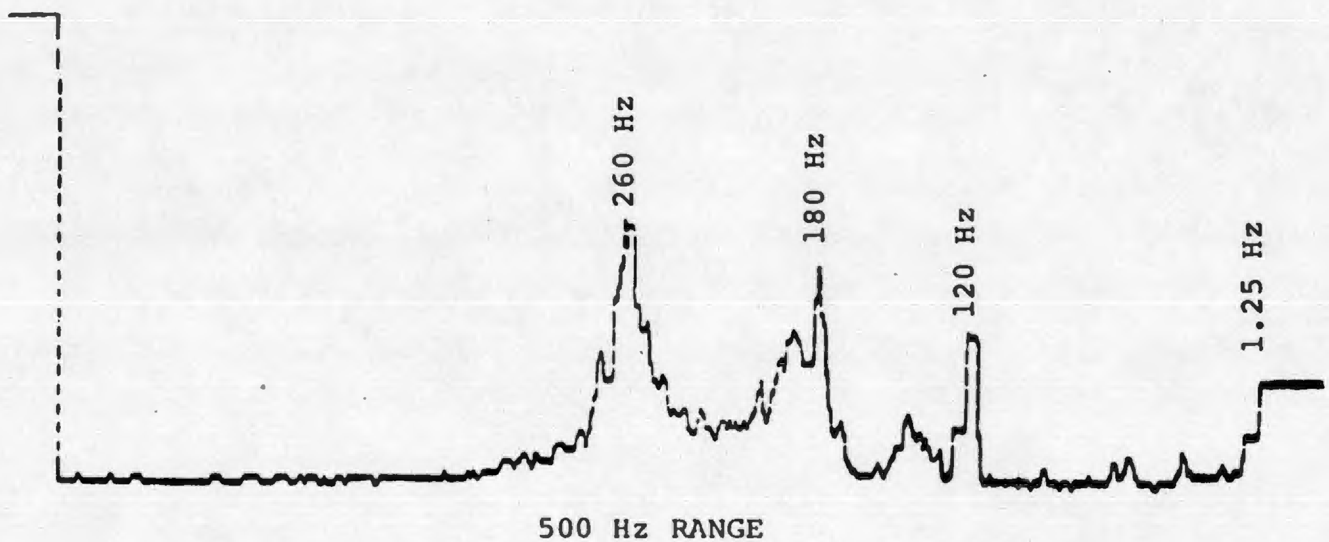

Figure 51. Friction Force Spectrum at 8 Newtons Normal Load and 5.1 cm Arm Length

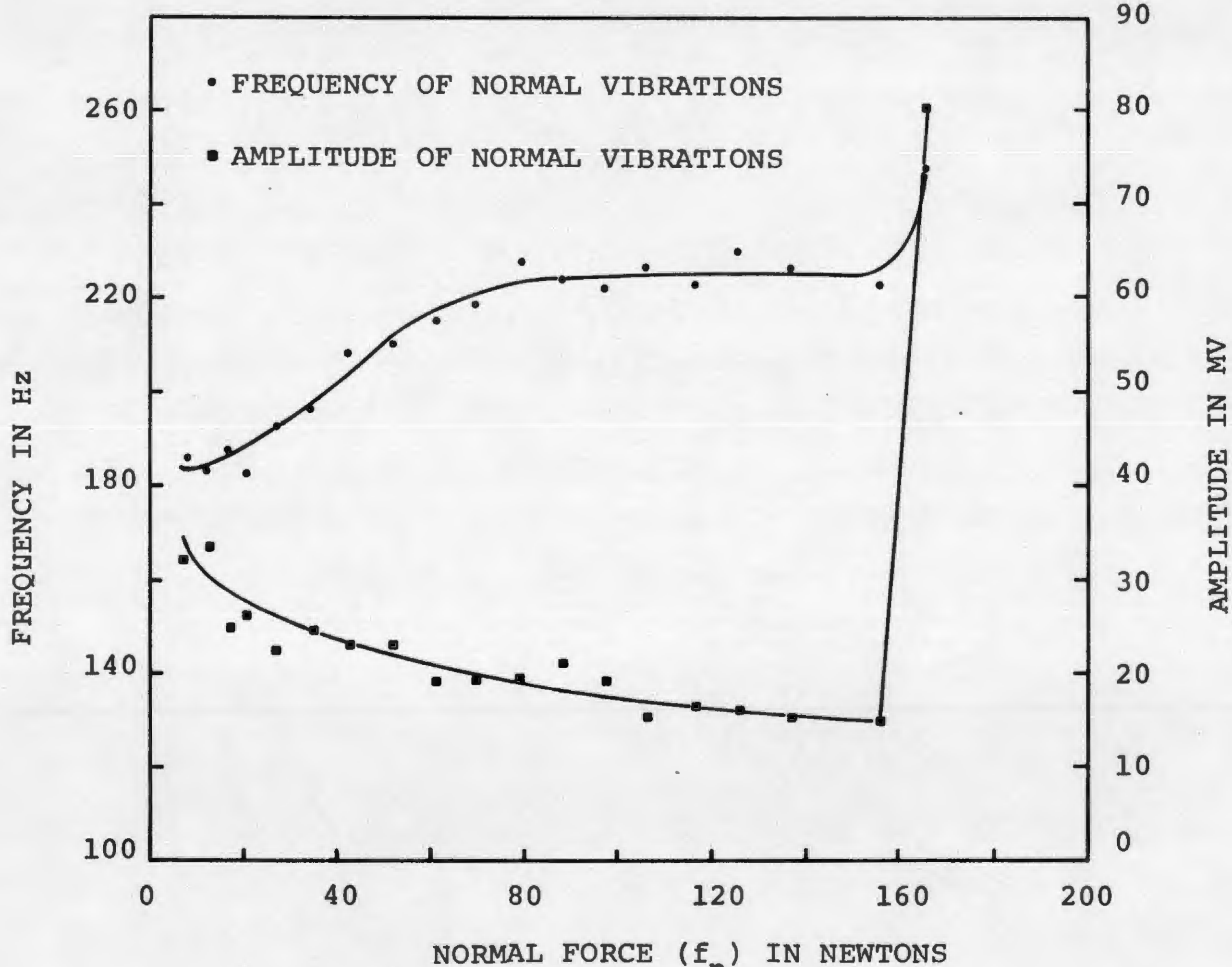

Figure 52. Variation of Frequency and Amplitude of Vibrations in Normal Direction vs. Normal Force for Sliding Speed of 46 cm/sec and stiffness K_1*

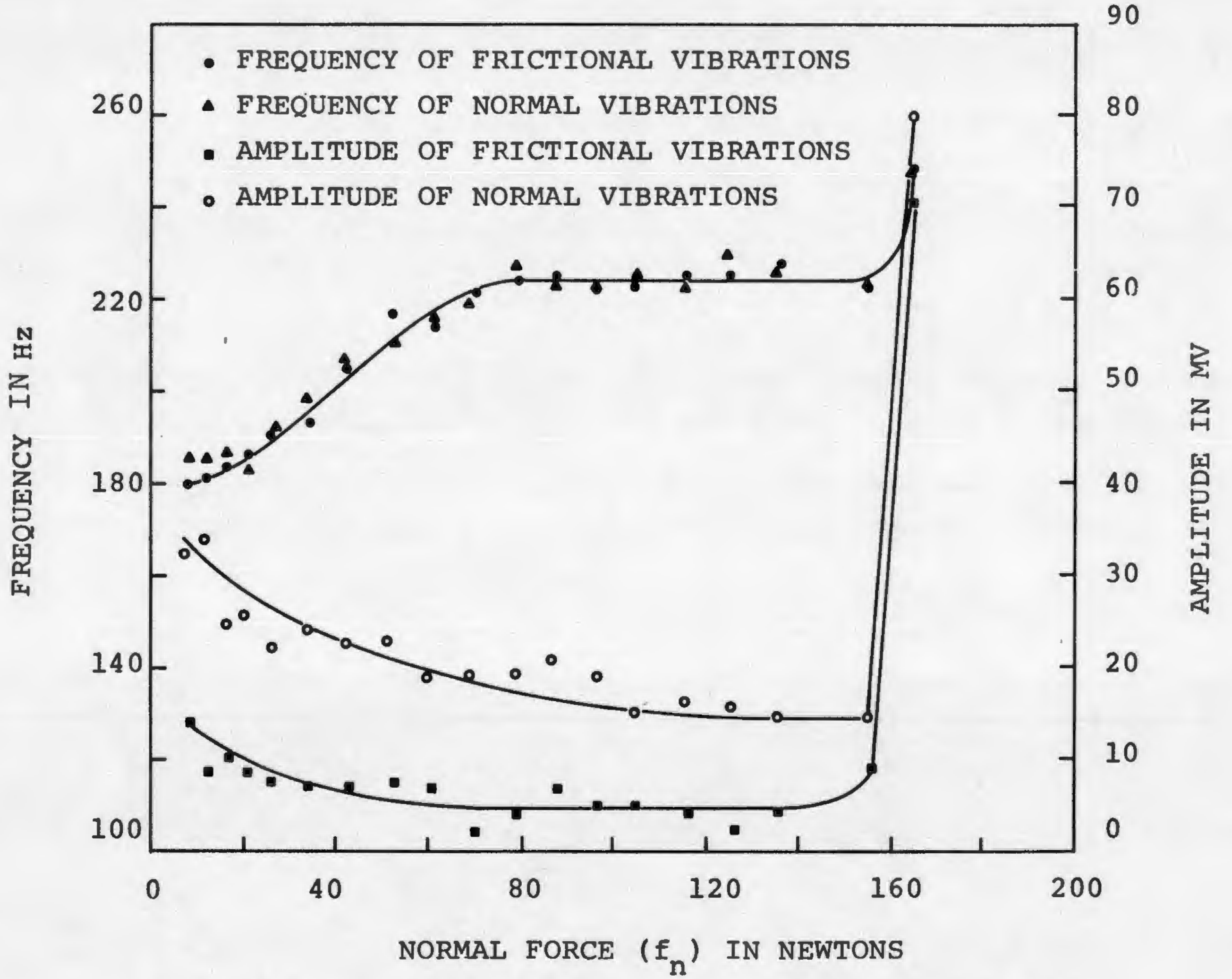

Figure 53. Variation of Frequency and Corresponding Amplitudes of Vibrations in Normal and Frictional Directions vs. Normal Force for Sliding Speed of 46 cm/sec and Stiffness K_1*

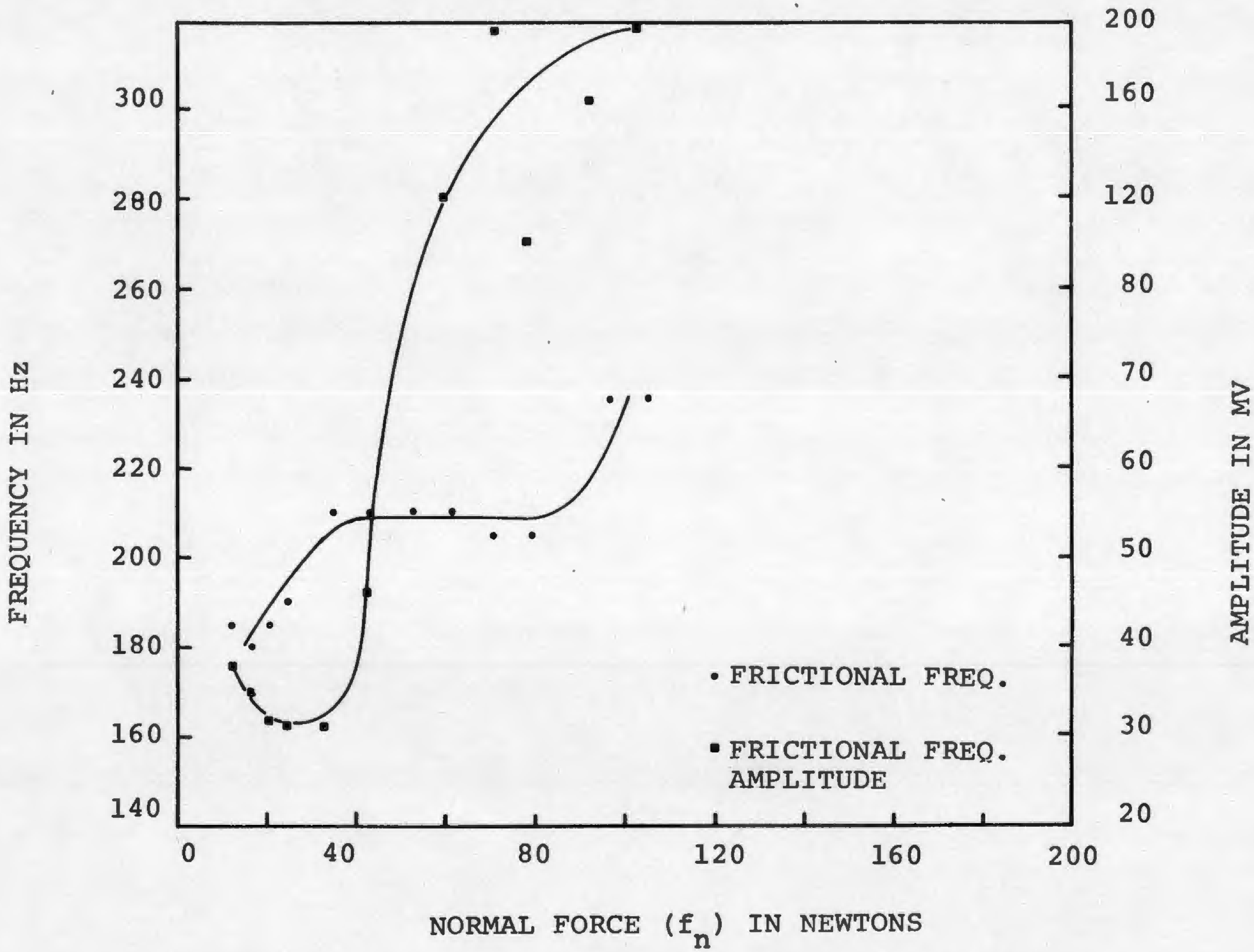

Figure 54. Frequency Variation and Its Amplitude vs. Normal Force for Sliding Speed of 70 cm/sec and Stiffness K_1*

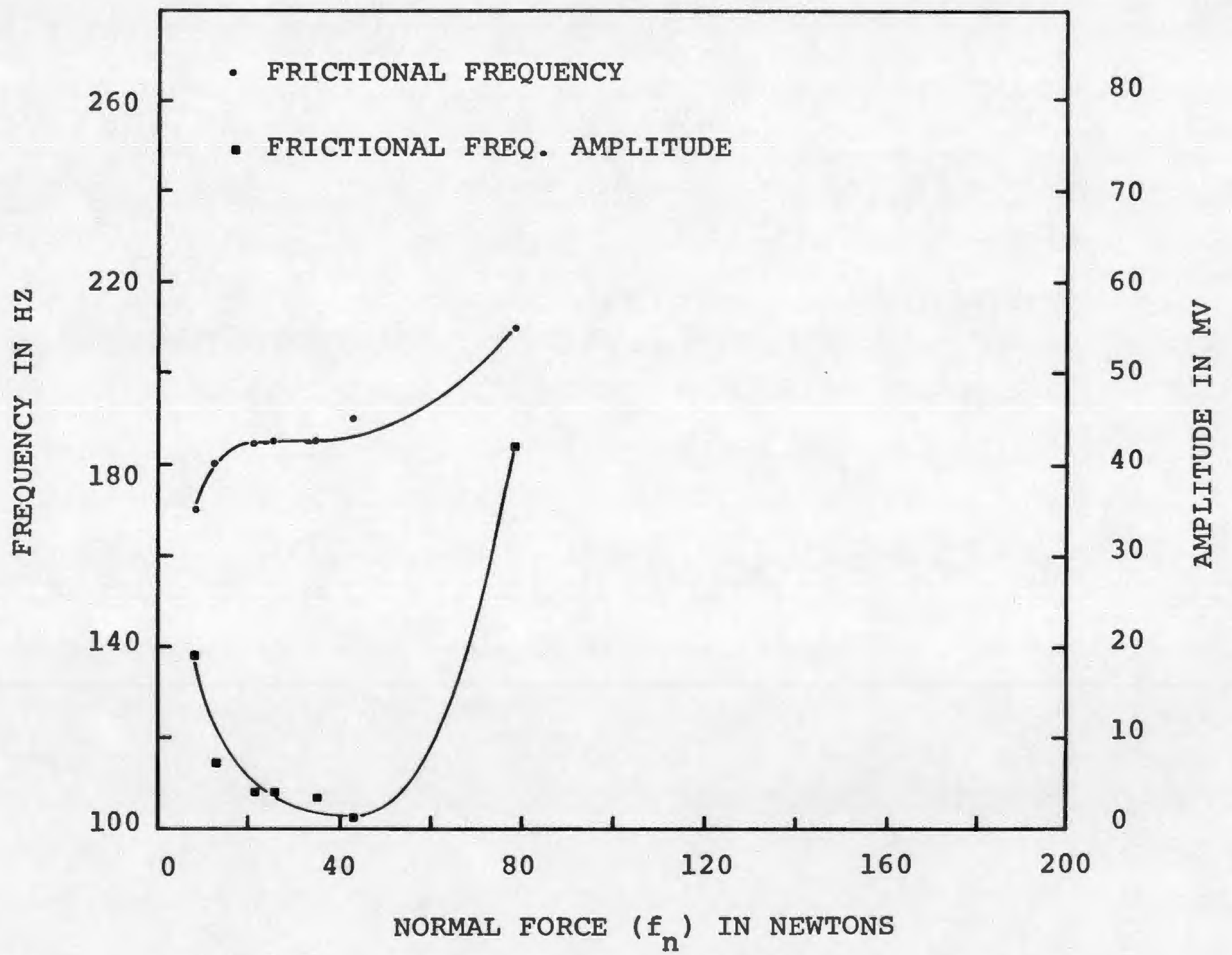

Figure 55. Frequency Variation and Its Amplitude vs. Normal Force for Sliding Speed of 94 cm/sec and Stiffness K_1*

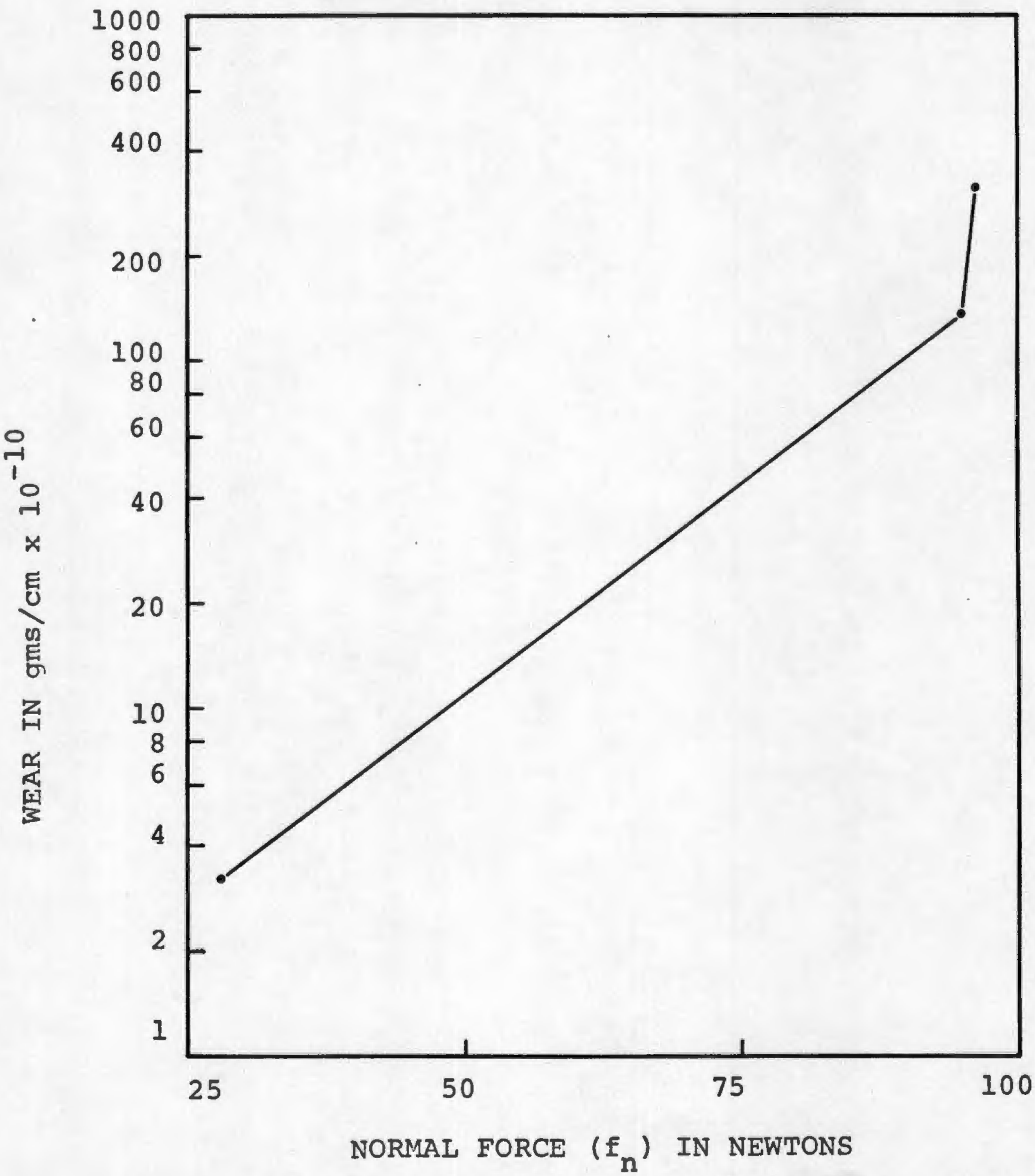

Figure 56. Wear vs. Normal Force for Sliding Speed of 46 cm/sec and Stiffness K_1*

ments the sliding speed and track diameter and normal load were maintained almost constant. Figure 57 shows the decrease in Ra value of the surface roughness across and along the direction of sliding for the 5.1 cm arm length. The decrease in Ra across appears to be sharper than the decrease along the lay. For the spring length of 8.9 cm, change of surface roughness is shown in Figure 58, while the surface roughness when the spring length is 12.7 cm is shown in Figure 59. The decrease of surface roughness with sliding distance for 5.1 cm (2") and 12.7 cm (5") arm length is shown in Figures 60 and 61, respectively.

For comparison purposes, the foregoing results are plotted in Figure 62. It is interesting to note that roughness across the sliding is largest for the stiffest spring, i.e., K_1*, and smallest for the least stiff spring, i.e., K_3*. Also, the rate of decrease of Ra across the sliding direction is highest for stiffness K_1*. In other words, the slope of the surface roughness curve (across the lay) increases with increasing system rigidity. This is shown in Figure 63. Also one sees in Figure 62 different Ra (across) values for different stiffnesses but at the same constant load. The roughness variation as a function of system rigidity is shown in Figure 64. One can see from this figure that the roughness is directly proportional to the stiffness of the system.

Another interesting feature to note in Figure 62 is that the roughness measured along the direction of sliding remains almost constant for all three spring stiffnesses.

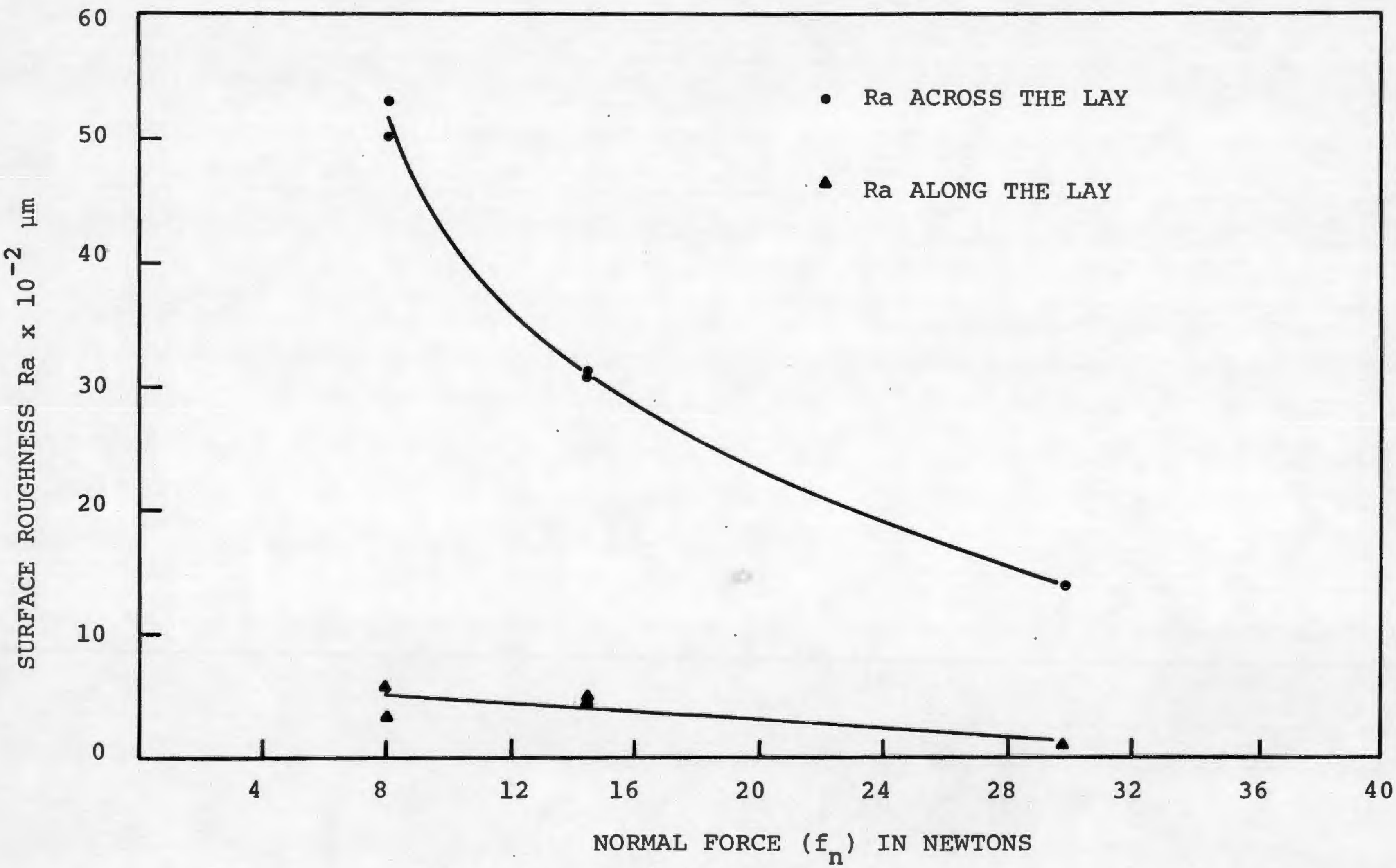

Figure 57. Surface Roughness vs. Normal Force for Sliding Speed of 46 cm/sec and Stiffness K_1*

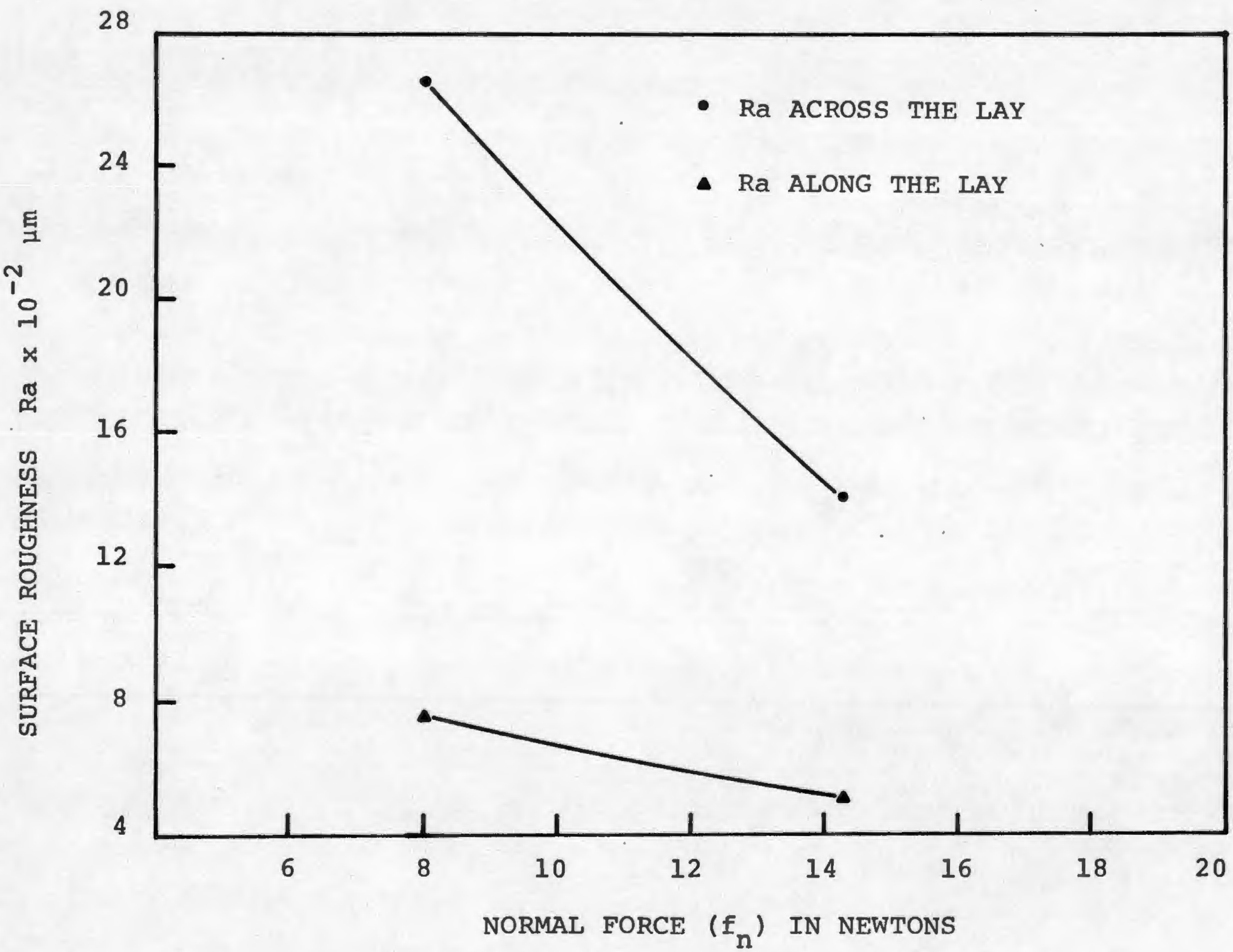

Figure 58. Surface Roughness vs. Normal Force for Sliding Speed of 46 cm/sec and Stiffness K_1*

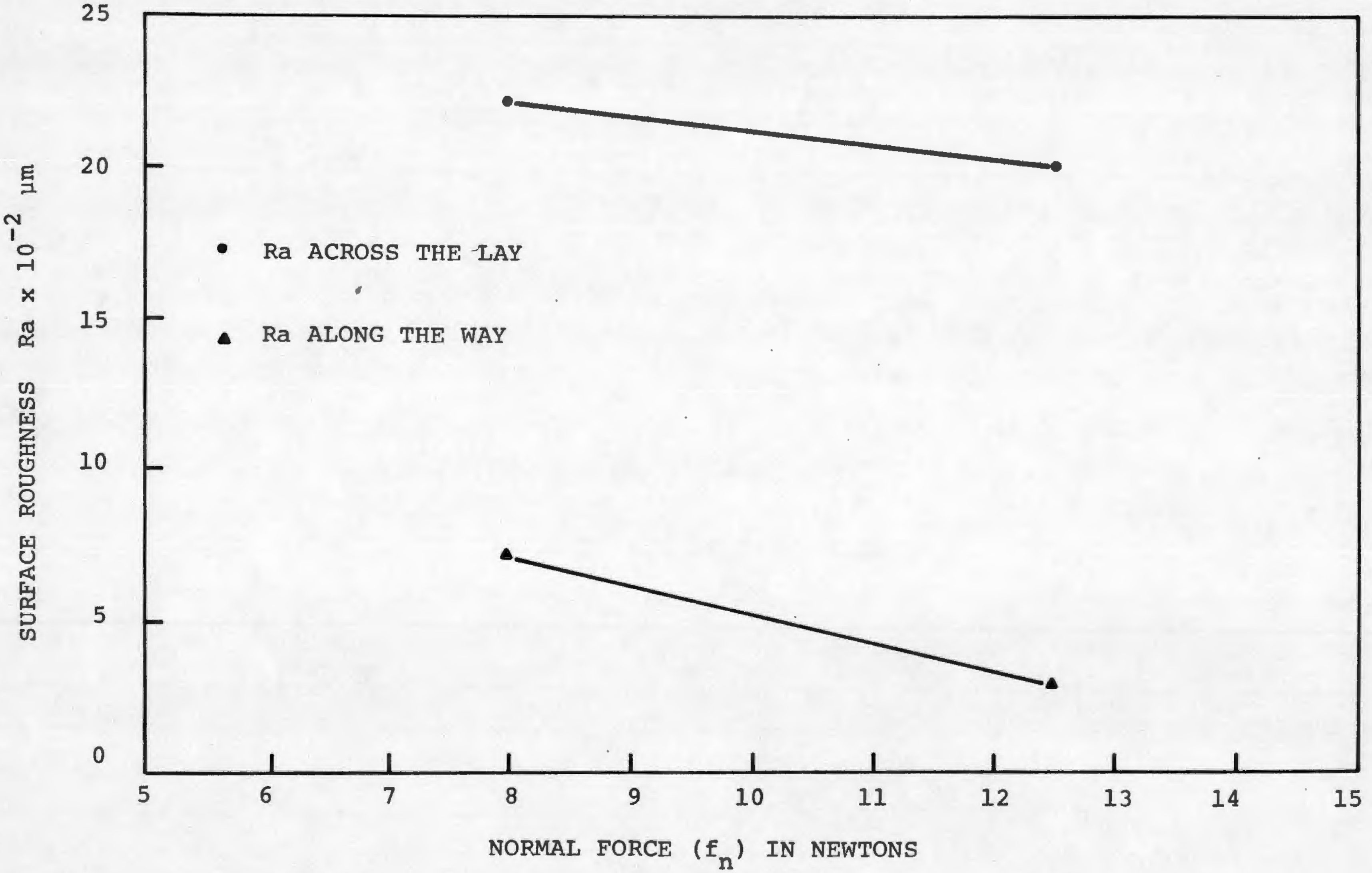

Figure 59. Surface Roughness vs. Normal Force for Sliding Speed of 46 cm/sec and Stiffness K_3*

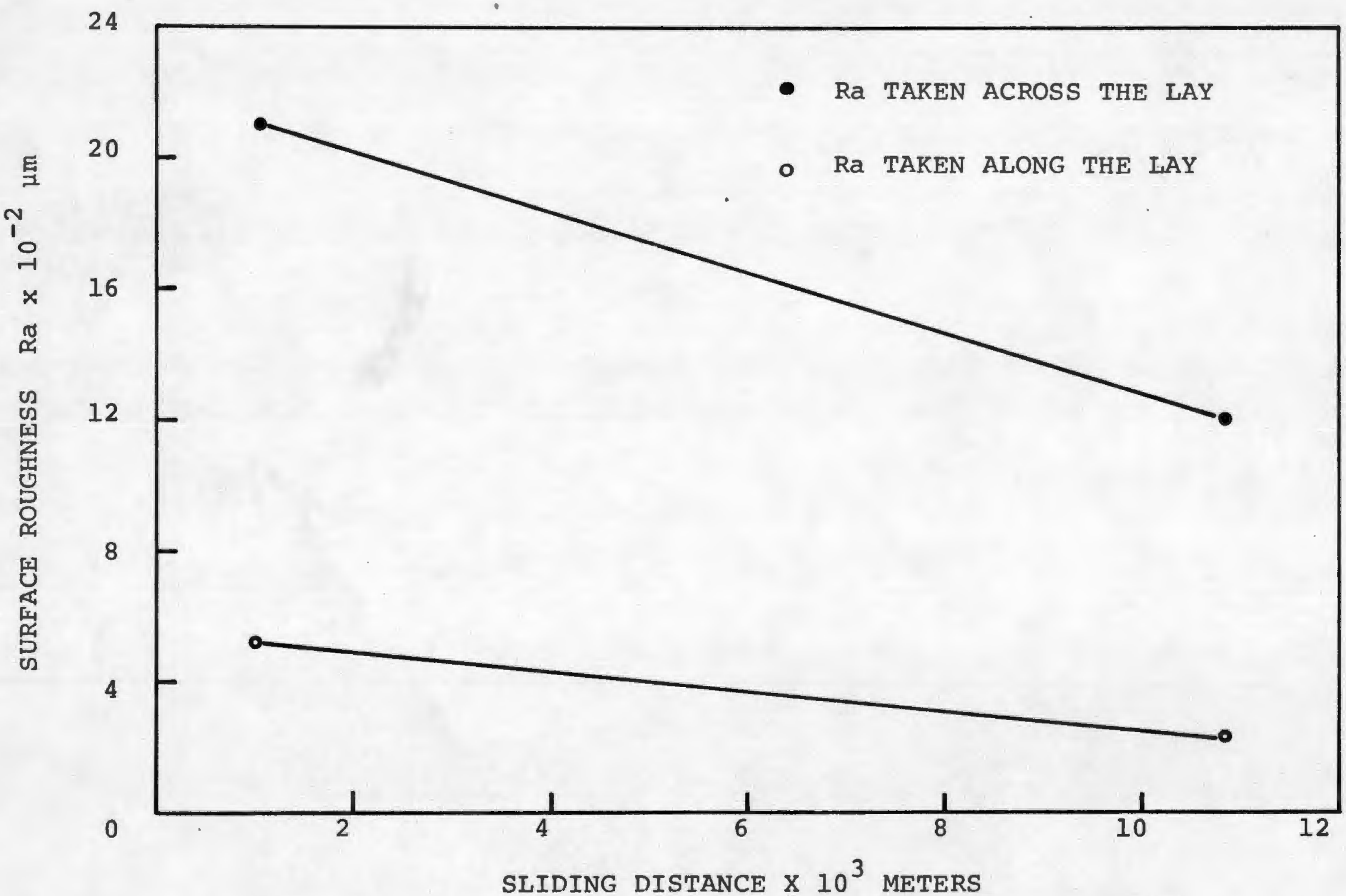

Figure 60. Variation of Surface Roughness with Sliding Distance for Stiffness K_1* (Arm length 5.1 cm) and Normal Force (f_n) 22 Newtons

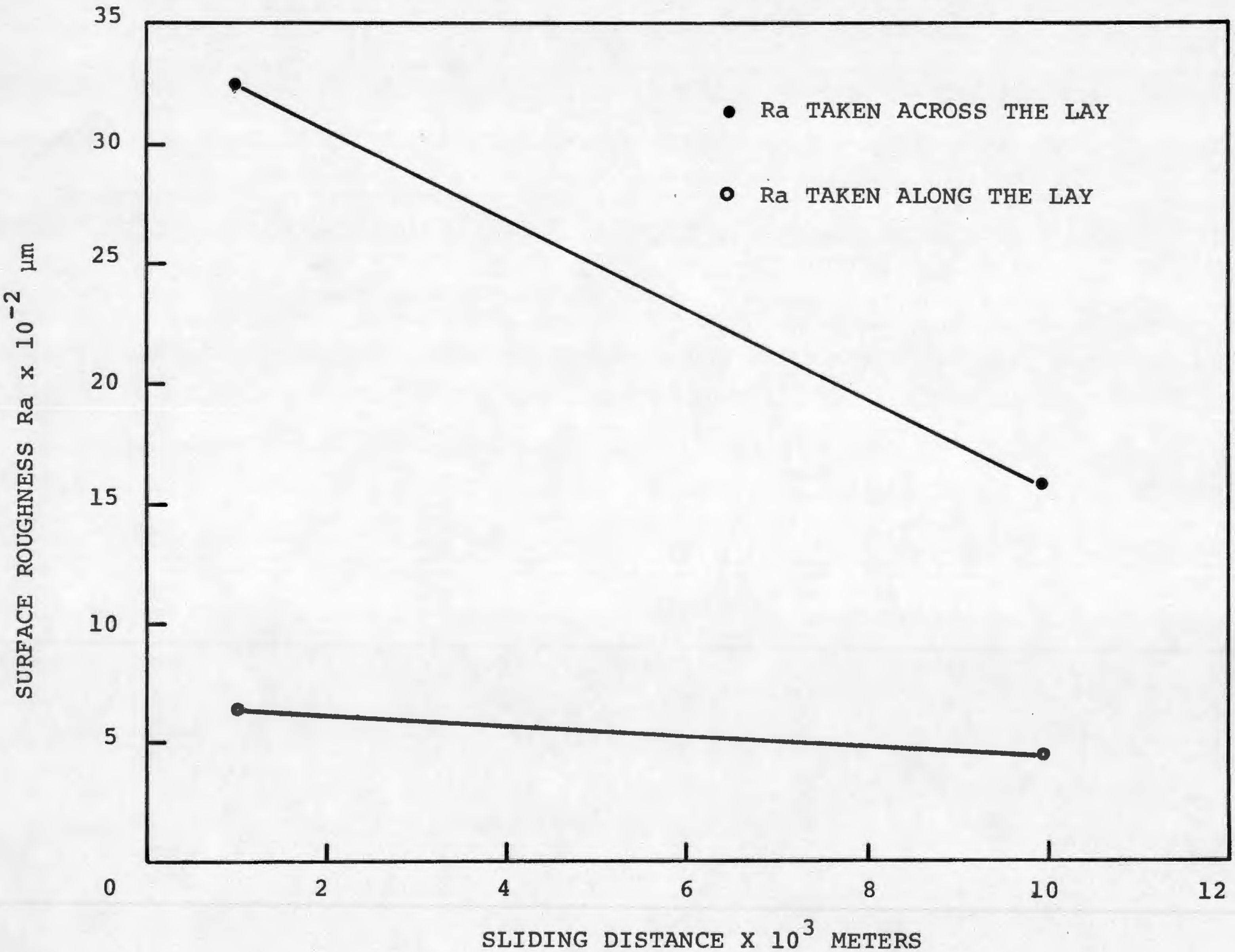

Figure 61. Variation of Surface Roughness with Sliding Distance for Stiffness K_3* (Arm length 12.7 cm) and at Normal Force (f_n) 14 Newtons

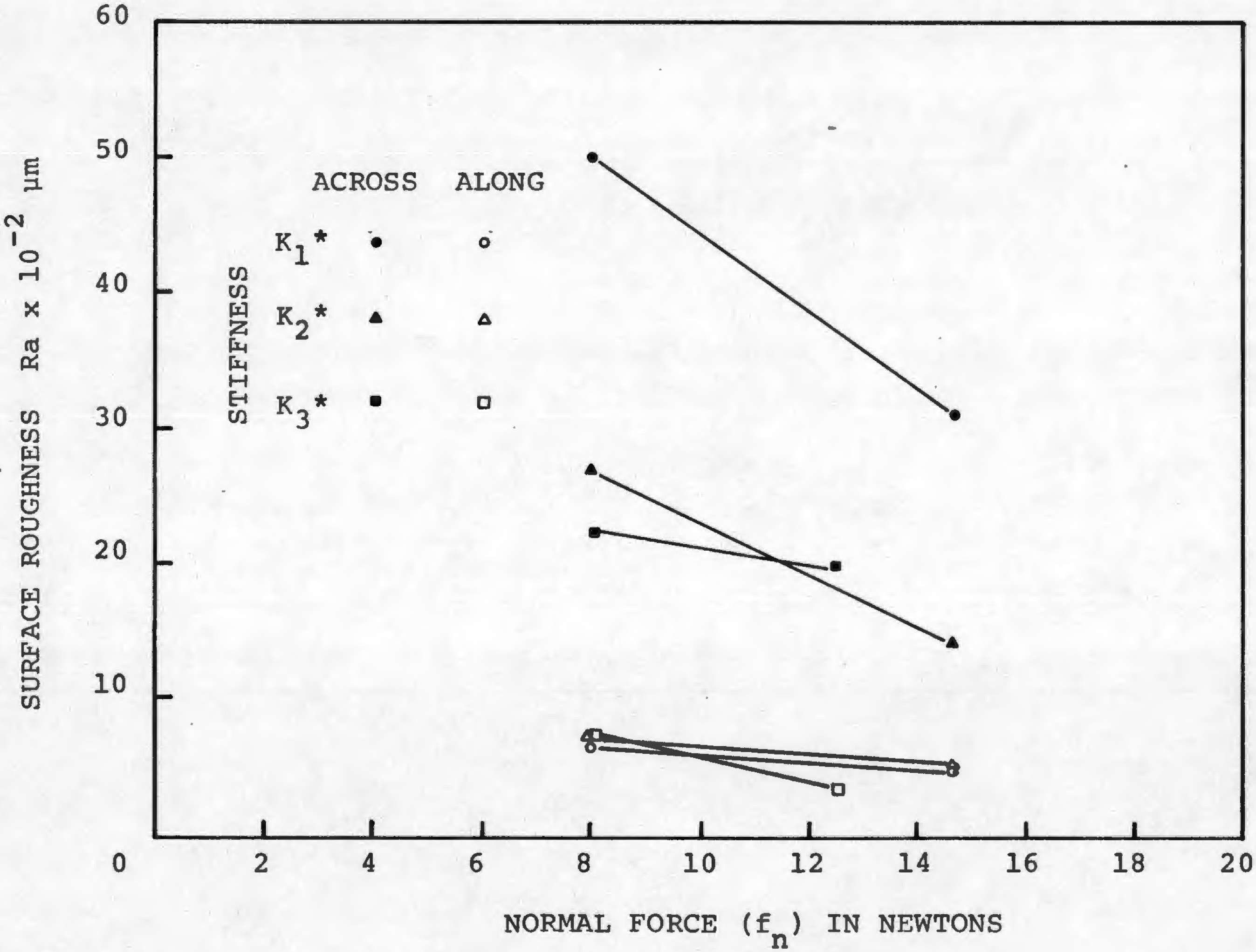

Figure 62. Variation of Surface Roughness Across and Along the Lay with Normal Force for Three Stiffnesses

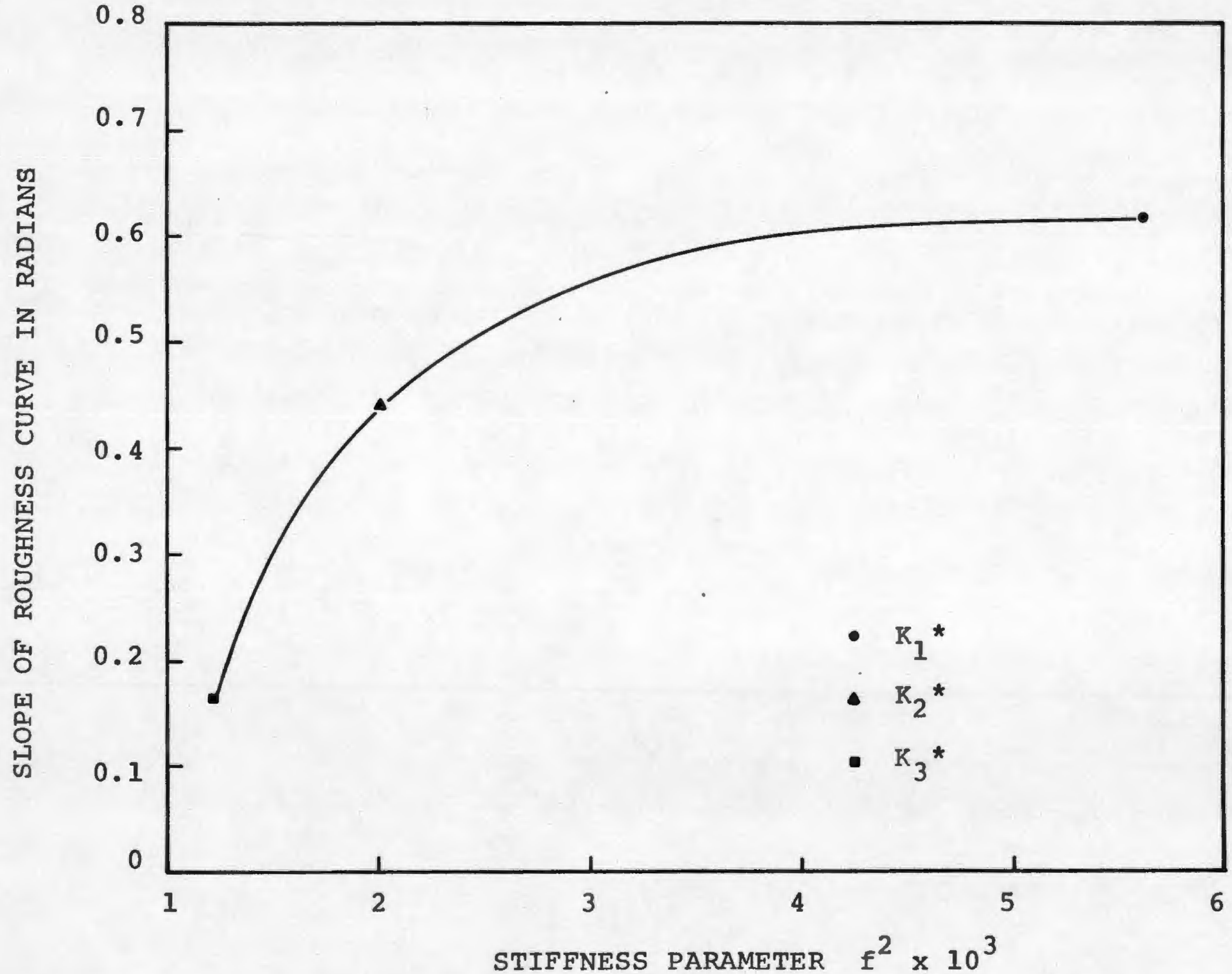

Figure 63. Slope of the Roughness Curve for Three Stiffnesses and at Constant Sliding Speed of 46 cm/sec.

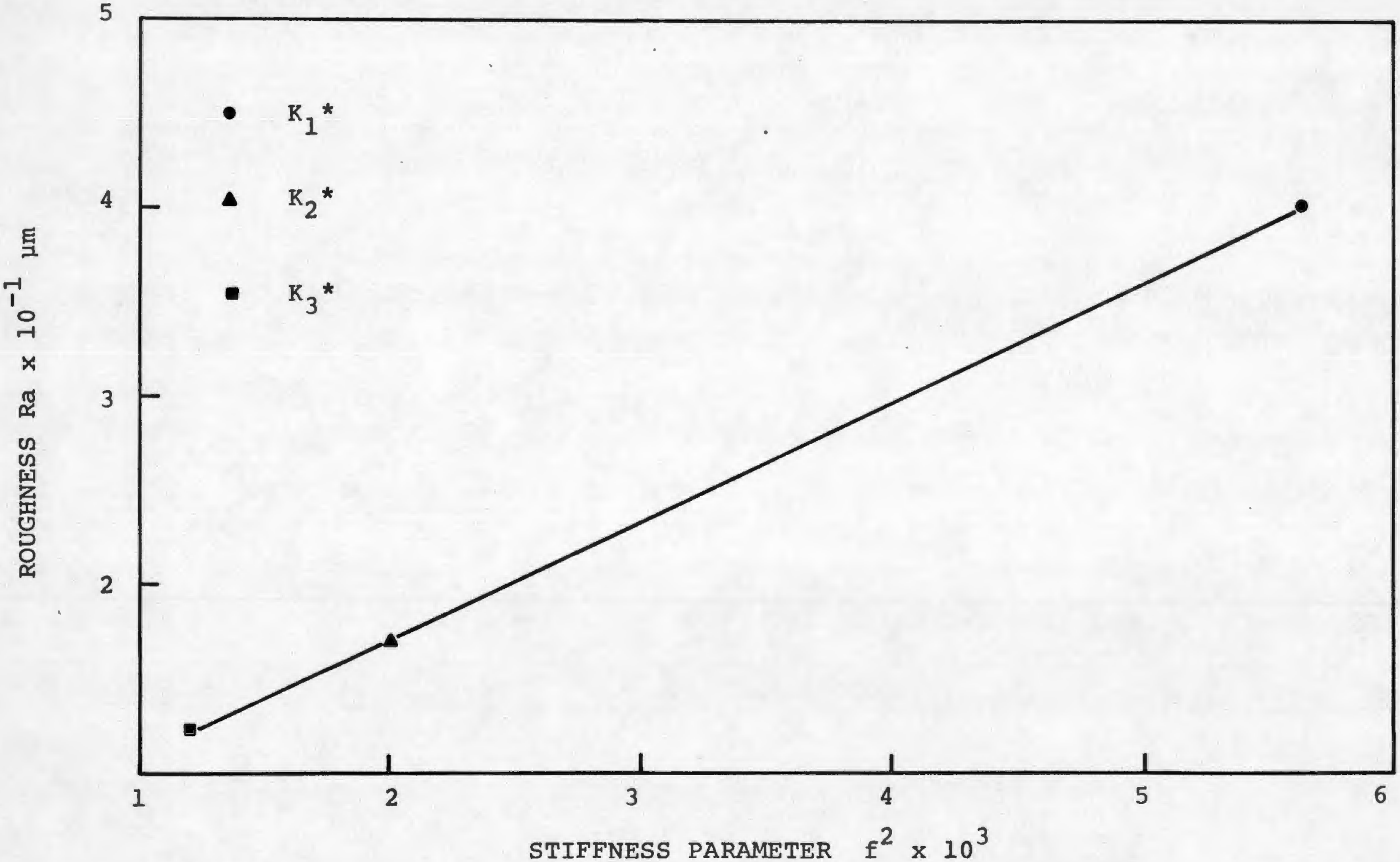

Figure 64. Surface Roughness (Across the Lay) Versus System Rigidity Measured at Constant Normal Load of 8 Newtons

Wear was also measured for different spring stiffnesses and at a constant normal load of 15 N and constant sliding speed of 46 cm/sec. The results obtained from these experiments are shown in Figure 65. This figure, once again, more firmly establishes an earlier finding that wear increases with system rigidity. It was suggested in section V.A.d.2. with water lubrication that wear rate tends to level off as rigidity increases beyond a certain limit. It appears from Figure 65 that the wear rate increases with rigidity and with further increase in rigidity the wear rate tends to become constant.

One more interesting correlation may be made between surface roughness, the frequencies of vibration and their amplitude of oscillation. It was stated earlier (Figures 50, 52 and 53) that the 180 Hz frequency changes with normal load f_n. Also Figure 57 shows the effect of normal load on surface roughness. Furthermore, Figure 15 indicates, at a particular normal load, the various frequencies occurring and their amplitude of oscillation (where spring length is 5.1 cm and sliding speed is 4.6 cm/sec.). Now if one plots the roughness versus amplitude of oscillation of various frequencies at a normal load of 8 and 15 N, we obtain Figure 66. It is interesting to note in this figure that the amplitude of oscillation of 4 different frequencies (1.25, 120, 180 and 260 Hz) in the frictional direction decrease in a very similar manner as the normal load increases and roughness simultaneously decreases.

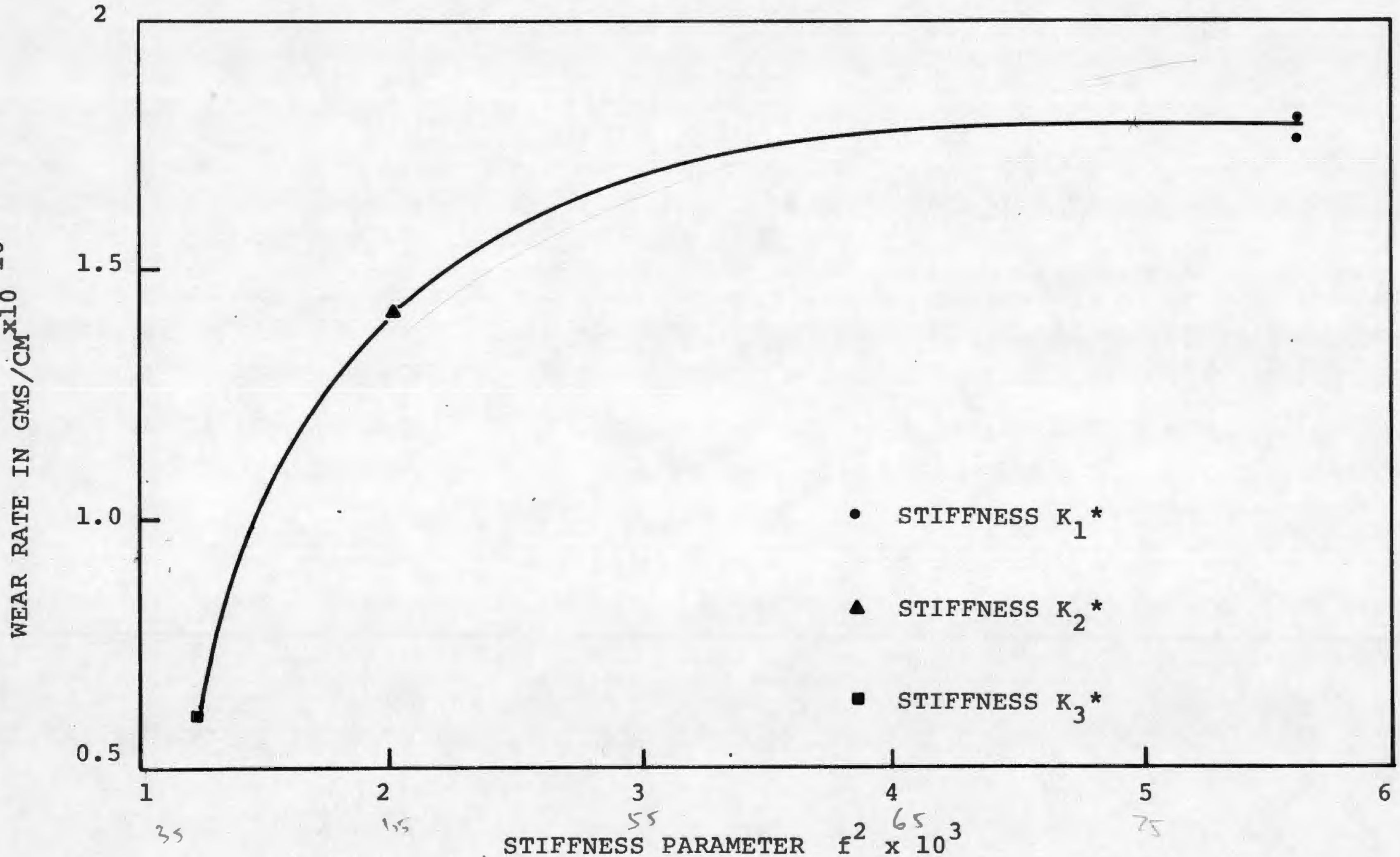

Figure 65. Wear Rate for Different Rigidities and at Constant Normal Load of 15 Newtons

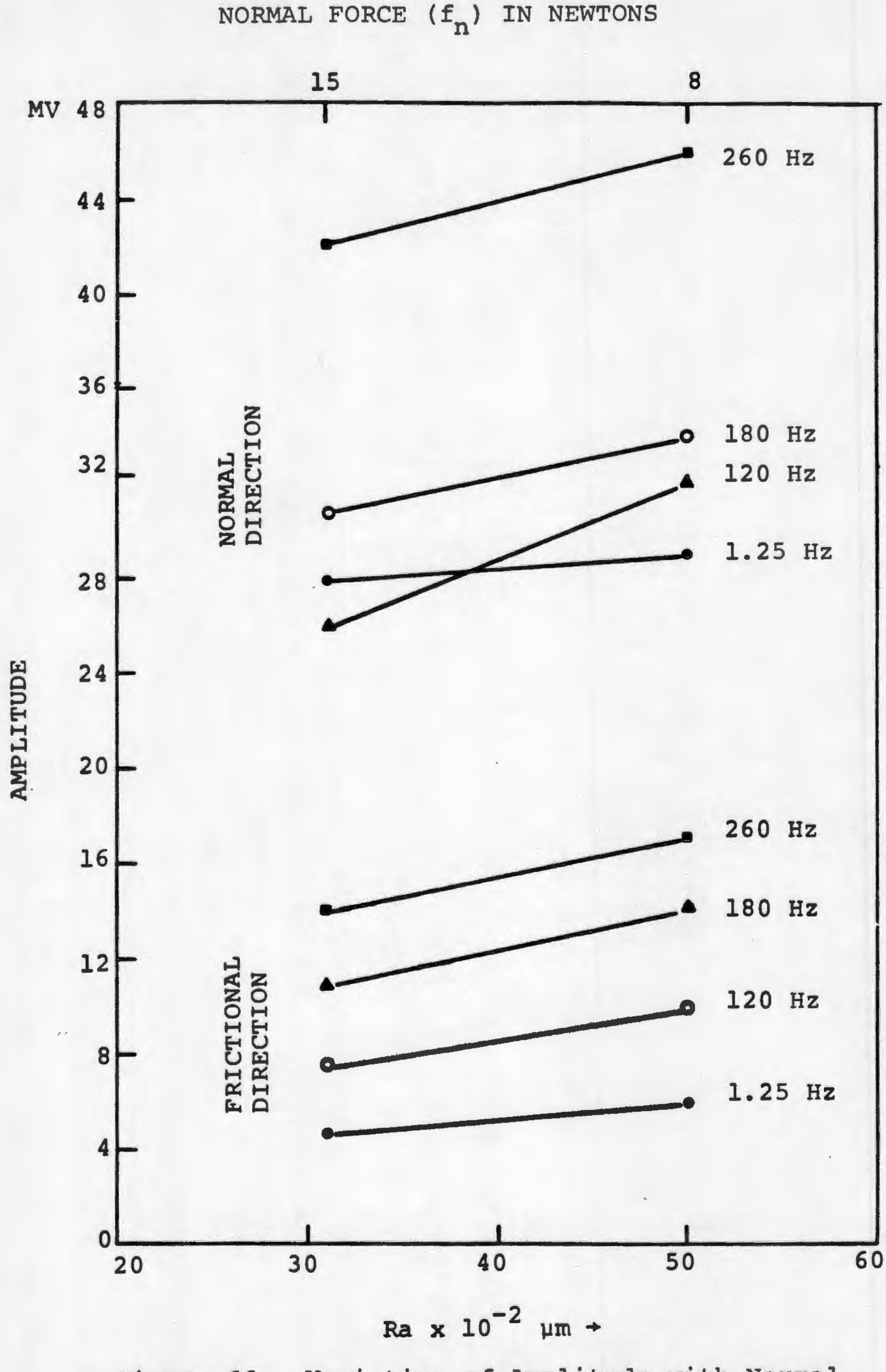

Figure 66. Variation of Amplitude with Normal Force (f_n) and Roughness for Different Frequencies

However, if one examines at the same time the behavior of the above frequencies in the normal direction it is found that all except 180 Hz frequency, have a similar decrease in their amplitude of oscillation as in the frictional direction. Unlike other frequencies, the 180 Hz frequency has a comparatively steep decline in its amplitude of oscillation. This shows that the 180 Hz frequency is sensitive to surface roughness.

C. ANALYSIS OF VIBRATIONS WITH DRY FRICTION

NATURAL FREQUENCIES OF THE SYSTEM

The natural frequencies and damping ratios of the arm in different directions were determined experimentally and the natural frequencies were also verified analytically. A (1/2" x 1/2") square steel bar was used for the arm. A (1/2" x 1/2" x 4-15/16") bar was welded to the arm as shown in Fig. 16ato form a T-section. A 2-1/2" x 2-1/2" x 5-1/16" steel block was bolted to the T-section. The pin was located at one end of the arm and the stiffness was altered by changing the arm length between the pin and the clamp. The vibration results discussed here are for the arm length of 12.7 cm (5 in.) corresponding to stiffness K_3*.

The coordinate system employed is shown in Fig. 67. The z-axis is in the normal direction and its positive direction is away from the disk. The x-axis is in the direction of the friction force on the pin and the y-axis is in the vertical direction. The positive directions of the normal force F_z and friction force F_x are also shown in Fig. 67.

The pin was hit impulsively in the normal and frictional directions, respectively, in order to determine the natural frequencies and damping in the z and x directions. The block was also hit impulsively off-center in order to determine the torsional natural frequency and damping about the vertical axis. The spectra of the impulse responses of the accelerometer in both the normal and frictional

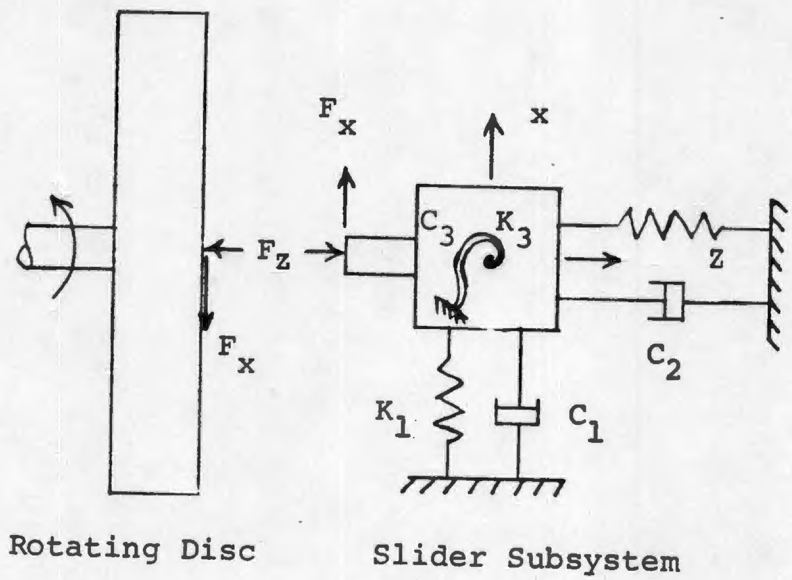

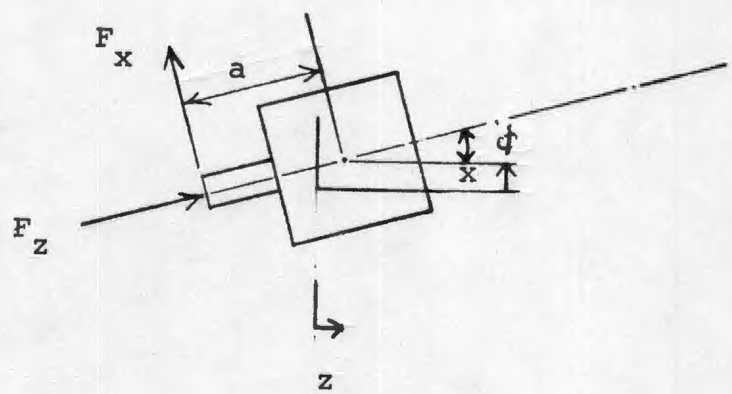

Figure 67. Mathematical Model of Slider System

directions were analyzed by the Fourier analyzer and were also observed on the storage oscilloscope. The fundamental natural frequencies in the normal and frictional directions were determined from the Fourier analyzer to be both equal to 35 Hz. The torsional natural frequency about the vertical axis was 85 Hz. These are the values of the natural frequencies for stiffness K_3^* when the pin is not in contact with the disk. It was observed as discussed later that when the pin was in contact with the rotating disk, only the natural frequency in the normal direction was changed and the natural frequencies in the frictional and torsional directions remained the same.

These experimentally observed natural frequencies, when the pin is not in contact with the disc, were verified analytically as follows. The natural frequencies in the x and z directions for a cantilever beam of length L and mass m loaded by a mass M at its tip are obtained as shown by Den Hartog [7] from the equation

$$\omega_n = \left[\frac{3EI}{L^3(M+0.236m)} \right]^{1/2}$$

where E is the Young's modulus and I is the moment of inertia of the square cross section. The weight of the block, T-section and accessories including the accelerometer, pin, pin holder, bolt and force transducer is 9.41 lbs., i.e., $M = 9.41/32.2 \times 12$ lbs. sec^2/in and the weight of the arm is 0.3525 lbs., i.e., $m = 0.3525/32.2 \times 12$ lbs. sec^2/in.

Letting $E = 29.5 \times 10^6$ psi, $I = \frac{1}{12}(0.5)^4$ and approximating the length of the cantilever beam shown in Fig.16b as 7 in., we obtain

$$\omega_n = 233.8 \text{ rad/sec}$$

i.e. $f_n = 37.2$ Hz

which checks with the experimental value of 35 Hz.

It has been shown by Timoshenko and Goodier [51] that the torsional stiffness of a rectangular bar is given by

$$k_s = \frac{\beta b c^3 G}{L}$$

where b is the long side and c the short side of the rectangular section, L the length, G the shear modulus and β is a parameter which depends on the ratio b/c. In our case $b = c = 0.5$ in. and $\beta = 0.141$. Letting $G = 12 \times 10^6$ psi and approximating the length of the cantilever beam of Fig.16b as 6.5 in., we obtain

$$k_s = 0.01627 \times 10^6 \text{ lbs. in.}$$

The natural frequency of a cantilever beam of mass moment of inertia I_b with a mass moment of inertia I at its tip is given by Den Hartog [7] as

$$\omega_n = \left[\frac{k_s}{I + \frac{1}{3} I_b}\right]^{1/2}$$

In our case, $I = \frac{8.92}{32.2\text{x}12} \times \frac{1}{12}(5^2 + 2.5^2)$ lb. in. sec^2

and $I_b = 0.0009619$ lbs. in. sec^2

Hence, we obtain

$$\omega_n = 519.62 \text{ rad/sec}$$

i.e. $f_n = 82.7$ Hz

as compared with the experimental value of 85 Hz. The slight discrepancies between the experimentally and calculated values of the natural frequencies are due to the fact that the analysis assumes that the mass M or mass moment of inertia I is located at the tip of the cantilever beam. However, as seen in Fig. 16b, the added mass contributes a length of 3 in. to the length of the arm which is 5 in. and hence the length of the equivalent beam has been approximated.

The damping ratios were obtained experimentally by displaying the impulse responses in the normal, frictional and torsional directions, respectively, in the time domain on a storage oscilloscope. Figures 68, 69 and 70 show these impulse responses in the x, z and torsional directions, respectively, for stiffness K_3*. The method of logarithmic decrement was employed to determine the damping ratios.

From Fig. 68, it is seen that in 7 cycles, the peak to peak amplitude decreased from 19 mm to 14 mm. Hence, the damping ratio in the x-direction is given by

$$[(7 \times 2\pi)^2 + (\log \frac{19}{14})^2]\ \zeta_1^2 = (\log \frac{19}{14})^2$$

i.e. $\zeta_1 = 0.0069$

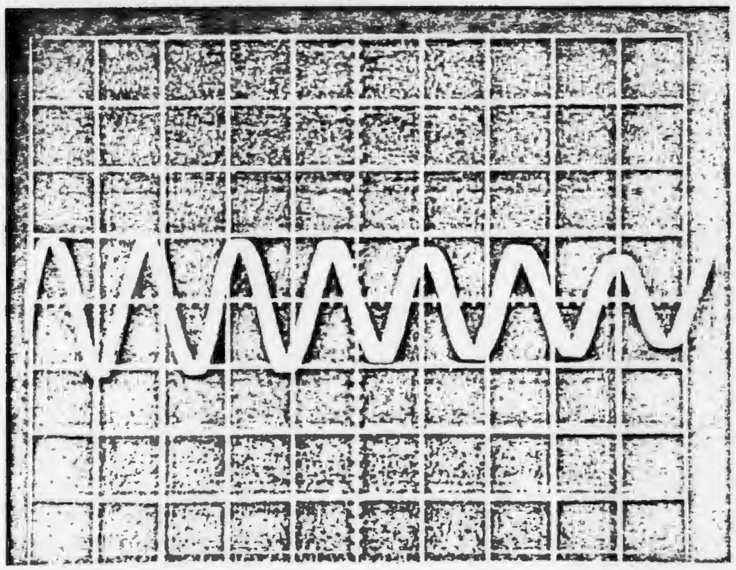

Figure 68. Impulse Response in the x-direction

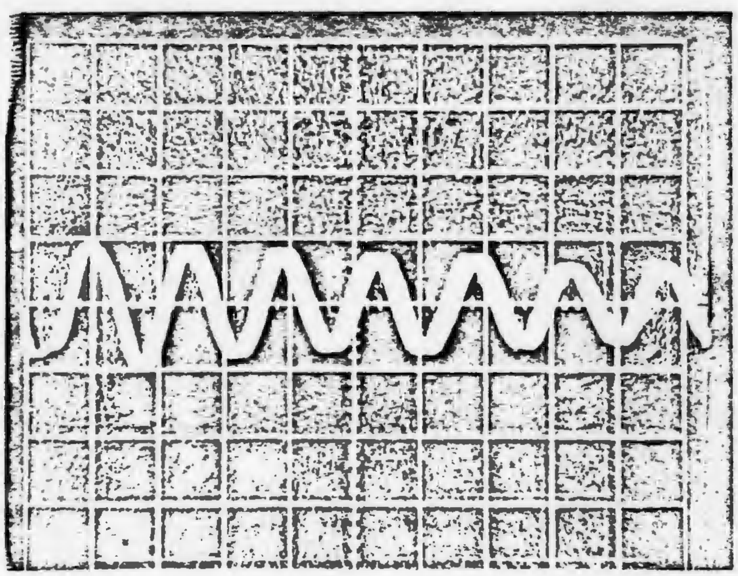

Figure 69. Impulse Response in the z-direction

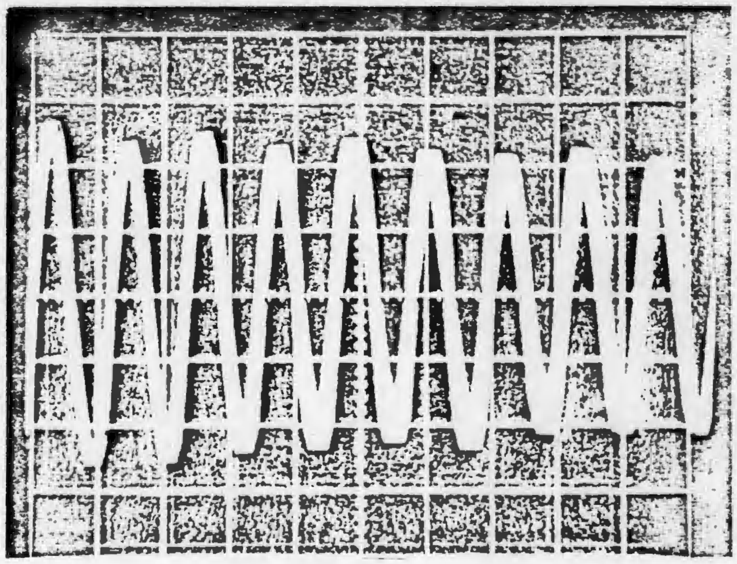

Figure 70. Impulse Response in the Torsional Direction

In Fig. 69, the peak to peak amplitude decreased from 17 mm to 11.5 mm in 7 cycles. Hence, the damping ratio in the z-direction is obtained from the equation

$$[(7 \times 2\pi)^2 + (\log \frac{17}{11.5})^2]\ \zeta_2^2 = (\log \frac{17}{11.5})^2$$

$$\text{i.e.}\quad \zeta_2 = 0.0089$$

In Fig. 70 which shows the impulse response in the torsional direction, the peak to peak amplitude decreases from 46 mm to 36 mm in 9 cycles. Hence,

$$[(9 \times 2\pi)^2 + (\log \frac{46}{36})^2\quad \zeta_2^2 = (\log \frac{46}{36})^2$$

$$\text{i.e.}\quad \zeta_3 = 0.0043$$

The natural frequencies were also determined from the experimental impulse response when the slider is in contact with the disk with a normal load of 90 N (20.3 lbs). It was observed that the natural frequencies in the frictional and torsional directions with contact remained unchanged from their values of 35 Hz and 85 Hz, respectively, without contact. In the normal direction, however, three natural frequencies of 30, 60 and 120 Hz were observed, their relative importance depending on the magnitude of the impulse. The experimentally obtained natural frequencies are shown in Table III.

Table III. Natural Frequencies for Stiffness K_3*

Direction	Pin Not in Contact with Disk Hz	Pin in Contact with Disk Hz
Frictional	35	35
Normal	35	30, 60, 120
Torsional	85	85

Vibrations with Pin in Contact with Rotating Disk

With the disk rotating at a certain nominal speed with the pin in contact with the disk, different regimes of operation were observed depending on the normal load and these are discussed here for the stiffness K_3*. As the normal load was increased from 4.45N (1 lb) to 71N (16 lbs), the mean value of the friction force increases with the normal load. In this region transient oscillations in the forces and velocities were observed. For a given normal load, both the amplitudes and frequencies of the vibrations would change with time.

It appears that these transient vibrations are caused by the interlocking and braking of random asperities in the contact zone. The frequency of vibrations then depends upon the mode excited by a disturbance. The various frequencies that appear are shown in Table IV. In this table, the frequencies of the velocities and forces for a given normal load are not equal because their spectrums were observed at different times. The effect of increasing the normal load was to increase the amplitude of the vibrations.

Between the normal loads of 71N (16 lbs) and 93N (21 lbs), large self-disturbances occurred and the mean value of the friction force would jump from its high value to a lower value. As time elapsed with the normal load held constant, the friction force would gradually climb to its higher value until another self-disturbance occurred. Beyond a normal load of 98N (22 lbs), self-excited vibrations appeared. These are periodic vibrations where the forces and velocities have the same constant frequency.

The steady state self-excited vibrations as recorded on the four channels of the visicorder are shown in Figure 28. In these experiments, the arm length was 5 in. (127 mm), the radius of the path of the pin on the disk was 180 mm and the disk was rotating at 35 rpm. This corresponds to a value of 0.105 m/s of the mean sliding speed. The normal load was 117.4N (26.4 lbs)

The frequency of these self-excited vibrations was observed on the Fourier analyzer and found to be 85Hz which is the torsional natural frequency of the system. Hence, it can be concluded that the self-excited oscillations are torsional vibrations. The visicorder paper was run at a speed such that the peak to peak distance in Figure 28 is 34 mm. The phase angles among the four oscillations were determined by measuring the distances between their respective peaks. The four channels of the visicorder were calibrated so that

TABLE IV. FREQUENCIES OF VIBRATIONS

Normal Load N	Frequency of V_x, Hz	Frequency of V_z, Hz	Frequency of F_x, Hz	Frequency of F_z, Hz	Remarks
4.4	30	90	120	120	Transient Vibrations
8.9	30	90	120	120	"
13.3	90	90	120	120	"
17.8	90	90	35	30	"
22.2	30	90	30	30	"
26.7	30	90	30	30	"
35.6	30	90	90	30	"
44.4	30	85	30	30	"
53.3	30	85	30	85	"
62.2	30	85	120	85	"
71.1	35	90	170	85	"
80.0	35	85	35	35	"
88.9	30	90	35	35	"
97.8	85	85	85	85	Almost periodic
117.4	85	85	85	85	Periodic

---

the forces could be read in Newtons and the velocities in m/s. Using these calibrations, we obtain the following expressions for the four oscillations

$$F_z = 34.54 \text{ Sin } \{2\pi\ (85)t\} \qquad \text{N}$$

$$F_x = 12.83 \text{ Sin } \{2\pi\ (85)t + \pi\} \qquad \text{N}$$

$$V_z = 0.011 \text{ Sin } \{2\pi\ (85)t + \frac{\pi}{2}\} \qquad \text{m/s}$$

and $$V_x = 0.027 \text{ Sin } \{2\pi\ (85)t - \frac{\pi}{2}\} \qquad \text{m/s}$$

The oscillations in the displacements can be obtained by integrating the velocities as

$$z = 20.5 \times 10^{-6} \sin \{2\pi (85)t\} \quad m$$

and $$x = 50.5 \times 10^{-6} \sin \{2\pi (85)t - \Pi\} \quad m$$

Since the mean value of the normal load was 117.4N, it is seen that the slider does not lose contact with the disk during the self-excited vibrations. Since the mean value of the sliding speed is 0.105 m/s, the relative speed between the disk and the pin does not change direction during the vibrations.

It is seen from Figure 28 that the waveforms of the velocities are quite sinusoidal but the waveforms of the forces are somewhat nonlinear and also there is a small high frequency component riding on the fundamental part. The frequency of the self-excited vibrations is 85Hz which is the natural frequency of the arm in the torsional direction.

ANALYSIS OF SELF-EXCITED VIBRATIONS

Several different types of friction-induced vibrations have been reported in the literature. It is apparent that there exist several distinct mechanisms that can excite different types of oscillations. As discussed in the technical background, these mechanisms could be generally grouped into the following three classes: 1) stick-slip, 2) mechanism of negative slope of friction-velocity curve, and 3) coupling among the different degrees of freedom.

It is clear from the waveforms of the oscillations shown in Figure 28 and the high value of the sliding speed that these self-excited vibrations do not belong to the stick-slip type. Several experiments were conducted in order to determine whether the friction force versus sliding speed curve has a negative slope. The disk was running at a given constant speed with a normal load below the value where self-excited vibrations occur. The speed of the disk was then increased and decreased from its nominal value but no significant change in the friction force with the sliding speed could be noted. Hence, the negative slope of the friction versus sliding speed curve as the cause of the instability can be ruled out. Hence, it appears that the coupling among the degrees of freedom is the cause of the instability.

Accordingly, the system is modeled as a coupled degrees of freedom system in order to simulate the essential experimental features. A mathematical model of the system is shown in Figure 67 . The pin subsystem is represented by three degrees of freedom, namely, translation in the x and z directions and torsional rotation about the vertical y axis. The disk is a large mass which is very rigidly supported. Hence, no degree of freedom is assigned to the disk except the rotation about its axis at a constant speed.

The slider subsystem is represented by a single body of mass m and moment of inertia I about a central axis y through its mass center. Let k_1, k_2, k_3 and c_1, c_2, c_3 be the stiffnesses and damping coefficients in the x, z and torsional directions, respectively. For small displacements, the structure behaves quite linearly and retaining only the fundamental frequencies of the coupled modes, the equations of motion may be represented as

$$m\ddot{x} + c_1\dot{x} + k_1 x = F_x \mathrm{Cos}\phi + F_z \mathrm{Sin}\phi$$

$$m\ddot{z} + c_2\dot{z} + k_2 z = -F\mathrm{Sin}\phi + F_z \mathrm{Cos}\phi$$

$$I\ddot{\phi} + c_3\dot{\phi} + k_3 \phi = -aF_x$$

where a is the moment arm of F_x as shown in Figure 15. The forces F_x and F_z can in general be nonlinear functions of the steady state sliding velocity V_s, the steady state normal force f_z, and of the displacements x, z, ϕ and their time derivatives. For small angle ϕ, Cos ϕ = 1 and Sin ϕ = 0. With this approximation, and after employing the natural frequencies and damping ratios, we obtain

$$\ddot{x} + 2\zeta_1\omega_{n1}\dot{x} + \omega_{n1}^2 x = \frac{1}{m}F_x$$

$$\ddot{z} + 2\zeta_2\omega_{n1}\dot{z} + \omega_{n1}^2 z = \frac{1}{m}F_z$$

$$\ddot{\phi} + 2\zeta_3\omega_{n3}\dot{\phi} + \omega_{n3}^2 \phi = \frac{a}{I}F_x$$

where we have earlier identified the parameters as $\omega_{n1} = \omega_{n2} = 2\pi(35)$ rad/s, $\omega_{n3} = 2\pi(85)$ rad/s, $\zeta_1 = 0.0069$, $\zeta_2 = 0.0089$, $\zeta_3 = 0.0043$, $m = 4.43$ kg and $I = 0.0069$ Kg.m^2.

An assumed relationship for F_x that can explain the observed self-excited vibrations is given by

$$F_x = -a_1\dot{\phi} + a_2\dot{\phi}^3 \qquad a_1 > 0, a_2 > 0$$

Letting $b_1 = a_1 a/I$ and $b_2 = a_2 a/I$ and substituting this relation for F_x in the third equation, we obtain

$$\ddot{\phi} + (2\zeta_3\omega_{n3} - b_1 + b_2\dot{\phi}^2)\,\dot{\phi} + \omega_{n3}^2\phi = 0$$

In this equation, if we assume that $\dot{\phi}$ is small so that the $\dot{\phi}^2$ term can be neglected, then it seems that the linearized equation is stable when $2\zeta_3\omega_{n3} > b_1$ and unstable when $2\zeta_3\omega_{n3} < b_1$. When the linearized equation is unstable, the $\dot{\phi}^2$ term limits the growth of the amplitude of ϕ. The nonlinear equation can be analyzed for limit cycles by the method of describing function [52, 53].

Assuming the existence of self-excited vibrations, the waveform of ϕ will be periodic. With the assumption that the harmonic components are filtered out by the structural dynamics, the filtered waveform can be represented by

ϕ = aSinωt where a is the amplitude and ω is the frequency of limit cycles. Then $\dot{\phi}$ = aωCosωt and we obtain

$$\dot{\phi}^3 = a^3\omega^3 Cos^3\omega t$$
$$= \frac{a^3\omega^3}{4}\ (3Cos\,\omega t + Cos^3\omega t)$$

Now in the frequency domain, d/dt = jω and Cosωt = jSinωt. Substituting these relations in the nonliear differential equation for ϕ and retaining only the fundamental frequency terms, we obtain

$$\left[-\omega^2 + j\omega(2\zeta_3\omega_{n3} - b_1 + 3/4a^2\omega^2) + \omega_{n3}^2\right] aSin\omega t = 0$$

Equating the real and imaginary parts to zero separately in the foregoing equation, we obtain

$$\omega^2 - \omega_{n3}^2 = 0$$

and $2\zeta_3\omega_{n3} - b_1 = 3/4a^2\omega^2 = 0$

Solving for the limit cycle frequency ω and amplitude a, we get

$$\omega = \omega_{n3}$$

and $a = \left[\frac{4}{3}\,\omega_{n3}^2 (b_1 - 2\zeta_3\omega_{n3})\right]^{1/2}$

Hence, the limit cycle frequency is the natural frequency of the slider system in the torsional direction and from the equation of the amplitude, self-excited vibrations occur when $b_1 > 2\zeta_3\omega_{n3}$, which is the condition for instability of the linearized system. It should be noted that the assumed relation for F_x as a function of $\dot{\phi}$ explains the experimentally observed behavior of the self-excited oscillations but it is only an hypothesis and requires further experimental verification. The functional relationship of the forces is currently being investigated. However, it appears that the cause of the instability is the torsional degree of freedom. Considering the work done by the forces in the normal and frictional directions, we obtain

$$W_z = \int_0^{\frac{2\pi}{\omega}} F_z v_z dt$$

and $$W_x = \int_0^{\frac{2\pi}{\omega}} F_x v_x dt$$

On substituting the expressions for the forces and velocities in the foregoing equations, we find that $W_z = W_x = 0$. This implies that the energy supplied to maintain the vibrations is through the torsional mode. This energy is then dissipated per cycle by the damping in all the three modes of vibrations. This topic requires further study.

VI. DISCUSSION

A. Discussion for Water Lubrication Experiments

From the analysis of the experimental data, an attempt is now made to develop a physical model of the friction processes of boundary lubrication with water. Steady state friction depends upon the ability of the lubricant and oxide films to separate metallic surfaces from direct contact. This ability is characterized by the kinetics of formation and breakdown of lubricant film between the contacting surfaces. Each of these kinetics is a function of the sliding speed and normal load. With increase in normal load, the dynamic equilibrium of the formation and breakdown of the film is shifted towards an increasing rate of breakdown. Therefore, the probability of metallic surfaces coming in direct contact with each other increases with the normal load.

At a certain value of the critical normal load (in these experiments, 18 to 27 N) direct contact between metallic surfaces becomes inevitable and finally direct contact does occur at certain spots. At this stage, transition takes place from steady state to unsteady state friction process. Apparently, this transition is independent, or at most weakly dependent, on the system rigidity. Observation of the SEM photos indicate that it is very probable that the deep pits are caused by the formation of metallic junctions, and the scratches are caused by their subsequent shearing. It has been observed earlier that the frequency of occurrence of disturbances was high soon after a change in the normal load and that it would decrease as the elapsed time from a change in the normal load increased. It is understandable that the probability for the formation of junctions would be high after a change in the normal load and would decrease with an increase in the elapsed time.

Using this hypothesis that a self disturbance is caused by the formation of a metallic junction between the surfaces, the sudden rise in the friction force as seen in Figure 22 can be attributed to this junction formation. The junction is soon sheared off and the friction force drops back to its nominal value.

The frequency of the low frequency oscillations that appear as soon as the friction force begins its rise in Figure 22 is seen to be close to the natural frequency of the pin and arm system with the pin not in contact with the disc. It appears that these low frequency oscillations are excited by the unsteadiness of the friction force. When the friction force increases to its high value in Figure 22, it is now in the range where high frequency self-excited oscillations exist. Hence, these high frequency oscillations soon appear. As the friction force decreases back to its nominal value, the high frequency oscillations cannot be maintained and immediately decay to zero. As the system is very lightly damped, the low frequency oscillations persist for a much longer time as they decay.

In the region of self-excited high frequency oscillations, there is a coupling between the degrees of freedom in the normal and frictional directions as seen in Figures 22 and 25, where the two force components and the two velocity components oscillate at the same frequency of 889 Hz. Here the conjecture is that the high frequency oscillations are caused by the coupling between the normal and frictional degrees of freedom and the difference in the phase angles of the oscillations.

Some energy is drawn from the steady state process and is supplied to the vibratory motion. The energy supplied is balanced by the energy dissipated per cycle by damping. This energy transforms mostly into heat, thereby shifting the dynamic equilibrium of formation and breakdown kinetics to an increased rate of formation of lubricant film (in the present case, most probably the formation of oxides). This then would explain the near absence of self disturbances when the operation is in the region of high frequency self excited vibrations.

The increase of wear rate with an increase in rigidity can be explained as follows: because of mechanical interactions between contacting surfaces, an increase in rigidity in the normal direction causes an increase in shear force; this, in turn, is responsible for higher wear rate.

It was felt that the sequence of the regimes, or even mechanisms of the friction-induced vibration, can be changed by changing lubrication conditions in the interface. This possibility may be very important as this change may cause a transition from mild to severe wear to be dependent on the system rigidity. With this aim a special oil-lubricated check-test experiment was conducted. Although further careful studies should be carried on, the results of this preliminary experiment showed that the sequence of the regimes of the friction-induced vibration did indeed change, and most probably will affect the transition from mild to severe wear.

Summary of the Current State of Knowledge

It has been recognized that the behavior of a frictional system depends on several conditions such as lubrication, normal load, sliding speed, contact temperature, system rigidity, and damping characteristics. These conditions can give rise to different types of friction regimes characterized by the absence or presence of various types of self-excited vibrations. There exist several different mechanisms by which friction can induce vibrations, and their classification and terminology are not well established in the literature. As expected, wear is closely related to friction to friction, as well as friction-induced vibration.

Several observations can be made on the basis of the foregoing discussions as follows:

i) When a frictional contact is an element of a mechanical system, self-excited vibrations may be induced by different friction mechanisms, namely:

   a) Stick-slip.

   b) Negative slope where the friction force is a decreasing function of the sliding velocity.

   c) Positive slope where the friction force is an increasing function of the sliding velocity.

This mechanisms may be due to the coupling between the degrees of freedom in the tangential and normal directions.

d) Intermittent self-disturbances.

e) Random fluctuations in the friction force due to the mechanical and physical heterogeniety of the contact surfaces.

ii) When self-excited vibrations are induced, the amplitude and frequency of vibrations depend on the nature and characteristics of the friction force and on the dynamic characteristics of both the structure and the frictional contact.

iii) Any type of vibration causes a change in the magnitude and distribution of stresses and temperature on the real contact areas and, thus, affects the rate of wear as well as the friction force.

iv) The dynamic characteristics of the frictional contact can vary depending on the temperature of the contact area and/or the mechanism of wear (which, in turn, depends on the characteristics of the system vibrations) causing a sharp transition from mild to severe wear and vice versa.

Among the main conclusions of our current study are the following: 1) There exist a few frictional regimes where the mechanisms of friction-induced vibrations are different; 2) The rate of wear in the regime of steady state friction is an increasing function of the system rigidity. In our experiments water was used for lubrication. The main reason for the use of water as a boundary lubricant was that it permits the continuation of the experiment in the region of severe wear without complete destruction of the contact surfaces as would occur in dry contact.

In water lubricated sliding contact, the following three different friction regimes were obtained:

a) Region of steady state friction with small irregular fluctuations in the normal and friction forces.

b) Region of self-disturbances caused by breakdown of the lubricant film, formation of metallic bonds between the surfaces in contact and subsequent shearing of these bonds. The friction force decreases back to its original value after the bond is sheared. This unsteadiness in the friction force produces decaying low frequency oscillations whose frequency is equal to the natural frequency of the slider. Also, when the friction force reaches its high value, additional high frequency oscillations are produced and these quickly disappear soon after the friction force decreases back to its original value.

c) Region of self-excited vibrations, characterized by periodic, high-frequency slider oscillations in both tangential and normal directions.

The wear rate, which is an increasing function of the system rigidity in the region of stable, steady-state friction, increases very sharply in the region of self-disturbances. This transition from low (mild) to high (severe) rate of wear is not a function of the system rigidity.

B. Discussion of Dry Friction Experiments

From the previous section on results, it is interesting to note and discuss the following.

It is clear from friction force (f_x) versus normal load (f_n) diagrams, Figures 29 and 31, that for the case of steady state sliding in the dry condition, the friction force f_x is proportional to the normal load f_n. Although it is a well established fact, it needs to be mentioned that due to the low frequency response of the strip chart recorder, the forces measured are average values.

From the dynamic analysis of the foregoing results it is very clear that at any instant of time the true friction force and normal force are not f_x and f_z, respectively. In fact, the actual friction force and normal force keep changing at all times of the friction process. The rate with which the forces change depends on the entire system rigidity of the test setup. Thus, as expected, the rate of change of forces, i.e., the frequency of this change, turns out to be a complex sum of various frequencies. These different frequencies and their amplitude of oscillation were found out in these experiments (Figures 44, 45, 46 and 47).

During the steady state friction process as the normal load f_n increases, the dynamic components of friction force (F_x) and normal force (F_z) and the corresponding velocities V_x and V_z decrease in their amplitude of oscillation. This decrease in the amplitude of oscillation becomes more significant before transition. If the scale of coefficient of friction μ_R ($\mu_R = f_x/f_n$) in Figures 29 and 31 is magnified considerably (not shown) then it is clearly seen that μ_R also falls significantly before transition takes place.

Furthermore, it is to be noted that just before transition, while the dynamic components F_x and F_z fall, the velocity of slider oscillation in both frictional and normal directions increases.

The dynamic component of the normal force (F_z) decreases as the normal load f_n increases in the steady state process, whereas, after transition F_z increases rapidly with an increase in the normal load f_n. On the other hand, friction force f_x and its dynamic component F_x decrease in the steady state region and, after transition, f_x behaves very randomly; at times, f_x increases sharply and at other times, it falls considerably, but the net effect of these fluctuations is towards an increase in f_x. During the same period, i.e., after transition, its dynamic component F_x increases but seldomly decreases. This continues up to the start of self excited vibration during which the friction force falls very sharply and, in a matter of few minutes, the f_x value falls to almost zero level. Whereas, at the same time, the dynamic component F_x increases by an order of magnitude. In fact, the magnitude of F_x during self excited vibrations is the highest and is much larger than at any other state of the entire friction process.

From foregoing results we have already seen that during steady state friction as the normal load increases, the surface roughness decreases; while after transition surface roughness increases. As surface roughness decreases before and increases after transition, the dynamic force components F_x and F_z also decrease before and increase after transition. Thus, there appears to be a direct correlation between the dynamic components of forces and the surface roughness.

In the steady state region, the decrease in surface roughness and dynamic force components with increasing normal load may be attributed to the increase in contact stiffness.

Furthermore, there appears to be one or more frequencies such as 180 Hz in Figure 50 which are very sensitive to surface roughness and also to transition. It is interesting to note that this particular frequency totally vanishes after the transition. This implies that there are one or more frequencies (depending on frictional setup) which are sensitive to transition and may even be the cause of transition. Although it is difficult to come to a conclusion from these results, it proves to be a very useful piece of information for future work.

So far the discussion pertained to the various frequencies and their amplitudes of a sliding system with a constant stiffness K_1*. The effect of different rigidities on the various parameters discussed above will now be outlined.

The normal load at which transition occurs for three different spring stiffnesses K_1*, K_2*, K_3* is compared in Figure 71 . It is clear from this figure that the magnitude of normal load at which transition occurs is proportional to the system rigidity.

For the same above mentioned three spring stiffnesses the magnitude of wear, at a constant normal load, is also found to be an increasing function of the system rigidity, as seen in Figure 65.

This means that for a particular range of mild wear it is possible to optimize the load carrying capacity of the frictional joint with respect to its rigidity.

The relationship of surface roughness to stiffness of the system, as seen from Figure 64, is also a linear function. This shows that the surface roughness is a function of system rigidity. Furthermore, the rate of decrease in roughness with normal load is also proportional to the

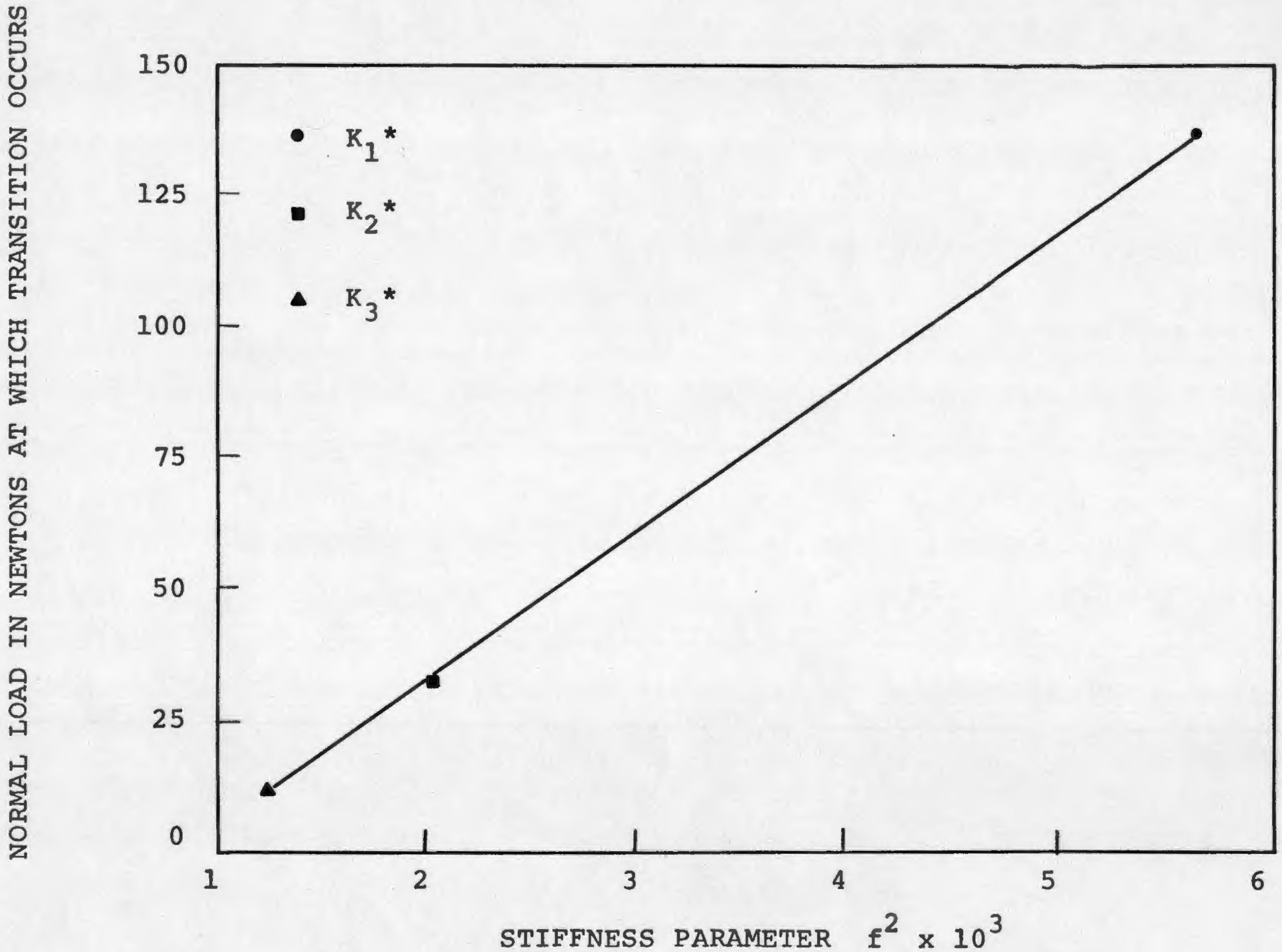

Figure 71. Plot of the Critical Load at Which Transition in Friction Process Occurs vs. the Stiffness Parameter for Three Stiffnesses K_1^*, K_2^* and K_3^*

system stiffness, i.e., under the same normal load the rate of decrease in roughness increases with increasing system rigidity, as seen in Figure 62.

VII. CONCLUSIONS AND RECOMMENDATIONS FOR FUTURE WORK

This report presents the results of an investigation undertaken to study the interaction between friction, wear and system rigidity. An experimental set-up has been built for this purpose and two different interfaces, namely, boundary lubrication with water and dry friction, have been studied for several system rigidities. Different friction, wear and vibration regimes are encountered, depending upon the lubricating conditions, normal load and system rigidity. The following conclusions can be drawn from this study:

1. There are three main regimes of friction affected by system rigidity; a) "steady state" friction process characterized by the smallest rate of wear (mild wear), smallest amplitudes of friction force and slider oscillation, absence of surface damage and smallest surface roughness; b) "self-disturbances" regime characterized by surface damage and unstable vibration of friction force and slider. The rate of wear is excessive in this regime; c) self-excited vibration characterized by friction force, normal force and slider oscillation with natural frequency of system vibration and highest amplitude.
2. The transition from mild to excessive wear is independent of system rigidity for lubricated friction and is an increasing function of the system stiffness for unlubricated regimes.

3. In the "steady state" friction regime the rate of wear is an increasing function of system rigidity, for both lubricated and dry friction.
4. The amplitudes of friction and normal force oscillations depend on surface roughness that is decreasing function of the normal load in the "steady state" friction. There is always one frequency of friction force oscillation which is most sensitive to roughness.
5. There is a critical value of the normal load at which transition from self-disturbance to the self-excited vibration takes place. This critical load is a function of system rigidity.
6. The frequency of the self-excited vibrations is the natural frequency of the slider in the torsional direction. The self-excited vibrations exhibit coupling among the normal, frictional and torsional degrees of freedom but, from the consideration of energy supply and dissipation, it appears that the cause of instability is the torsional degree of freedom.

On the basis of the above conclusions, the following is recommended for the future study:

1. Development of the physical and mathematical models of the slider oscillation in the steady state friction regime. These models should include roughness formation on the surface and wear as they depend on system stiffness.

2. Development of the physical and mathematical model of the transition from mild to severe wear and its dependence on the system rigidity.

3. Development of a stability theory to explain the onset of friction-induced self-excited vibrations and the cause of instability. To determine a functional relationship of the friction force with the other variables including sliding speed, stiffness, normal load and displacements.

4. Combine above analyses to establish guidelines for optimum design of frictional interfaces and joints.

REFERENCES

1. Hardy, W.B. and Hardy, J.K., "Note on Static Friction and on the Lubricating Properties of Certain Chemical Substances", Phil. Mag., Series 6, Vol. 38, No. 223, July 1919, pp. 32-49.

2. Tomlinson, G.A., "A Molecular Theory of Friction", Phil. Mag., Series 7, Vol. 7, June 1929, pp. 905-939.

3. Rabinowicz, E., "A Study of the Stick-Slip Process", Proceedings of the Symposium on Friction and Wear, Detroit, 1957, pp. 149.

4. Ko, P.L. and Brockley, C.A., "The Measurement of Friction and Friction-Induced Vibration", Journal of Lubrication Technology, Trans. ASME, October 1970, pp. 543-549.

5. Brockley, C.A., Cameron, R. and Potter, A.F., "Friction-Induced Vibration", Journal of Lubrication Technology, Trans. ASME, April 1967, pp. 101-108.

6. Brockley, C.A. and Davis, H.R., "The Time-Dependence of Static Friction", Journal of Lubrication Technology, Trans. ASME, January 1968, pp. 35-41.

7. Den Hartog, J.P., "Mechanical Vibrations", McGraw-Hill Book Company, New York, New York, 1940, Chapter VII.

8. Brockley, C.A. and Ko, P.L., "Quasi-Harmonic Friction-Induced Vibration," Journal of Lubrication Technology, Trans. ASME, October 1970, pp. 550-556.

9. Fuller, D.D., "Theory and Practice of Lubrication for Engineers," J. Wiley and Sons, Inc., 1956, p. 133.

10. Kummer, H.W. and Meyer, W.E., "Measurement of Skid Resistance," Symposium on Skid Resistance, ASTM Special Technical Publication, No. 326, 1962, pp. 3-28.

11. Tolstoi, D.M., "Significance of the Normal Degree of Freedom and Natural Normal Vibrations in Contact Friction," Wear, Vol. 10, 1967, pp. 94-102.

12. Yokoi, M. and Nakai, M., "A Fundamental Study on Frictional Noise," Bulletin of the J.S.M.E., Vol. 22, No. 173, 1979, pp. 1665-1671.

13. Bhushan, B., "Stick-Slip Induced Noise Generation in Water-Lubricated Compliant Rubber Bearings," Journal of Lubrication Technology, Vol. 102, April 1980, pp. 201-212.

14. Krauter, A.I., "Generation of Squeal/Chatter in Water-Lubricated Elastometric Bearings", Journal of Lubrication Technology, Trans. ASME (in press).

15. Bowden, F.P. and Tabor, D., "The Friction and Lubrication of Solids," Part II, Oxford, Clarendon Press, 1964.

16. Welsh, N.C., "The Dry Wear of Steels," Phil Trans. Roy. Soc. 1965 257, pp. 31-70.

17. Kostetskii, B., "Friction, Lubrication and Wear in Machines," Tekhnica, Kiev, 1970.

18. Rabinowicz, E., "Friction and Wear of Materials," J. Wiley, 1965, pp. 94-102.

19. Quinn, R.F.J., "The Application of Modern Physical Techniques to Tribology," Butterworths, London, 1971.

20. Aronov, V., "Formation and Destruction Kinetics of Transformed Structures of Metals in Frictional Contact," Wear, 38, 1976, pp. 305-310.

21. Aronov, V., "Kinetic Characteristics of the Transformation and Failure of the Surface Layers of Metals Under Dry Friction," Wear 41, 1977, pp. 205-212.

22. Rabinowicz, E., "Lubrication of Metal Surfaces by Oxide Films." ASME Transactions, 10, 1967, pp. 400-407.

23. Buckley, D.H. and Johnson, R.L., "Effect of Inert, Reducing and Oxidising Atmospheres on Friction and Wear of Metals to 1000F", NASA Tech. Note, D1103, 1961.

24. Hirst, W. and Lancaster, S.K., "The Influence of Oxide and Lubricant Films on the Friction and Surface Damage of Metals," Proc. Roy. Soc. London, Ser. A223 pp. 324-338, 1954.

25. Molgaard, J., "A Discussion of Oxidation, Oxide Thickness and Oxide Transfer in Wear," Wear 70, 1976, pp. 277-291.

26. Zaporogetz, V., "Friction and Wear Investigations by Spectrum Analysis," Friction, Lubrication and Wear of Machine Elements, V. 5, 1969.

27. Zaporogetz, V., "Friction Force Oscillation," UCXA, V. 51, 1970.

28. Aronov, V., "Investigation of Mild Wear," Ph.D. Thesis, Kiev, 1970.

29. Aronov, V. and Yahalom, J., "Studies on the Behavior of Copper During Friction under Electrolyte Immersion Conditions," Wear, 97, 1978, pp. 293-299.

30. Aronov, V., unpublished results.

31. "Friction and Wear Devices," 2nd ed., Am. Soc. of Lubrication Engineers, 1976.

32. Swinnerston, B.R.G., and Turner, M.J.B., "Blistering of Graphite Films in Sliding Contacts", Wear, Volume 9, 1966, pp. 142-159.

33. Hirst, W., in Proceedings Conference on Lubrication and Wear, Institution of Mechanical Engineers, London, 1957, pp. 675.

34. Lancaster, J.K., "The Influence of the Conditions of Sliding on the Wear of Electromagnetic Brushes", British Journal of Applied Physics, Vol. 13, No. 9, Sept. 1962, pp. 468-477.

35. Rabinowicz, E., "Friction - Especially Low Friction," Proceedings of the International Conference on the Fundamentals of Tribology, MIT, June 1978, pp. 351-363.

36. Rabinowicz, E., "The Determination of the Compatibility of Metals Through Static Friction Tests," Trans. of American Society of Lubrication Engineers, Vol. 14, Number 3, July 1971, pp. 198-205.

37. Kimura, Y., "Some Problems in the Adhesion Theory of Friction," Proc. of the Intl. Conf. on the Fundamentals of Trib., MIT, June 1978, pp. 385-389.

38. Gwathmey, A.T., et al., "Friction and Cohesion Between Single Crystals of Copper," Proceedings of Royal Society of London, Series A., Vol. 212, May 1952, pp. 464-467.

39. Takagi, R., and Tsyua, Y., Japan Society of Lubrication Engineers, Journal, Vol. 6, 1961, p. 81.

40. Kimura, Y., Japan Society of Lubrication Engineers, Journal, Vol. 9, 1964, p. 475.

41. Mochlin, E.S. and Yankee, W.R., "Friction of Clean Metals and Oxides with Special Reference to Titanium," Journal of Applied Physics, Vol. 25, Jan.-Dec. 1954, pp. 576-581.

42. Rabinowicz, E., "Theoretical Criteria for the Effectiveness of a Lubricant Film," Lubrication Science and Technology, ASLE Transactions, Vol. 1, Number 1, 1958, pp. 96-100.

43. Aronov, V., D'Souza, A.F., Kalpakjian, S., and Shareef, I., "Experimental Investigations of the Effect of System Rigidity on Wear and Friction-Induced Vibrations," to be published in Trans. ASME, Journal of Lubrication Technology.

44. Earles and Lee, C.K. "Instabilities Arising from the Frictional Interaction of a Pin-Disk System Resulting in Noise Generation," Trans. ASME, Jr. Eng. Ind., Vol. 98, 1976, pp. 81-86.

45. Yamada, K., Takeda, N. and Naoi, T., "Surface Density of Asperities and Real Distribution of Asperity Heights on Rubbed Surfaces", Wear, Vol. 47, March 1978, pp. 5-20.

46. Sasada, T., Norse, S. and Mishina, H., "The Behaviour of Adhered Fragments Interposed Between Sliding Surfaces and the Formation Process of Wear Particles", Trans. ASME, J. of Lubrication Technology, Vol. 103, April 1981, pp. 195-202.

47. Kato, S., Yamaguchi, K. Marui, E. and Tachi, K., "Frictional Properties of a Surface Covered with a Soft Metal Film- Part 1: Experiments on Friction Between a Single Protuberance and a Surface", Trans. of ASME, J. of Lubrication Technology, Vol. 103, April 1981, pp. 236-242.

48. Moore, D.F., "A Precise Wear Screening Machine", Tribology International, Vol.12 , August 1979, pp. 180-184.

49. Moore, D.F. and Noah, S., "Simple Reciprocating Friction and Wear Tester", Tribology International, Vol. 13, February 1980, pp. 11-15.

50. Throp, J.M., "A Novel Tri-pin-on-disc Tribometer Designed to Retain Lubricants", Tribology International, Vol. 14, April 81, pp. 121-125.

51. Timoshenko, S. and Goodier, J.N., Theory of Elasticity, Third Edition, McGraw-Hill Book Company, New York, New York, 1970, p. 312.

52. Hsu, J. and Meyer, A.U., Modern Control Principles and Applications, McGraw-Hill Book Company, New York, New York, 1968.

53. Gelb, A. and Vander Velde, W.E., Multiple-Input Describing Functions and Nonlinear System Design, McGraw-Hill Book Company, New York, New York, 1968.